Dissertation zur Erlangung des Doktorgrades

der Fakultät für Chemie und Pharmazie

der Ludwig-Maximilians-Universität München

Evaluation of the actin binding natural compounds
Miuraenamide A and Chivosazole A

Shuaijun Wang

Changchun, Jilin Province, P.R.China

2019

Erklärung

Diese Dissertation wurde im Sinne von §7 der Promotionsordnung vom 28. November 2011 von Herrn Prof. Dr. Stefan Zahler betreut.

Eidesstattliche Versicherung

Diese Dissertation wurde eigenständig und ohne unerlaubte Hilfe erarbeitet.

München, den 17.05.2019

_____

Shuaijun Wang

Dissertation eingereicht am: 17.05.2019
1. Gutachter: Prof. Dr. Stefan Zahler
2. Gutachter: Prof. Dr. Angelika M. Vollmar
Mündliche Prüfung am: 02.07.2019

To my family

Contents

1 Introduction

1.1 Actin and actin dynamics

Actin is one of the most abundant proteins in any eukaryotic cell as an essential component of the cytoskeleton and plays a central role in a number of motile activities such as cell migration, cell division and intracellular transport. It comprises a highly conserved family of proteins that fall into three broad classes: α-, β-, and γ-isoforms. It is mainly located in the cytoplasm, but it is also found in the nucleus. Actin exists in two principal forms, globular, monomeric actin (G-actin), and filamentous polymeric actin (F-actin). The globular form is a 43 kDa monomer, while the filamentous form is a long-chained polar polymer. G-actin monomers have tight binding sites that enable head-to-tail interactions with two other actin monomers, so that they polymerize into thin, flexible F-actin, and F-actin also can depolymerize into single G-actin monomers reversibly. So, actin filaments are in a continuous state of assembly/disassembly (Fig. 1.1). This steady state is dependent on solvent conditions, particularly on the presence of certain actin binding proteins (ABPs) and/or actin ligands such as jasplakinolide[1] or latrunculin B[2].
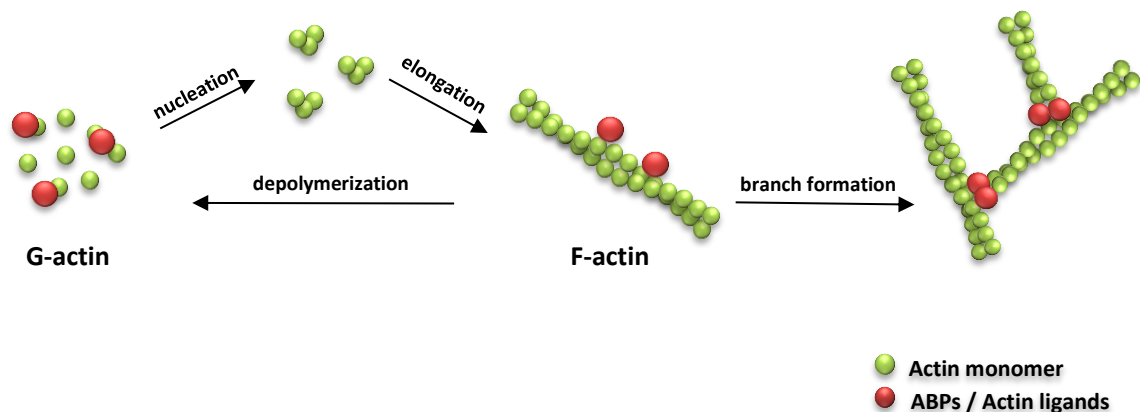
Figure 1.1 Actin dynamics-polymerization, depolymerization and branch formation
The actin polymerization is divided into two steps. 1) Nucleation: G-actin monomers form an unstable dimer, and then become stabilized by addition of another G-actin monomer to form a tight trimer. 2) Elongation: Actin-trimers then polymerize to form filaments (F-actin) by further G-actin monomer addition. Actin binding protein Arp2/3 complex can nucleate filaments from the side of existing filaments to allow the filaments branch formation. In the meantime, F-actin can also depolymerize into G-actin by losing G-actin monomers from the side of filament.

Actin is a protein with the greatest variety of binding partners (such as ABPs, actin binding compounds). Due to its common expression and its many biological functions, actin has not been pushed as a clinically relevant drug target.

1.2 Actin binding proteins

1.2.1 Actin dynamics is regulated by actin binding proteins

Actin binds a vast number of proteins called actin binding proteins (ABPs). Actin participates in more protein-protein interactions than any other known protein, including the interaction of actin with itself and with ABPs[3]. In cells, the assembly and disassembly of actin filaments, and also their functions are modulated by various of ABPs [4-6] (Fig. 1.2). The activities of these proteins are in turn under the control of specific signaling pathways. Actin polymerizes from both ends of the filament, but the rate of polymerization at either end is different. The fast-growing end is called the barbed end (or plus-end) and the slow-growing end is called pointed end (or minus-end). Actin filaments elongate when ATP-actin monomers are combined at the barbed end. As the filament elongating, ATP bound in the central cleft of actin is hydrolyzed and phosphate is released. As a result, the ADP-actin filament is disassembled by losing monomers from the pointed end. The released ADP-actin monomers then undergo nucleotide exchange to generate ATP-actin monomers that can be used for a new round of polymerization. This typical phenomenon of steady filament dissociation/association is called actin treadmilling. For actin alone, the equilibrium is a dynamic exchange of monomers between the G-actin and the F-actin pool. This dynamics is modulated by various ABPs. These proteins include actin depolymerization proteins (like e.g. ADF/cofilin), capping/sequestering proteins (like e.g. thymosin β4, Arp2/3 complex), severing proteins (like e.g. gelsolin), actin bundling protein (α-actinin), ABPs that facilitate nucleotide exchanging (like e.g. profilin), and ABPs that promote branching (like e.g. Arp2/3 complex)[6].
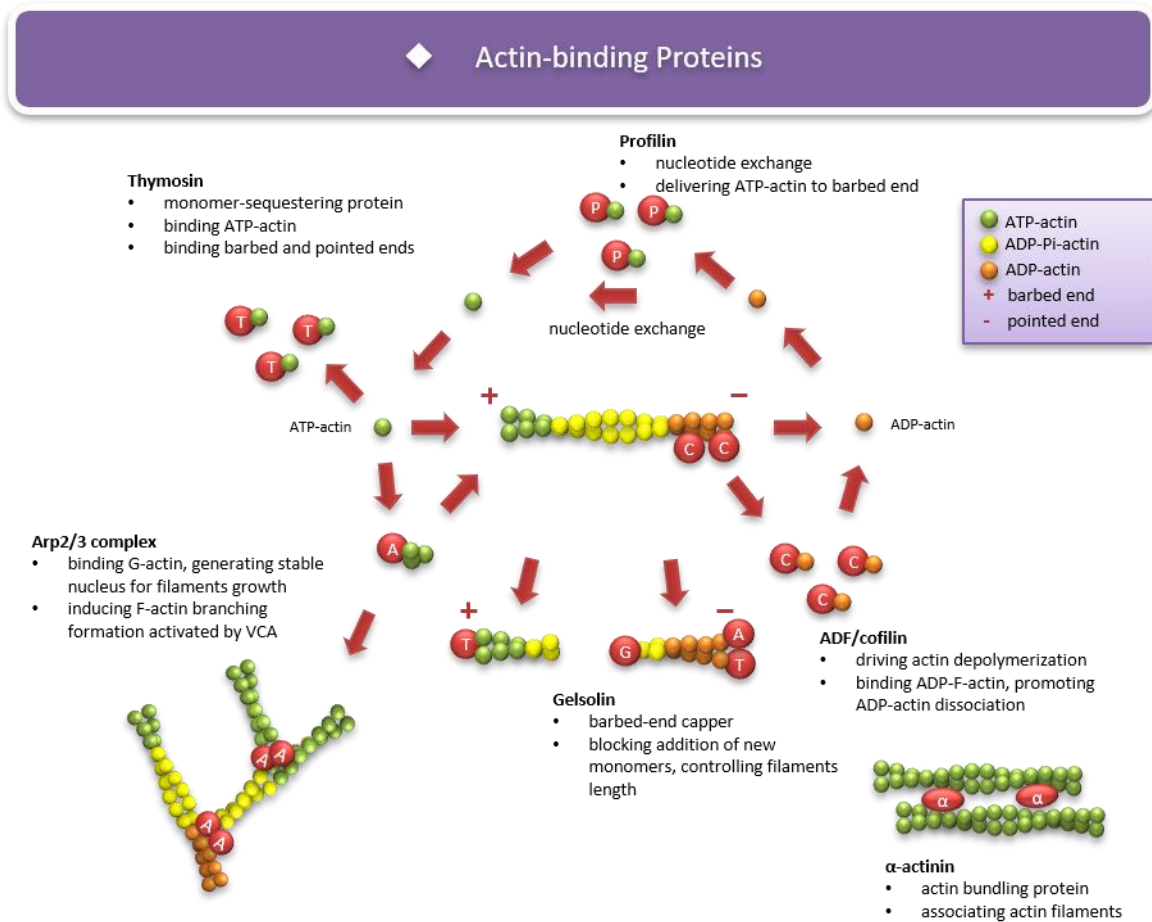
Figure 1.2 Actin binding proteins regulate actin dynamics

The monomer-binding protein ADP/cofilin is involved in binding ADP-actin when it is released from pointed end. And profilin facilitates the nucleotide exchange of ADP-actin for ATP-actin and delivers the new ATP-actin monomers to barbed ends to facilitate new rounds of polymerization. As a monomer-sequestering protein, thymosin β4 can clamp ATP-actin to effectively block both barbed and pointed ends, preventing ATP-actin combined into the filaments. So that a large amount of ATP-monomer actins can be stored. When triggered by a certain signal, a rapid release of thymosin β4 binding will happen, and leads to a rapid filament extension. ADF/cofilin binds to ADP-F-actin and promotes dissociation of ADP-actin from the pointed end of filament, driving actin depolymerization. Arp2/3 complex can nucleate filament formation, elongate filaments, and establish branch points in actin networks. It also caps the pointed end, reduces the loss of monomers from pointed end and thereby leads to rapid filament extension. By contrast, the barbed end cappers such as gelsolin, it caps filament barbed end, blocks the addition of new ATP-monomers, controlling the overall length of the filament. As an actin bundling protein, α-actinin can form an association of actin filaments[6].

1.2.2 Actin competes with ABPs and actin itself in a limited G-actin pool

The actin cytoskeleton controls cells interaction with each other and their environment in a precise way. This is depending on the rearrangement of actin dynamics which is regulated by numerous different actin regulators, such as ABPs. A number of recent findings suggest that different actin assembly factors compete with one another for a finite G-actin pool. This competition limits actin and actin regulators activities and therefore a specific actin network and structures were formed as cell needs. Increasing or decreasing cellular G-actin influences the generation of F-actin network. For example, the actin monomer binding protein profilin is responsible for producing ATP-G-actin for assembly. Profilin also enhances formin-mediated and Ena/VASP-mediated actin filament elongation, leading linear filaments assembly[7, 8], which consequently inhibit Arp2/3 complex-mediated actin nucleation and branch formation. Thymosin β4 clamps ATP-G-actin and control the amount of available ATP-G-actin for assembly. It was found that the formin and Arp2/3 complex compete with each other for G-actin and disruption of one frees more actin monomers for the other[9]. The competition between actin monomers, F-actin filaments and ABPs for binding to the available G-actin pool ensures cytoskeletal homeostasis and coordination between the different actin regulators to support dynamic cell behavior.

1.3 Actin cytoskeleton and disease

1.3.1 The actin cytoskeleton is involved in fundamental functions in cell

The actin cytoskeleton (actin and ABPs) plays a key role in intracellular transport, cell motility, control of cell shape and polarity, and distribution of macromolecules within cells[10] (Fig. 1.3). Reorganization of the actin cytoskeleton and expression of different actin isoforms are closely associated with cell differentiation processes[11]. This system is also involved in cell division[10]. The actin skeleton was shown to play an important role during programmed cell death, especially in apoptosis[12-14]. It has been shown that actin is also present in nuclei, where it plays a key role in nuclear matrix association, chromatin remodeling, RNA polymerase I, II, and III transcription, and mRNA processing[15].
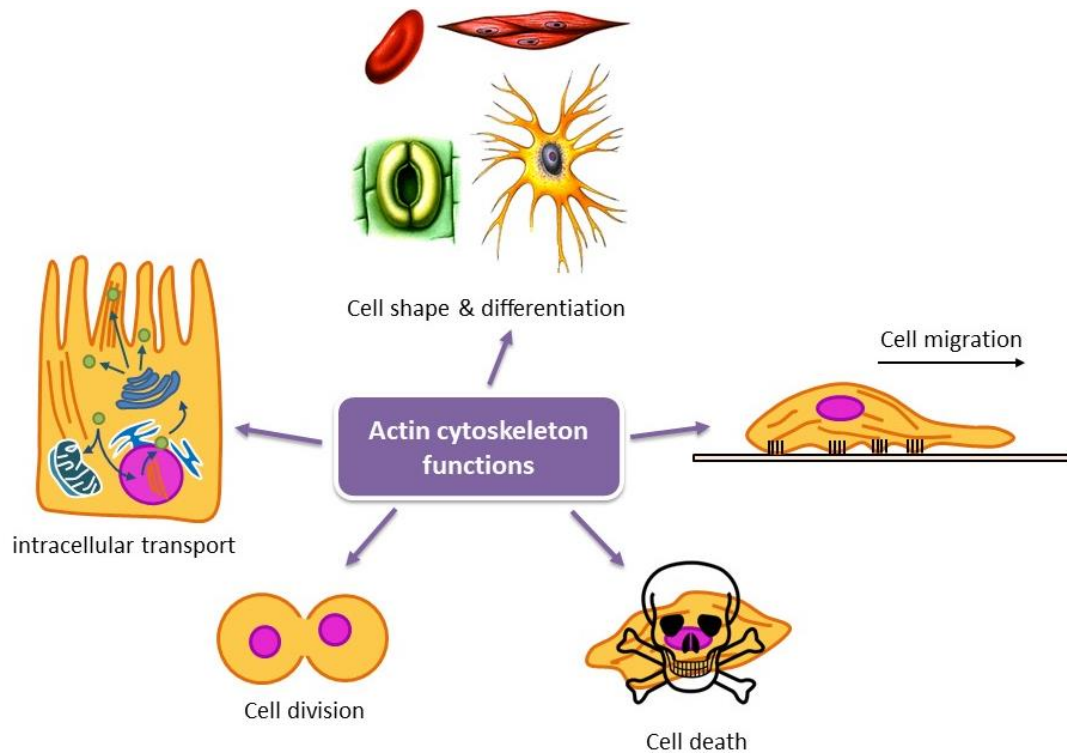
Figure 1.3 Biological functions of actin cytoskeleton in cells

Cell shape picture is retrieved from http://www.scienceline.ucsb.edu/images/cell-shapes.

1.3.2 The actin cytoskeleton plays important role in the development of different diseases

The actin cytoskeleton, besides the above-mentioned fundamental functions in cell vital activity, also plays a key role in the development of different diseases. The role of the cytoskeleton and ABPs in disease is an emerging story. The actin microfilament system is involved in oncological processes (cell transformation, invasion[16], and metastasis[17]) and tissue fibrosis[18]. In particular, the metastatic disease, or the cancer cells movement, is a complex process requiring dramatic remodeling of the cell cytoskeleton[17]. Actin dynamics defects are a common feature contributing to neurodegeneration[19, 20]. The actin cytoskeleton is essential for invasion and infection by various viruses, bacteria, and other parasites[21]. All these processes largely depend on the polymerization and depolymerization of actin filaments, and the organization of actin into functional networks is of course regulated by ABPs. Factors regulating actin assembly become potential targets for preventing dissemination and invasion of tumor cells. Actin-dependent cellular processes, including tumor invasion, can be pharmacologically modulated by small-molecule inhibitors of actin assembly[22]. The inseparable element of the cancer progression, Epithelial-to-mesenchymal transition (EMT) and its reverse process MET

involve the acquisition of features such as invasiveness and migration potential. And the cell movement is due to changes in actin cytoskeleton reorganizations including polymerization and depolymerization of actin filaments[23]. The dynamics of this process can be regulated by actin-binding proteins such as cofilin-1 (CFL1) or special AT-rich sequence-binding protein 1 (SATB1)[24]. Profilin1 is required for normal mouse brain development, which relies on profilin1 regulation of actin[25].Thus, a better understanding of the molecular mechanisms of ABPs controlling actin cytoskeleton provides cues for the treatment of these diseases. The feasibility of modifying the behavior of ABPs as a therapeutic approach for disease is a considerable need.

1.4 Actin binding natural compounds

1.4.1 Actin binding natural compounds: promising actin targeting compounds in a therapeutic setting

Though actin binding natural compounds are known for more than 45 years[26], none of them has made it into clinics yet for reasons of lacking functional selectivity. The large number of actin binding compounds we know today is mainly of natural origin (fungi, bacteria, marine organisms) and can be roughly divided into two groups: 1) actin filament stabilizers (phalloidin 1975[27], jasplakinolide 1994[28]), and 2) actin filament assembly inhibitors or destabilizers (kabiramide C 1993[29], latrunculin 1983[30]). The discovery of actin binding compounds has immensely fueled our knowledge about the biology of actin, and these natural compounds mentioned above have already become standard tools in cell biology.

Although, during the past years, we have learned that the complexity of actin biology goes far beyond the regulation of overall polymerization and depolymerization[31]: actin does not merely form polymers with other actin molecules and subsequently depolymerize again. Rather, ABPs continuously compete with each other for binding sites on actin (e.g. thymosin β4 with profilin[32], or MRTF with G-actin[33]) and with actin itself[31]. This complex network allows for subtle control of the "actin-interactome" and related cell functions. Small actin-binding molecular compounds have been found to, in turn, compete with specific actin-binding proteins. For example, kabiramide C has been shown to compete with actin capping proteins like gelsolin in a kind of "molecular mimicry"[34]. This aspect of the interaction between small molecular inhibitors and actin has been largely neglected during the characterization discovery. The effect of actin-binding compounds on the cellular level has

yet to be discovered. And the use of actin targeting natural compounds in a therapeutic setting has to be considered in spite of their availability. It would open a new field of biological tools or even therapeutic options by developing novel and much more specific actin targeting compounds.

1.4.2 Miuraenamide A - a new actin stabilizer

Myxobacteria produce a variety of natural compounds that interfere with the dynamics of cytoskeleton structures of eukaryotic cells, such as chondramides[35], disorazoles[36], and rhizopodins[37].

A novel myxobacterial compound miuraenamide A, is presumed to be an actin filament stabilizing agent[38]. Miuraenamide A is a cyclodepsipepide antibiotic that was isolated from Paraliomixa miuraensis, a slightly halophilic myxobacterium discovered in Japan in 2006[39]. The absolute stereostructure of miuraenamide A was soon determined in 2008[40]. Miuraenamide A shows antimicrobial activity, inhibits NADH oxidase, and stabilizes actin filaments[38-40]. Miuraenamide A also shows high cytotoxicity to a range of tumor cell lines[41]. The β-methoxyacrylate moiety of miuraenamide A is known to be important for its antimicrobial activity[40], but its influence on actin binding is still unclear. Comparable biological effects of Miuraenamide A were observed with other cyclodepsipeptides, such as chondramide[42] and jasplakinolide[35], which is not surprising on the basis of their closely related structures (Fig. 1.4). Owing to its interesting biological activities, the synthesis of miuraenamides was soon obtained by a peptide modification approach in 2015[41]. Further investigations on the characterization of miuraenamide A binding to actin is promising.

Miuraenamide A: R=H, X=Br (*E*)
             B: R=H, X=Cl (*E*)
             C: R=H, X=I (*E*)
             D: R=H, X=Br (*Z*)

Chondramide A: R^1=OMe, R^2=H
             B: R^1=OMe, R^2=Cl
             C: R^1=H, R^2=H
             D: R^1=H, R^2=Cl

Jasplakinolide
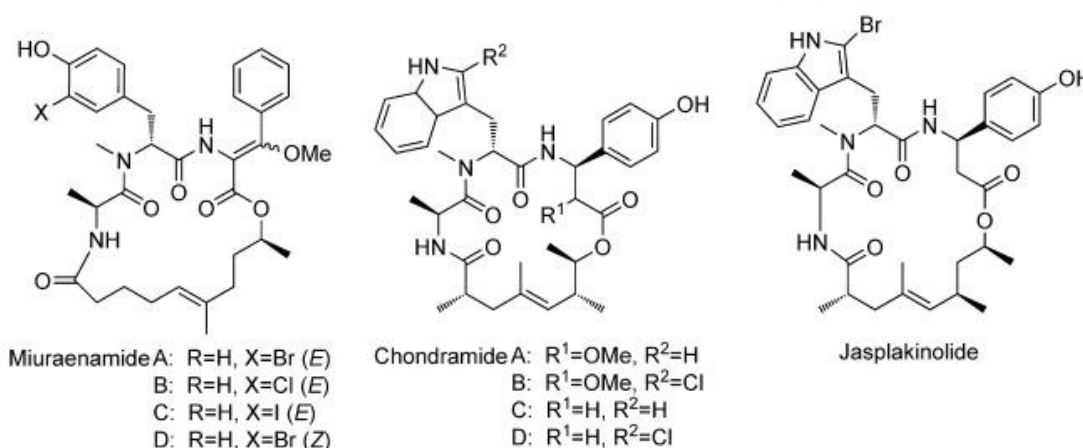
Figure 1.4 Structures of cyclodepsipeptides

(adapted from Karmann L et al. 2015[41])

1.4.3 Chivosazole A - a new actin destabilizer

Chivosazoles are 31-membered macrolides with one oxazol ring that were originally discovered in different strains of the myxobacterium Sorangium cellulosum, the main representative of which is chivosazole A[43] (Fig. 1.5). The chivosazoles are glycosides of 6-deoxyglucose derivatives. Additionally, the simple aglycon of chivosazole A, was isolated and named chivosazole F. The chivosazole family shows a potent antiproliferative activity against different mammalian cell lines including human cancer cell lines. Chivosazoles show antimicrobial activity against yeasts and filamentous fungi[43]. Chivozazoles are cytotoxic against mouse fibroblasts (L-929), inducing a clearly morphological changes different from those induced by rhizopodin. Chivosazoles destabilize pryrene F-actin, while rhizopodin and cytochalasin D do not[44]. This reveals that chivosazoles inhibit actin polymerization through specific binding to G-actin, thereby leading to disruption of cytoskeletal dynamics. The absolute and relative configuration of chivosazole A has been assigned in 2007 [45], prompting the chemical synthesis of this very potent natural product. The synthesis of the chivosazoles was shown to be feasible in 2017[46]. As a result, the exact binding site and action mode of chivosazole A are likely to be distinct, thus making it a novel, selective tool for the investigation of actin cytoskeleton, as well as a promising antimicrofilament lead candidate for drug discovery.

Chivosazole A   R = 2,3-dimethoxy-6-deoxy-glucosyl
Chivosazole F   R = OH
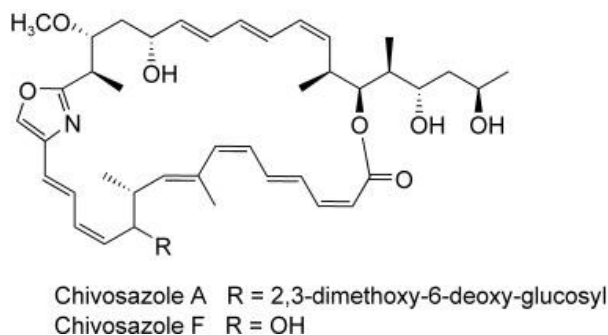
Figure 1.5 Structure of chivosazole A and F

(adapted from Diestel R et al. 2009[44])

1.5   Aim of the study

We wanted to perform an in-depth characterization of these two novel myxobacterial compounds miuraenamide A (in comparison to the classical actin stabilizer jasplakinolide) and chivosazole A (in comparison to a structurally unrelated actin filament inhibitor latrunculin B[2])

> ➢   in vivo on cellular function and on transcriptional regulation
> ➢   in vitro on actin dynamics and protein-protein-interactions of actin
> ➢   through co-crystallization and structure determination to reveal their actin binding mode

in order to find out new and more specific actin targeting compounds and develop them into a new field of biological tools or even therapeutic options instead of just "stabilizers" or "destabilizers".

2 Materials and Methods

2.1 Materials

2.1.1 Compounds

Miuraenamide A (MiuA) was kindly provided by Prof. Dr. Uli Kazmaier (Institute for Organic Chemistry, Saarland University, Saarbrücken, Germany). Jasplakinolide (Jaspla) was purchased from Santa Cruz (Heidelberg, Germany). Chivosazole A (ChivoA), Chivosazole F (ChivoF) and Rhizopodin were kindly provided by Prof. Dr. Rolf Müller (Helmholtz Center for Infection Research, Saarland University, Saarbrücken, Germany), isolated from myxobacterial strains. Latrunculin B was purchased from Biomol GmbH (Hamburg, Germany).

All compounds were dissolved in dimethyl sulfoxide (DMSO) and stored at -20 °C. For cell experiments, they were further diluted in endothelial cell growth medium (ECGM) with a maximum end concentration of DMSO of 0.1% (v/v). For TIRF and actin-binding experiments, they were further diluted in DMSO.

2.1.2 Chemicals and reagents

The following table contains a list of all chemicals, reagents and kits used in this study. Buffers and solutions are listed separately.

Table 2.1: Chemicals and reagents

Reagent	Producer
Adenosine 5′-triphosphate (ATP)	Sigma-Aldrich, Taufkirchen, Germany
Actin (rabbit skeletal muscle)	Hypermol, Bielefeld, Germany
Actin-Toolkit G-actin binding	Hypermol, Bielefeld, Germany
Actin-Toolkit F-actin binding	Hypermol, Bielefeld, Germany
α-actinin (turkey gizzard smooth muscle)	Hypermol, Bielefeld, Germany
Arp2/3 complex (porcine brain)	Hypermol, Bielefeld, Germany
ATP-Sucrose cushion	Hypermol, Bielefeld, Germany
Atto488-Actin (rabbit skeletal muscle)	Hypermol, Bielefeld, Germany
Amphotericin B	PAN-Biotech, Aidenbach, Germany
Bovine Serum Albumin (BSA)	Sigma-Aldrich, Taufkirchen, Germany
$CaCl_2$	Sigma-Aldrich, Taufkirchen, Germany
Catalase	Sigma-Aldrich, Taufkirchen, Germany

Cofilin (non muscle cofilin)	Hypermol, Bielefeld, Germany
Collagen G	Biochrom AG, Berlin, Germany
Coomassie Brilliant Blue R-250 staining solution	Bio-Rad, Munich, Germany
Coomassie Brilliant Blue R-250 destaining solution	Bio-Rad, Munich, Germany
Crystal violet	Carl Roth, Karlsruhe, Germany
D-glucose	Sigma-Aldrich, Taufkirchen, Germany
Dimethyl sulfoxide (DMSO)	Sigma-Aldrich, Taufkirchen, Germany
Dithiothreithol (DTT)	SERVA Electrophoresis, Heidelberg, Germany
Dulbecco's Modified Eagle Medium (DMEM)	PAA Laboratories, Pasching, Austria
Endothelial cell growth medium (ECGM)	Pelobiotech, Martinsried, Germany
Ethanol	Carl Roth, Karlsruhe, Germany
Ethylendiaminetetraacetic acid (EDTA)	Sigma-Aldrich, Taufkirchen, Germany
Ethylene glycol-bis(2-aminoethylether)-N,N,N′,N′-tetraacetic acid (EGTA)	Sigma-Aldrich, Taufkirchen, Germany
F-Actin BufferKit REF 5300-01	Hypermol, Bielefeld, Germany
Fetal calf serum (FCS)	Biochrom AG,Berlin
FluorSave® reagent mounting medium	Merck, Darmstadt, Germany
Glucose oxidase from Aspergillus Niger	Sigma-Aldrich, Taufkirchen, Germany
GST-VCA (recombinant, human)	Hypermol, Bielefeld, Germany
Hoechst 33342	Sigma-Aldrich, Taufkirchen, Germany
Imidazole	Sigma-Aldrich, Taufkirchen, Germany
KH_2PO_4	Carl Roth, Karlsruhe, Germany
KCl	Carl Roth, Karlsruhe, Germany
Corning®, Matrigel®, REF 356231	Corning, NY, USA
Methanol	Carl Roth, Karlsruhe, Germany
Methylcellulose	Sigma-Aldrich, Taufkirchen, Germany
$MgCl_2$	AppliChem, Darmstadt, Germany
$MgSO_4 \cdot 7H_2O$	Carl Roth, Karlsruhe, Germany
$Na_3C_6H_5O_7$	Carl Roth, Karlsruhe, Germany
NaCl	Carl Roth, Karlsruhe, Germany
Na_2HPO_4	Merck, Darmstadt, Germany
Formaldehyde, 16%, methanol free, Ultra Pure	Polysciences Inc., Warrington,PA, USA
Penicillin/Streptomycin	PAN Biotech, Aidenbach, Germany
Prestained protein ladder PageRuler™	Bio-Rad, Munich, Germany

Pyrene Actin 10% (rabbit skeletal muscle)	Hypermol, Bielefeld, Germany
Rhodamin phalloidin	Sigma-Aldrich, Taufkirchen, Germany
Sodium dodecyl sulfate (SDS)	Carl Roth, Karlsruhe, Germany
Streptomycin	PAN Biotech, Aidenbach, Germany
Tris-Base	Sigma-Aldrich, Taufkirchen, Germany
Tris-HCl	Sigma-Aldrich, Taufkirchen, Germany
Triton X-100	Merck, Darmstadt, Germany
Trypsin	PAN Biotech, Aidenbach, Germany
β-Mercaptoethanol	Sigma-Aldrich, Taufkirchen, Germany

Table 2.2: Consumables

Product	Producer
Cell culture flasks 75cm^2	TPP, Trasadingen, Switzerland
Corning® 96 Well Black Polystyrene Microplate REF3686	Corning Incorparated, NY, USA
Cover slip (8 × 8 mm)	H.Saur Laborbedarf, Reutlingen, Germany
Cover slip (22 × 22 mm)	Th.Geyer GmbH, Renningen, Germany
Disposable pipettes: 5 ml, 10 ml, 25 ml	Greiner Bio, Frickenhausen, Germany
Falcon tubes: 15 ml, 50 ml	VWR, Bruchsal, Germany
Glass slide (Microscope Slides 76 × 26 mm)	Thermo scientific, Braunschweig, Germany
Microcentrifuge Tubes: 1.5ml	Beckman Coulter, Krefeld, Germany
Microtiter plates: 96 well	Greiner Bio, Frickenhausen, Germany
Microtubes: 1.5 ml, black	Carl Roth, Karlsruhe, Germany
Microtubes: 1.5 ml, brown	Sarstedt AG & Co.KG, Nuembrecht, Germay
Parafilm	American National Can, Chicago, USA
Pipette tips: 10 µl, 100 µl, 1000 µl	Sarstedt, Nümbrecht, Germany
Safe-Lock Tubes: 0.5 ml, 1.5 ml, 2.0 ml	Eppendorf, Hamburg, Germany
µ-Slide 8 Well	Ibidi GmbH, Munich, Germany
µ-Slide Angiogenesis	Ibidi GmbH, Munich, Germany

µ-Slide Chemotaxis	Ibidi GmbH, Munich, Germany

2.1.3 Technical equipment

Table 2.3 Technical equipment

Technical equipment	Producer
Axiovert 25 / m200	Zeiss, Jena, Germany
ChemiDoc™ Touch Imaging System	Bio-Rad Laboratories, Munich, Germany
Digital block heater HX-1	PEQLAB Biotechnologie, Erlangen, Germany
Heracell CO_2 Incubator 150i	Thermo Fisher Scientific, MA, USA
Heraeus Megafuge 1.0 RS centrifuge	Kendro Laboratory Products, Hanau, Germany
Ibidi stage top incubation system	Ibidi GmbH, Munich, Germany
IKA Vibrax VXR Basic shaker	IKA-Werke, Staufen Germany
Infinite® 200 PRO microplate reader	Tecan, Männedorf, Switzerland
LSM 510 Meta confocal microscope	Zeiss, Jena, Germany
Mikro 220 / 220 R microliter centrifuge	Hettich, Tuttlingen, Germany
Mini-PROTEAN® 3	Bio-Rad, Dreieich, Germany
Nanodrop® ND-1000	Peqlab,Wilmington, USA
Optima TLX Ultracentrifuge	Beckman Coulter, Fullerton, CA, USA
Power Pac 300 blotting device	Bio-Rad, Dreieich, Germany
SpectraFluor Plus™ microplate reader	Tecan, Männedorf, Switzerland
Thermo Haake W19 open-bath circulator	Thermo Fisher Scientific, MA, USA
Total internal reflection fluorescence microscope (TIRFM)	Leica Microsystems, Wetzlar, Germany
Vi-Cell™ XR	Beckman Coulter, Fullerton, CA, USA
Nikon inverted microscope Eclipse Ti	Nikon corporation, Tokyo, Japan

2.2 Methods

2.2.1 Cell culture

The human umbilical vein endothelial cells (HUVECs) are primary cells purchased from Promocell (Heidelberg, Germany). The company guarantees an ongoing quality control (e.g. expression of endothelial markers). Further authentication is not necessary, since these are primary cells. The cells were cultured with endothelial cell growth medium (Promocell), supplemented with 10% FCS under constant humidity at 37 °C and with 5% CO_2. Upon confluency, cells were splitted in a ratio 1:3 in a 75 cm^2 cell culture flasks. Cells were used for functional assays at passage 6.

Table 2.4 Cell culture solutions and reagents

Endothelial cell growth medium (ECGM)		Freezing medium	
Endothelial cell growth medium (with supplement kit)	500 ml	DMEM	70%
FCS (heated)	50 ml	FCS	20%
Amphotericin*	5 ml	DMSO	10%
Pen / Strep*	5 ml		

Stopping medium		Starvation medium	
DMEM	500 ml	DMEM	500 ml
FCS (heated)	50 ml	Amphotericin*	5 ml
		Pen / Strep*	5 ml

PBS (pH 7.4)	
NaCl	132.2 mM
Na_2HPO_4	10.4 mM
KH_2PO_4	3.2 mM
H_2O	

PBS+Ca^{2+}/Mg^{2+} (pH 7.4)	
NaCl	137 mM
KCl	2.68 mM
Na_2HPO_4	8.10 mM
KH_2PO_4	1.47 mM
$MgCl_2$	0.25 mM
H_2O	

Trypsin/EDTA (T/E)	
Trypsin	0.05%
EDTA	0.20%
PBS	

Collagen G	
Collagen G	0.001%
PBS	

* Pen / Strep: Penicillin 10 000 Units/ml, Streptomycin 10 mg/ml

* Amphotericin: Amphotericin B 250 µg/ml

2.2.2 Passaging

For passaging, cell medium was removed, cells were washed twice with PBS and detached with 1.5 ml Trypsin/EDTA (37 °C, 3 min). After incubation, tryptic digestion was stopped by adding 15 ml stopping medium. Cells were centrifuged (1000 rpm, 5 min, 20 °C), resuspended in ECGM. Cell concentration and vitality were determined by using Vi-Cell™ XR. Then cells were either transferred into a new cell culture flask (75 cm^2, pre-coated with Collagen G) or seeded for experiments.

2.2.3 Freezing and thawing

For long time storage, a 75 cm^2 flask of confluent HUVECs were detached by Trypsin/EDTA and collected by centrifugation (1000 rpm, 5 min, 20 °C). Cells were then resuspended in 3 ml ice-cold freezing medium. 1.5 ml aliquots were frozen in cryovials and stored at -80 °C for 24 h before being moved to liquid nitrogen (-196 °C) for longtime storage. In order to thaw cells, cells in cryovials were immediately dissolved in pre-warmed stopping medium.

DMSO was removed by centrifugation, cells were resuspended in 15 ml pre-warmed ECGM and transferred into a 75 cm² flask (pre-coated with Collagen G).

2.3 Proliferation Assay

HUVECs (1.5×10^3 cells/well) were seeded in 96-well plates (pre-coated with Collagen G). After 24 h incubation, cells in a reference plate were stained with crystal violet and served as initial control. The cells in a treatment plate were either left untreated or treated with indicated concentrations of compounds respectively for 72 h. After treatment, the medium was removed and cells were stained with crystal violet staining solution for 10 min, then washed with water and dried overnight. Cell-bound crystal violet was dissolved with sodium citrate solution (5 min, shaking) and the absorbance which correlates with cell number was measured at 550 nm using a microplate reader (SpectraFluor PlusTM). For statistical analysis, cells treated with vehicle control were set to be 100%.

Table 2.5 Crystal violet and sodium citrate buffer.

Crystal violet staining solution		Sodium citrate solution	
Crystal violet	0.5%	$Na_3C_6H_5O_7$	0.05 M
Methanol	20%	Ethanol	50%
H_2O		H_2O	

2.4 Fluorescence imaging

HUVECs (25×10^3 cells/well) were seeded in an 8 well ibidi µ-slide (pre-coated with Collagen G), pretreated with indicated concentrations of compounds. After 1 h treatment, cells were rinsed with PBS + Ca^{2+}/Mg^{2+} and fixed with 4% (v/v) formaldehyde for 10 min. After 5 min washing with PBS, samples were permeabilized for 2 min with 0.2% Triton X-100 in PBS. After 3×5 min washing with PBS, cells were incubated with rhodamine phalloidin (1:400) and Hoechst 33342 (1 µg/ml) for 1 h at room temperature, then washed again 3×5 min with PBS and sealed with one drop of FluorSave reagent mounting medium and covered by cover slips (8×8 mm). Images were taken using a Zeiss LSM 510 META confocal microscope.

2.5 Cell migration assay

2.5.1 Scratch assay

To examine the migratory ability of HUVEC cells under the influence of various compounds, scratch assay was performed first. For the scratch assay, HUVECs were seeded into 96-well plates (Collagen G pre-coated), incubated overnight. Then confluent HUVECs were scratched with a custom-made tool and either left untreated or treated with the indicated concentrations of compounds. Cells were allowed to migrate for 16-24 h, then washed with 100 µl/well PBS (including Mg^{2+}, Ca^{2+}), stained with 100 µl/well Crystal Violet solution for 10 min, washed with water, and dried. Images were taken using a standard inverted microscope. Image analysis was performed with ImageJ. Migration was quantified as the percentage of cell covered area compared with the total image area.

2.5.2 2D and 3D Chemotaxis

Chemotaxis experiments were conducted according to the manufacturer's instructions. For the 2D-chemotaxis assay, HUVECs (50×10^3/well) were seeded in a µ-Slide Chemotaxis, either left untreated or treated with indicated concentrations of compounds and incubated to be slightly adherent to the surface of the observation area. After 2 h, ECGM with a gradient of FCS between 0 and 10% (v/v) was applied into the slide (Fig. 2.1). For 3D-chemotaxis assay, HUVECs (50×10^3/well) were seeded in matrigel in the observation area of a µ-Slide Chemotaxis, either left untreated or treated as indicated and incubated. After 0.5 h, ECGM with a gradient FCS between 0 and 10% (v/v) was applied (Fig. 2.2).

Time lapse image sequences of HUVEC cell migration were taken every 10 min for 21 h using a Nikon inverted microscope Eclipse Ti, equipped with ibidi stage top incubation system (37 °C, 5% CO_2, 80% humidity). Single cell tracking was performed using ImageJ software plugin "Manual tracking" (Version 2.0 with ImageJ Plugin). Images were analyzed using the Chemotaxis and Migration Tool (ibidi, Martinsried, Germany). Cell mean velocity, directness and X-forward migration index (X-FMI) were calculated as parameters.
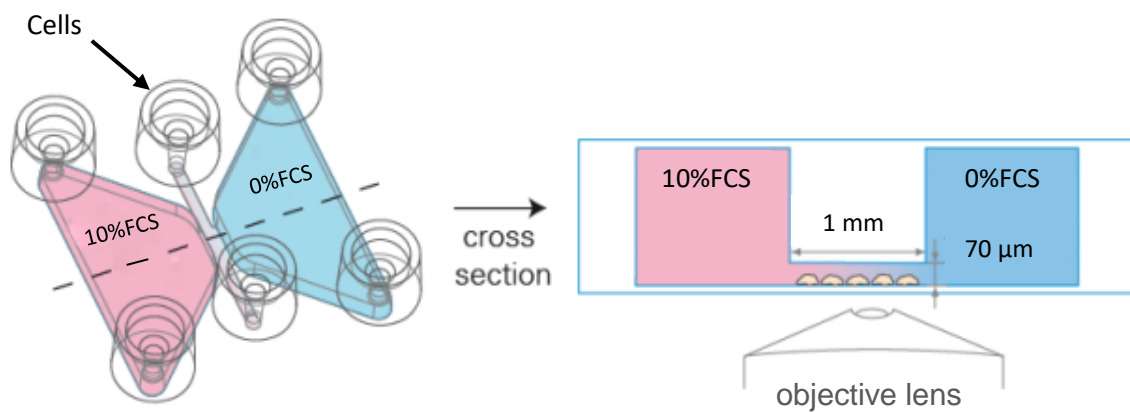
Figure 2.1 2D Chemotaxis experiments without gel

(adapted from Application note 17: Chemotaxis 2D and 3D, ibidi GmbH, Munich, Germany)
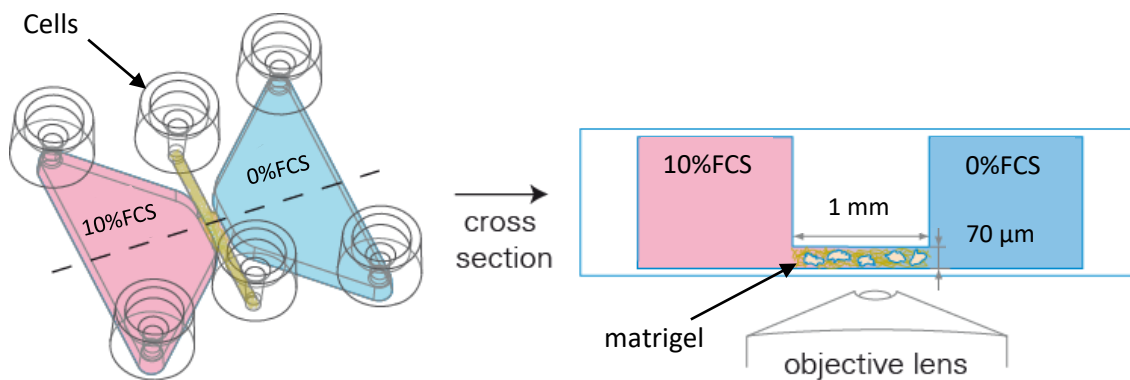
Figure 2.2 3D Chemotaxis experiments in matrigel

(adapted from Application note 17: Chemotaxis 2D and 3D, ibidi GmbH, Munich, Germany)

2.6 Tube formation assay

To investigate the effect of our compounds on HUVECs tube formation ability, tube formation assay was performed. For tube formation assay, HUVECs (10×10^3 cells/well) were seeded in matrigel in a μ-Slide Angiogenesis, either left untreated or treated with various compounds as indicated and incubated for tube formation. After 16 h, images of the cells were taken using a Nikon standard inverted microscope Eclipse Ti and analyzed by Wimasis GmbH (Munich, Germany). As parameters of tube formation, total branching points, total loops, total tubes and mean tube length were used.

2.7 Pyrene assay

To investigate the effect of our compounds on actin polymerization, pyrene assay was performed. This assay is based on the enhanced fluorescence of pyrene conjugated actin that occurs during polymerization. The enhanced fluorescence that occurs when pyrene G-actin (monomer) forms pyrene F-actin can be measured in a fluorimeter to follow polymerization over time.

Pyrene assay was performed using Pyrene Actin (10%) and F-Actin BufferKit according to the manufacturer's instructions. Pyrene Actin (10%) was diluted with H_2O to a 1 mg/ml (24 µM) stock solution. Before use, spontaneously formed actin aggregates were removed by ultracentrifugation for 1 h at 40,000 rpm and 4 °C. 50 µl samples for the pyrene assay consisted of: 30 µl H_2O, 10 µl 10 mM $MgCl_2$ or 250 mM KCl, 5 µl F-actin Buffer (100 mM Imidazole-Cl pH 7.4, 10 mM ATP) as well as 5 µl DMSO (containing indicated concentrations of compounds/proteins) were added into a 96 well black polystyrene microplate immediately before the rapid addition of 10 µl pyrene actin to start polymerization. Pyrene fluorescence was monitored every 20 s over 1 h in a 96-well fluorescence plate reader (Infinite® 200 PRO) at 360 nm excitation and 400 nm emission wavelength.

2.8 TIRF assays

2.8.1 Flow cell preparation

Flow cells containing 15 - 20 µl of fluid were prepared as a sandwich of a cover slip (22 × 22 mm), 2 parafilm strips forming an approximately 5 mm wide channel, and a glass microscope slide (76 × 26 mm). Both, the coverslip and the glass slide were cleaned by ethanol and dried. The chamber was heated briefly and cooled to melt the parafilm strips to the glass slide surface and the cover slip. For TIRF microscope, chambers were used with the cover slip down, facing the objective lens, and slide up (Fig. 2.3). Solutions were loaded directly into the chamber via capillary action.
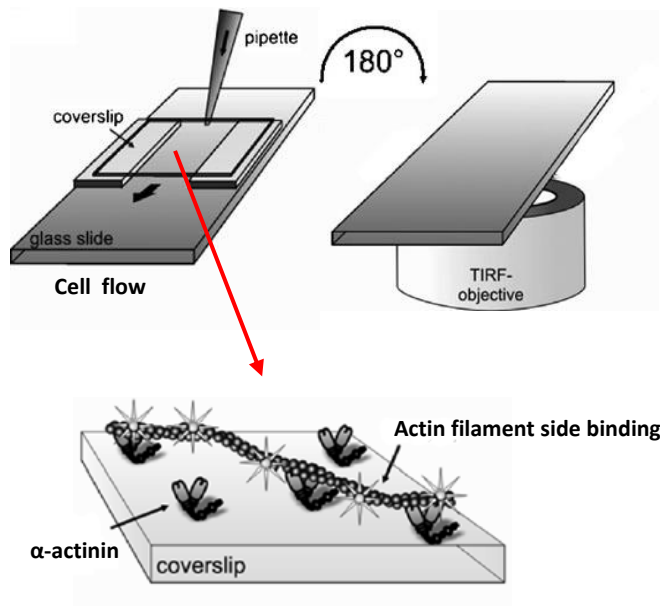
Figure 2.3 Scheme of flow cell and the visualization of single actin filaments using TIRF microscopy

Growing actin filaments attach to α-actinin on the coverslip surface. (adapted from Breitsprecher D et al. 2009[47])

2.8.2 Protein and TIRF buffer preparation

Atto488-Actin and Actin from rabbit skeletal muscle were purchased from Hypermol (Bielefeld, Germany). Both Atto488-Actin and Actin were reconstituted with H_2O to obtain a 1 mg/ml stock. Labeled actin was prepared by mixing Atto488-Actin and Actin 1:1 v/v. Protein concentration was determined by measuring OD at 290 nm (ε_{290} = 26,600 $M^{-1}cm^{-1}$) using Nanodrop® ND-1000[48].

α-actinin from turkey gizzard smooth muscle was purchased from Hypermol (Bielefeld, Germany) and was prepared by adding 1 ml H_2O to the tube with α-actinin to obtain a working stock of 1 mg/ml.

Table 2.7 Buffers for TIRF assays

G-buffer (pH 7.8)		10 × KMEI buffer (pH 7.1)	
Tris-HCl (pH 8.0)	2 mM	KCl	500 mM
$CaCl_2$	0.2 mM	$MgCl_2$	20 mM
DTT	0.5 mM	EGTA	20 mM
ATP	0.2 mM	Imidazole	300 mM
H_2O		H_2O	
Added before use:			
MgATP	0.2 mM		

2 × TIRF buffer (pH 7.4)		F-buffer	
10 × KMEI buffer	20% (v/v)	10 × KMEI buffer	10% (v/v)
D-glucose	30 mM	G-buffer	90% (v/v)
Catalase	40 µg/ml		
Glucose oxidase	400 µg/ml		
Methylcellulose	1%(w/v)	**10 × Mg exchange buffer**	
β-mercaptoethanol	2%(v/v)	$MgCl_2$	400 µM
G-buffer		EGTA	2 mM

2.8.3 Nucleation and polymerization assay

Freshly prepared flow cells were first incubated with 25 µl 1% (w/v) BSA for 10 min, then 25 µl α-actinin (1 mg/ml) was applied into the flow cell and incubated for 5 min. In the meantime, labeled actin (10 µM) was incubated 1:1 v/v with 1/10 volume of 10 × Mg exchange buffer and 1:8 v/v with G-buffer for 5 min on ice to convert Ca-ATP-actin to Mg-ATP-actin. Flow cell was then washed with 30 µl of G-buffer. 2 × Mg-ATP-actin (1 µM) was mixed 1:1 v/v with 2 × TIRF buffer containing different compounds as indicated, and the polymerization started. 30 µl polymerizing actin were immediately loaded into the flow cell chamber and placed on the TIRF microscope to start image acquisition. For nucleation

assay, the amount of actin nuclei present in each frame was analyzed using programs custom-written in MATLAB (The MathWorks, Natick, MA) R2017a. For polymerization assay, fluorescence image sequences of actin polymerization were taken every 1 s for 5 min. Elongation rates were calculated by Image J software (version 1.49).

2.8.4 Depolymerization assay

Labeled F-actin was obtained by incubating labeled actin (10 µM) 1:1 v/v with 1/10 volume of 10 × KMEI buffer and 1:8 with G-buffer for 1 h at room temperature. 20 µl 1:4 v/v diluted F-actin filaments (with F-buffer) were loaded into a flow cell previously blocked with 1% BSA and coated with 1 mg/ml α-actinin. Then 50 µl 2 × TIRF buffer with indicated compounds were applied gently into the flow chamber and immediately placed on the TIRF microscope to start image acquisition. The real time actin depolymerization process in a single frame was captured as image sequence every 15 s for 90 min. The average length of actin filaments was quantified as depolymerization parameter by using custom-written programs in MATLAB.

2.8.5 Phalloidin competition assay

For the phalloidin competition assay, labeled F-actin (prepared as described) was loaded into a freshly coated flow cell. TIRF buffer with 16.5 nM rhodamine-phalloidin, as well as different concentrations of Miuraenamide A as indicated were applied into the flow chamber and immediately placed on the TIRF microscope to start image acquisition. Different frames of fluorescent actin filaments were taken. Phalloidin Δintensity and IC 50 of Miuraenamide A were calculated by using ImageJ software (version 1.49).

2.8.6 Branch formation assay

To observe actin branch formation, labeled actin was incubated with Mg exchange buffer to obtain Mg-ATP-actin as described. 2 × Mg-ATP-actin (1 µM) was mixed 1:1 v/v with 2 × TIRF buffer containing Arp2/3 complex, GST-VCA and various compounds as indicated, then immediately loaded into a coated flow chamber and placed on the TIRF microscope to start image acquisition. A single frame of actin fluorescence was recorded every 2 s for 10 min.

2.9 Actin binding assay

2.9.1 G-actin binding assay

The G-actin binding assay was performed using 'Actin-Toolkit G-Actin Binding' according to manufacturer's instructions. In this kit G-actin is coupled to Sepharose^{TM} as G-actin beads. Binding of ABPs to G-actin is highly specific, and thus, the ABPs bound to G-actin will be co-precipitated under low centrifugal forces. G-actin beads (1/4 volume of 1 tube) were pre-treated with our compounds as indicated for 30 min at room temperature under agitation, then the ABPs (gelsolin, profilin, cofilin or Arp2/3 with GST-VCA) were added respectively, incubated for 1 h at room temperature. After incubation, sample was spun (6,000 × g, 4°C, 4 min) and 40 µl supernatant were mixed with 10 µl 5 × SDS-sample buffer. Then the G-actin beads were washed, resuspended in 25 µl of 1 × SDS-sample buffer and boiled at 95°C for 5 min. Both the supernatant and the G-actin beads (15 µl of each) were separately loaded onto an SDS-PAGE gel for analysis. After electrophoresis, the gel was stained in Coomassie Brilliant Blue R-250 staining solution for 60 min, rinsed in deionized water and then fixed in Coomassie Brilliant Blue R-250 destaining solution for 60 min at room temperature or overnight at 4°C. The stained gel was imaged using a ChemiDoc Imaging System. The amounts of each protein were quantified by using Image Lab 6.0 Software.

2.9.2 F-actin binding assay

F-actin binding assay was performed using 'Actin-Toolkit F-Actin Binding' according to manufacturer's instructions. F-actin is prepared by polymerizing G-actin with PolyMix (1 M KCl, 0.02 M MgCl$_2$, 0.01 M ATP, 0.1 M imidazole pH 7.4) for 30 min at room temperature. 250 µl F-actin sample mix were prepared by incubating F-actin with each of our compounds as indicated for 30 min in PolyMix at room temperature, then the respective F-actin binding protein (cofiln, gelsolin, or Arp2/3 complex with GST-VCA) was added, incubated for 1 h at room temperature (the molar ratio of F-actin and ABP was 1:1). During sample incubation the sucrose cushions was prepared by adding 50 µl sucrose solution to the centrifuge tube. After incubation, 40 µl of the sample mix were prepared (mixed with 10 µl of 5 × SDS-sample buffer) for a total SDS-PAGE sample. 200 µl of the rest sample was added into the centrifuge tube overlaying the sucrose cushion. Pelleting of F-actin binding proteins was achieved by spinning the rest of the sample at 100,000 × g, at 4 °C for 1 h. After centrifugation, 40 µl of the supernatant were prepared (mixed with 10 µl of 5 × SDS-sample buffer) as a supernatant sample for SDS-PAGE. The pellets were dissolved in 200 µl 1 ×

SDS-sample buffer, boiled at 95°C for 5 min and then 15 µl of each SDS-sample (total, supernatant and pellet) was loaded into an SDS-PAGE gel separately to observe F-actin binding after electrophoresis. The gel was then stained by coomassie blue as described in G-actin binding assay. After staining the gel was captured by using a ChemiDoc Imaging System. The amounts of each protein were quantified by using Image Lab 6.0 Software.

2.9.3 Crosslink assay

Cross-linking of thymosin β4 to G-actin was performed by using EDC as a cross-linker. Binding of thymosin β4 to G-actin could be detected after crosslinking. The molecular weight of cross-link product was approximately 47.5 kDa.

G-actin (27 µM) was dissolved in crosslink G-buffer (3 mM triethanolamine-HCl, 0.2 mM $CaCl_2$, 0.2 mM ATP, NaN_3, pH 7.5) and incubated with either ChivoA or LatB as indicated at 4 ºC for 30 min. Then thymosin β4 was applied and incubated at 4 ºC for 45 min at a weight ratio of 9:1, corresponding to 0.94 molecules of thymosin β4 per actin monomer. Aliquots of 10 µl were then mixed with 12.2 µl of 5.4 mM EDC (1-ethyl-3-(3-dimethylaminopropyl)- carbodiimide) in 0.1 M MES (2-(N-morpholino)-ethanesulfonic acid), pH 6.5, and incubated for 2 h at 25 ºC. Equal aliquots were taken up into SDS sample buffer and analyzed by SDS-PAGE on a 10% gel to detect cross-link product. After electrophoresis gel was then stained by coomassie blue as described in G-actin binding assay. After staining the gel was captured by using a ChemiDoc Imaging System. The amounts of each protein were quantified by using Image Lab 6.0 Software. Cross-link product was quantified as a normalized gray intensity of cross-link product band compared with actin.

2.9.4 SDS-PAGE

The SDS-PAGE gels were prepared in a discontinuous manner, with a stacking gel on top of the separation gel. The concentrations of acrylamide in the separation gels were adjusted to optimize the separation of proteins according to their molecular weights.

The Mini-PROTEAN 3 electrophoresis module was used. Prior to sample loading, the apparatus was assembled according to manufacturer's protocol and the chamber was filled with electrophoresis buffer. Equal amount of samples were loaded on to the stacking gel. An equal volume of 1 x SDS-sample buffer containing 2 µl of prestained protein ladder PageRuler™ was loaded on each gel to estimate the molecular weights of the separated proteins. Electrophoresis was carried out at 100 V for 21 min for protein stacking, then at 200 V for 35-45 min for protein separation.

Table 2.8 Buffers for SDS-PAGE analysis

5x SDS-sample buffer	
3.125 M Tris-Base, pH6.8	10%
Glycerol	50%
SDS	5%
DTT	2%
Pyronin Y	0.025%
in H_2O	

1x SDS-sample buffer	
5x SDS sample buffer	20%
H_2O	80%

Table 2.9 Acrylamide gels

Separation gel 10 / 12 / 15 %	
Rotiphorese™ Gel 30	33/40/50%
1.5 M Tris-Base (pH 8.8)	25%
SDS	0.1%
TCE	10%
TEMED	0.1%
APS	0.05%
in H_2O	

Stacking gel	
Rotiphorese™ Gel 30	17%
1.25 M Tris-Base (pH 6.8)	10%
SDS	0.1%
TEMED	0.2%
APS	0.1%
in H_2O	

Table 2.10 Electrophoresis buffer

Electrophoresis buffer	
Tris-Base	4.9 mM
Glycine	38 mM
SDS	0.1%
in H_2O	

2.10 Assessment of the transcriptome

HUVECs at 80 % confluency were treated with equipotent concentrations of 60 nM MiuA, 120 nM Jaspla, 20 nM ChivoA or 250 nM LatB respectively for 4 h. The concentrations were chosen in order to stay below levels causing visible alterations of cell morphology and overall actin structure. Samples for transcriptome analysis were prepared by F. Gegenfurtner. Transcriptome analysis was performed by Prof. Dr. Wolfgang Enard (Department Biology II, Ludwig-Maximilians University Munich, Germany).

2.11 Quantification and statistical analysis

Quantitative data are expressed as mean ± SEM. Statistical analysis was performed using the software GraphPad Prism Version 7.02 (GraphPad Software, Inc., La Jolla, CA, USA). Statistical differences were evaluated by using Kruskal - Wallis test or one-way analysis of variance (ANOVA). P-values lower than 0.05 were considered to be significant. For all tests, three independent replicates (n = 3) were used respectively. Specific information on the statistical procedures used can be found in the respective figure legends.

3 Results - Part 1:

Miuraenamide A, a novel actin stabilizing compound, selectively inhibits cofilin binding to F-actin

3.1 Miuraenamide A induces actin nucleation and polymerization, as well as stabilization of filaments

Based on previous findings[38], we investigated the molecular mechanism of the interaction of miuraenamide A with actin alone. First, we examined the effect of Miuraenamide A on the actin polymerization process in a pyrene assay. With 1 µM Miuraenamide A, actin nucleation and polymerization were faster (Fig. 3.1A) but, interestingly, peak fluorescence was lower. This might result from substrate consumption by the rapid formation of small actin aggregates. Monitoring actin filament assembly by TIRF microscopy showed that Miuraenamide A increased the overall rate of formation of actin filaments (Fig. 3.1B). This increase in the number of filaments formed over time suggested a stabilizing effect during nucleation.

Next, we investigated the influence of Miuraenamide A on the rate of actin filament elongation using TIRF microscopy. In the absence and presence of 250 nM of Miuraenamide A, we monitored the length of individual filaments as a function of time and found that the elongation rate doubled compared to control samples (Fig. 3.1C). To determine whether Miuraenamide A plays any role in stabilizing actin filaments, we monitored the disassembly of labeled actin filaments in the presence and absence of 5 µM Miuraenamide A by TIRF microscopy. As expected, the length of actin filaments decreased in a time-dependent manner in the absence of Miuraenamide A. In the presence of Miuraenamide A, disassembly of filaments was retarded (Fig. 3.1D). These results indicate that the binding of Miuraenamide A promotes both, the assembly and stabilization of actin filaments.
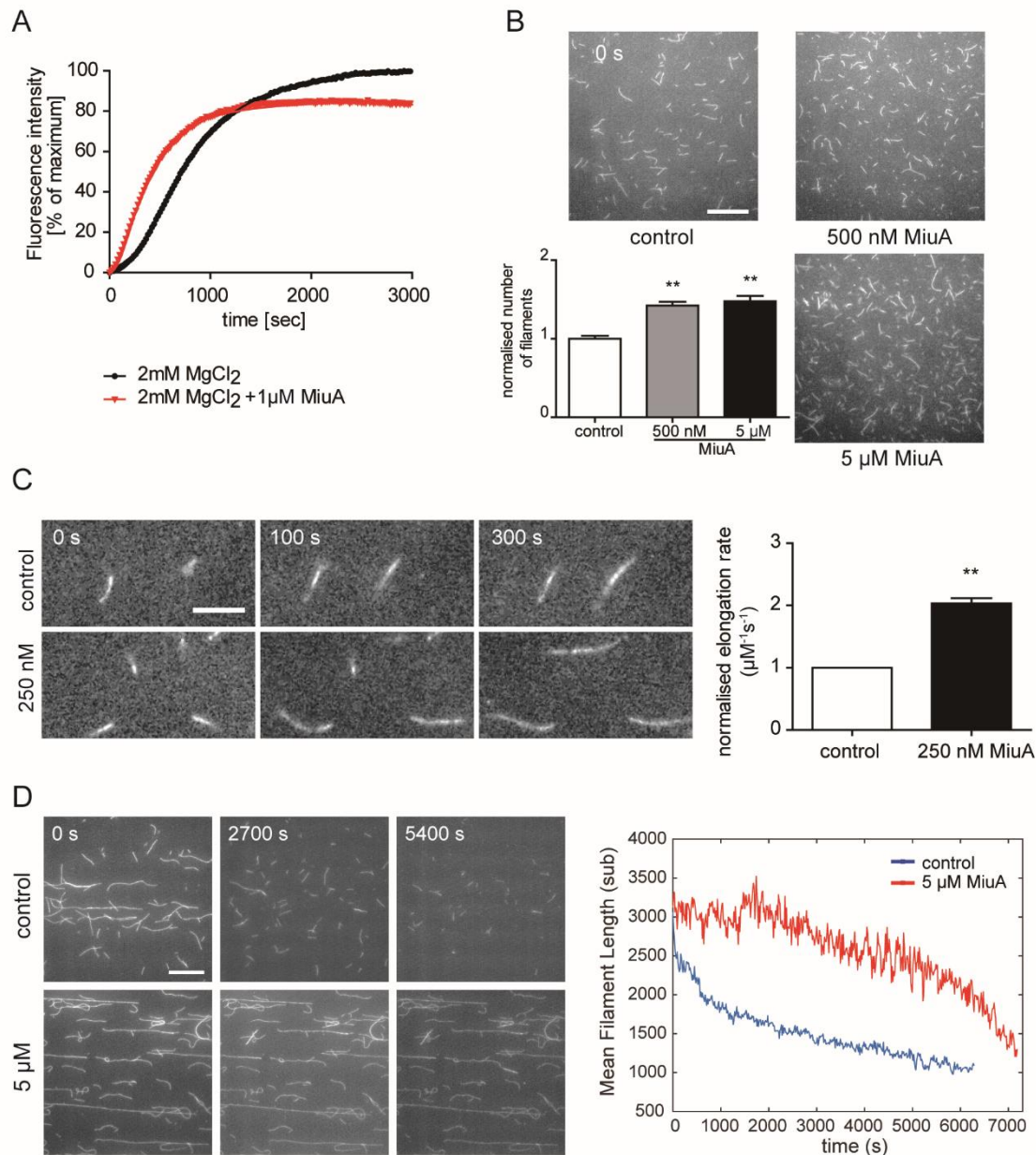
Figure 3.1 Miuraenamide A enhances actin polymerization and nucleation, and inhibits depolymerization

(A) The pyrene assay shows an accelerated polymerization of actin after treatment with Miuraenamide A. (B) The TIRF assay shows increased number of filaments indicating more nucleation of actin upon addition of Miuraenamide A. (C) Actin elongation measured using TIRF microscopy. Left panel: Representative time series of fluorescence images show the elongation of actin filaments. Right panel: The calculated actin elongation rate. (D) Miuraenamide A reduces actin depolymerization as shown by TIRF microscopy. Left panel: Representative fluorescence images at different time points during F-actin depolymerization. Right panel: The average length of actin filaments was quantified as depolymerization parameters. Scale bars in (B) and (D) represent 15 µm.

*Scale bar in (C) represents 5 µm. (Kruskal–Wallis test with Dunn's test as post hoc, **P<0.01 vs. control, n=3).*

3.2 Miuraenamide A competes with phalloidin for binding to F-actin

Phalloidin is a well-known F-actin stabilizing compound with a well characterized binding site[49]. To investigate whether Miuraenamide A binding to actin competes with phalloidin binding, we performed a competition assay with rhodamine-labeled phalloidin. Rhodamine-labeled phalloidin could be displaced from actin filaments by Miuraenamide A in a concentration dependent manner (Fig. 3.2A) with an IC 50 of about 5 nM (Fig. 3.2A-right panel). This indicates that Miuraenamide A may share a proximal binding site with phalloidin on F-actin, or that Miuraenamide A allosterically influences binding of phalloidin.

3.3 Effect of Miuraenamide A on actin filament branch formation

Subsequently, we measured the effects of Miuraenamide A on actin filament dynamics, which is more complex but also more physiologically relevant. First, we studied Arp2/3-mediated actin filament nucleation. The actin-related protein Arp2/3 complex is a key actin filament nucleation factor that binds to actin and rapidly assembles distinctive branched filament networks. Addition of Miuraenamide A enhanced the overall polymerization in the presence of activated Arp2/3 (i.e. Arp2/3 in complex with the VCA domain of the WAVE protein) (Fig. 3.2C, upper panel). To visualize the effect of Miuraenamide A on actin Arp2/3-mediated branch formation, we used TIRF to measure Atto488 labeled actin in the presence of Arp2/3 (activated by the VCA domain of the WAVE protein). The formation of branched filament networks is accelerated by an increasing concentration of Miuraenamide A (500 nM, 1 µM). At 5 µM Miuraenamide A, a large number of actin nuclei were observed with very few branches (Fig. 3.2B, bottom panel). We made a similar observation in the pyrene assay: in the presence of 50 mM potassium, actin steadily polymerized, resulting in a linear growth curve. Addition of Arp2/3 complexes induced a sigmoidal curve of nucleation and polymerization. In the presence of an excessive concentration of Miuraenamide A (50 µM), the onset of actin nucleation was so fast that it could not be substantially accelerated by the addition of Arp2/3 complexes (Fig. 3.2C, lower panel).
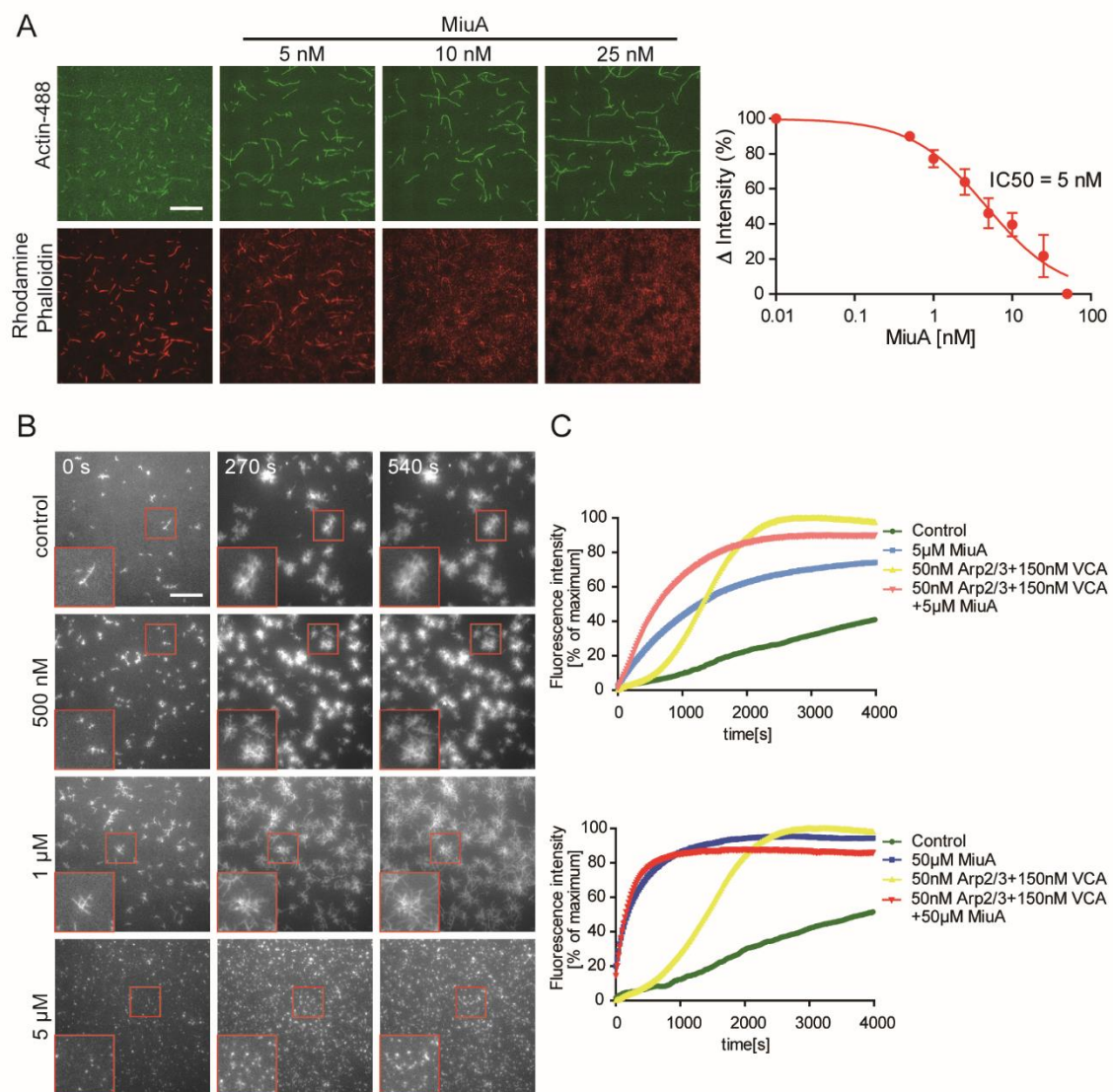
Figure 3.2 Miuraenamide A competes with phalloidin for binding to F-actin and increases branch formation induced by Arp2/3 and CST-VCA

(A) Miuraenamide A competes with phalloidin binding to actin filaments. Labeled F-actin was incubated with 16.5 nM rhodamine phalloidin and increasing concentrations of Miuraenamide A. Images of actin filaments were taken by TIRF microscopy. Left panel: TIRF images showing the Atto488-labeled actin filaments (upper panels) and rhodamine-labeled phalloidin (lower panels). At increasing concentrations of Miuraenamide A, the binding of phalloidin to actin filaments decreased. Right panel: The IC50 of Miuraenamide A was calculated (n=3). (B) Actin branch formation was triggered by addition of the Arp2/3 complex and GST-VCA during polymerization, and the process of branch formation was measured using TIRF microscopy. The representative time series of fluorescence images show actin branch formation. Red inserts: zoom-ins of single actin nuclei at 2× magnification. (C) The results of pyrene assays show the fast nucleation induced by 5 µM Miuraenamide A and Arp2/3/VCA. Scale bar in A and B represents 15 µm.

3.4 Miuraenamide A inhibits proliferation of endothelial cells at nanomolar concentration and leads to actin aggregation

To assess the effect of Miuraenamide A on cells, we first measured proliferation. At nanomolar concentrations, Miuraenamide A inhibited the proliferation of HUVEC cells with an IC 50 value of around 9 nM (Fig. 3.4A), which is comparable to that in tumor cell lines (HCT116, HepG2, HL-60, U-2OS)[41]. Phalloidin staining of F-actin revealed that one hour of incubation with 30 nM of Miuraenamide A reorganizes the actin cytoskeleton into clusters or aggregates (Fig. 3.4B). At 100 nM Miuraenamide A, the actin cytoskeleton was completely destroyed and perinuclear actin aggregates were observed (Fig. 3.4B).

3.5 Miuraenamide A inhibits HUVEC cell migration

To examine the effect of Miuraenamide A on the ability of cells to migrate, we performed a scratch assay. The migration of HUVEC cells was inhibited by Miuraenamide A in a concentration-dependent manner with an IC 50 of approximately 80 nM (Fig. 3.4C). Since migration normally occurs in a gradient of growth factors, we studied the effect of Miuraenamide A on the chemotactic properties of HUVECs. In a 2D-chemotaxis assay, the directed migration of HUVECs was inhibited by 10 nM Miuraenamide A, as seen by the reduction of the forward migration index (FMI) and directness, while the mean velocity of movement was not affected (Fig. 3.4D). In 3D-chemotaxis, at 10 nM Miuraenamide A, cell migration directness, mean velocity and FMI were all significantly reduced (Fig. 3.4E). These results indicate that Miuraenamide A has an overall effect on both cell motility and directionality of the movement, both in a simple 2D and in more physiological 3D environments. The reduced velocity in the 3D system could be explained by the cells having a reduced ability to squeeze through a small meshwork.

Overall, the cellular response to Miuraenamide A was typical for actin nucleating compounds[50].
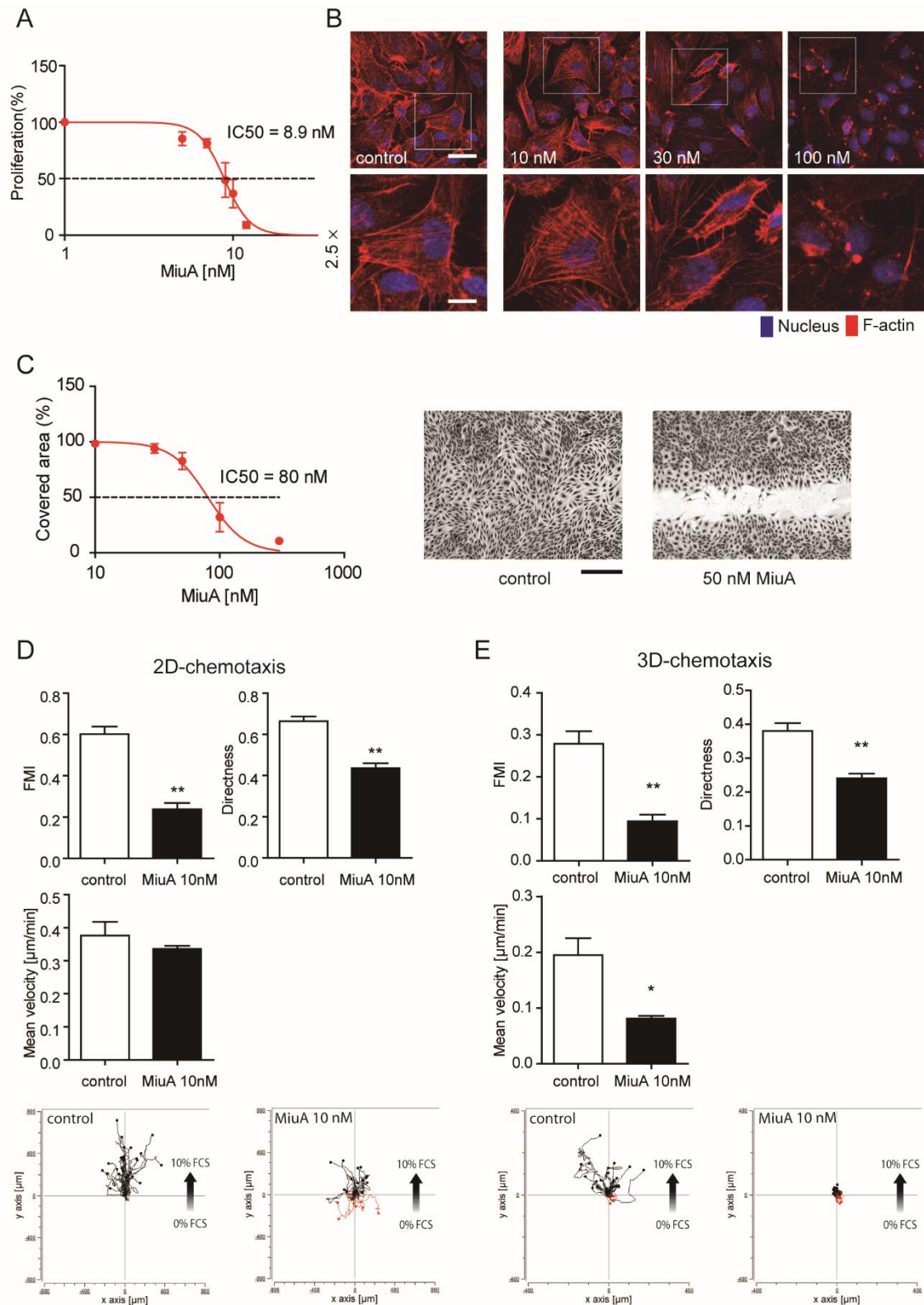
Figure 3.3 Miuraenamide A inhibits proliferation of HUVEC cells, induces actin aggregation and inhibits migration

(A) Half inhibitory concentration (IC 50) on proliferation of Miuraenamide A (n=3). (B) HUVEC cells were treated with the indicated concentrations of Miuraenamide A for 1 h, fixed and stained for F-actin (red) and DNA to highlight the nuclei (blue). Representative images out of 3 independent experiments performed in triplicates are shown. The upper scale bar in (B) represents 75 µm, and the lower scale bar represents 30 µm. The white frame indicates the zoomed in area. (C) Confluent HUVECs were scratched and treated with Miuraenamide A (indicated concentrations). After 16 h, images were collected and the cell covered area was analysed. Left panel: the measured IC 50 of Miuraenamide A from a scratch assay is shown (n=3). Right panel: Representative images of the scratch assay. The scale bar represents 200 µm. Miuraenamide A inhibits endothelial cells migration (D) in 2D- and (E) in 3D-chemotaxis assays. Quantitative evaluation of the parameters X-Forward migration index, directness and mean velocity are shown (n=3). Analysis of one representative experiment (out of triplicates in three independent experiments) is shown. (Kruskal– Wallis test with Dunn's test as post hoc, *P<0.05, **P<0.01 vs. control, n=3).

3.6 Effect of Miuraenamide A on HUVECs tube formation

To study the effect of Miuraenamide A on a morphogenetic process in vitro, a tube formation assay on matrigel was performed. The tube structure when compared with control could not be established after 16 – 20 h incubation with increasing concentration of Miuraenamide A (Fig. 3.5A). The maturation of the network, which is characterized by a reduction of branching points, tube loops and tube number, as well as by an increase of tube length in control, did not occur after treatment with 10 nM and 30 nM Miuraenamide A (Fig. 3.5B). Treatment led to a fragmented phenotype of the tubular network with a higher number of shorter tubes. At 100 nM Miuraenamide A, HUVEC cells could not build a network at all, the cell-cell contacts were clearly disrupted. Thus, Miuraenamide A interferes with the stability of tubes and development of cell-cell contacts.
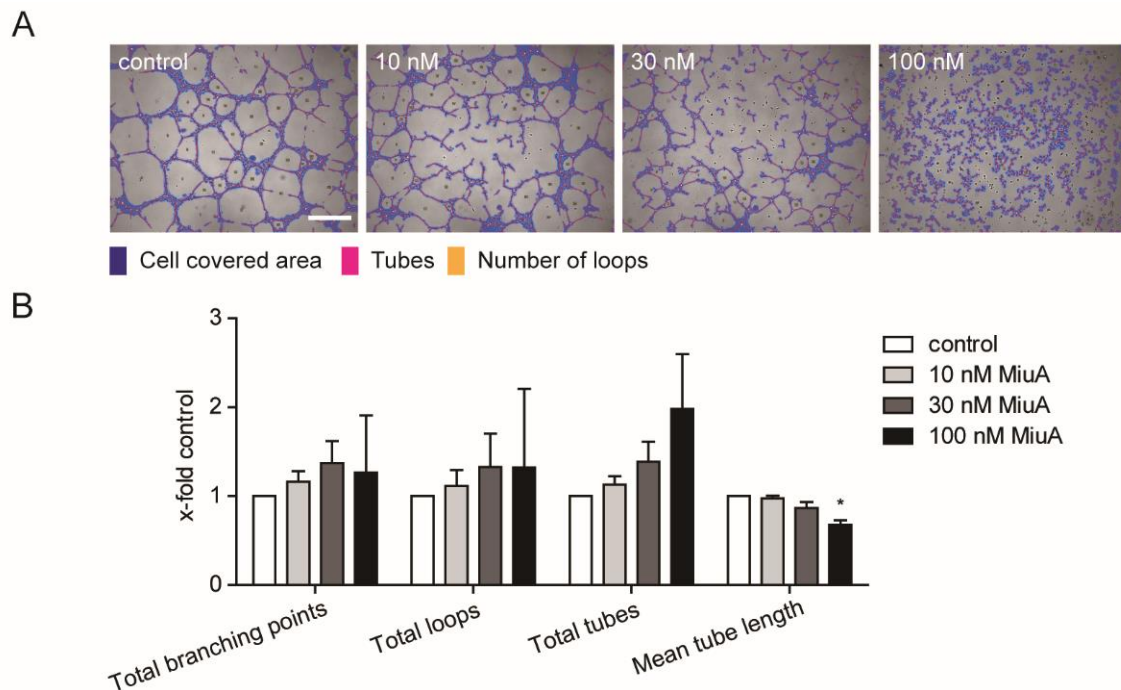
Figure 3.4 Miuraenamide A disturbs tube maturation of endothelial cells on Matrigel

HUVECs were seeded on matrigel, treated with the indicated concentration of Miuraenamide A respectively and incubated for 16 h. Images were taken and analyzed. (A) Representative images in one experiment (out of triplicates in three independent experiments each) are shown. Cell covered areas recognized by software are indicated in blue, tubes are indicated in pink, and loops are indicated by yellow numbers. (B) Tube length, number of total loops, total tubes, and total branching points were analyzed (n=3). The scale bar represents 30 µm. (One-way ANOVA with Tukey post hoc test for multiple comparisons, *P<0.05 vs. control, n=3).

3.7 Effect of Miuraenamide A on the binding of proteins to G-actin

We next investigated whether Miuraenamide A affects the binding of ABPs to G-actin. To this end, we performed pulldown experiments with G-actin immobilized on beads and added single ABP (gelsolin, profilin, cofilin or Arp2/3 complex with GST-VCA). As depicted in Fig. 3.6A-D, the total amount of the tested ABPs in G-actin pellets did not increase or decrease even if treated with a high amount of Miuraenamide A (10 or 100-fold excess), indicating that Miuraenamide A does not compete with gelsolin, profilin, cofilin or Arp2/3 complex for binding to G-actin.
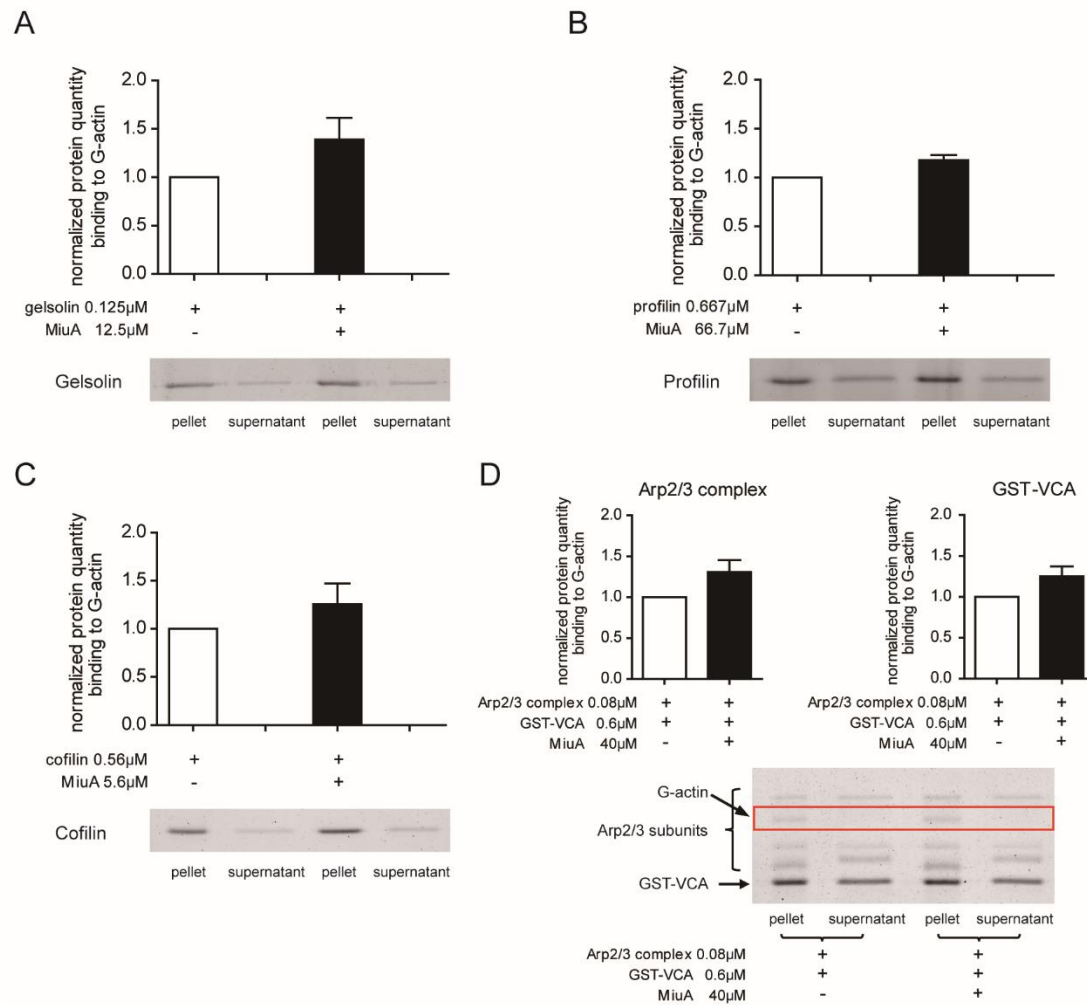
Figure 3.5 Miuraenamide A does not change the binding of ABPs to G-actin

G-actin beads were incubated with indicated concentrations of Miuraenamide A for 30 min at room temperature, then 0.01mg/ml of the G-actin binding proteins (A) gelsolin, (B) profiling, (C) cofilin and (D) Arp2/3 complex & GST-VCA was added respectively and incubated for 1 h at room temperature. After 1 h, the mixture of actin beads and ligands was spun and only the ligands bound to G-actin will be co-precipitated in the pellet. The amount of G-actin binding protein in the pellets was quantified. Representative images of protein bands and quantifications are shown. (Kruskal–Wallis test with Dunn's test as post hoc, no significant differences vs. control, n=3).

3.8 In contrast to jasplakinolide, Miuraenamide A influences cofilin binding to F-actin

To investigate potential competition of Miuraenamide A and ABPs for binding to F-actin, we also performed a binding assay with cofilin, gelsolin and Arp2/3 complex (together with GST-VCA) to F-actin. In the absence of Miuraenamide A, cofilin was largely found in the F-actin pellet (Fig. 3.7A), as expected from the known interaction between cofilin and F-actin. In the presence of Miuraenamide A, a significant reduction of cofilin was observed in the pellet (Fig. 3.7A, upper panel). Jasplakinolide did not change binding of cofilin to F-actin, even when added at a ten-fold concentration in comparison to Miuraenamide A. (Fig. 3.7A, lower panel). Neither Miuraenamide A, nor jasplakinolide influenced binding of gelsolin (Fig. 3.7B), and Miuraenamide A did not affect Arp2/3 complex binding to F-actin, since the amounts of Arp2/3 complex in F-actin pellet were similar in the presence or absence of Miuraenamide A (Fig. 3.7C). These results suggest that Miuraenamide A selectively interferes with the binding of cofilin to F-actin, and that this action is specific for Miuraenamide A, since it was not mimicked by jasplakinolide.

Figure 3.6 Miuraenamide A selectively inhibits binding of cofilin to F -actin

(A) Miuraenamide A inhibits binding of cofilin to F-actin filaments (upper panel), while jasplakinolide does not (lower panel). F-actin was incubated with (A) cofilin, (B) gelsolin or (C) Arp2/3 complex & GST-VCA, together with Miuraenamide A or jasplakinolide (molar ratio 1:10). Binding of gelsolin (B) or Arp2/3 (C) to F-actin were not influenced by Miuraenamide A or jasplakinolide. The amount of F-actin binding protein in the total sample, supernatant and pellets was quantified. Representative images of protein bands and quantifications are shown. (Kruskal–Wallis test with Dunn's test as post hoc, **P<0.01 vs. control, n=3).

4 Results - Part 2:

Chivosazole A modulates protein-protein-interactions of actin

4.1 Chivosazole A sequesters G-actin, inhibits actin nucleation, polymerization and branch formation and destabilizes F-actin in vitro

To characterize the functional effects of chivosazole A in comparison with a prototypic actin depolymerizer with a different binding site and mode of action (latrunculin B), we performed a pyrene assay with pyrene labeled actin and TIRF assay with Atto488 labeled actin. In the pyrene assay, chivosazole A concentration dependently inhibits actin polymerization (Fig. 4.1A), as previously described by others[44]. When investigating the underlying mechanisms, we found that the critical concentration of actin in the presence of either latrunculin B or chivosazole A, was increased to a similar degree (Fig. 4.1B). This indicates a similar sequestering action of both compounds. Accordingly, we found a decreased nucleation of actin in TIRF assays (Fig. 4.1C), and a lower rate of polymerization (Fig. 4.1D). In addition, we observed a destabilizing effect of chivosazole A on F-actin filament stability (Fig. 4.1E). In addition, we observed the formation of branched filament networks triggered by Arp2/3 complex and GST-VCA. Branches formed slower and shorter with 5 µM chivosazole A (Fig. 4.1F). Taken together, our data suggest that chivosazole A inhibits actin filament branch formation by sequestering G-actin, so that less actin nuclei were formed for forming actin filament branches.
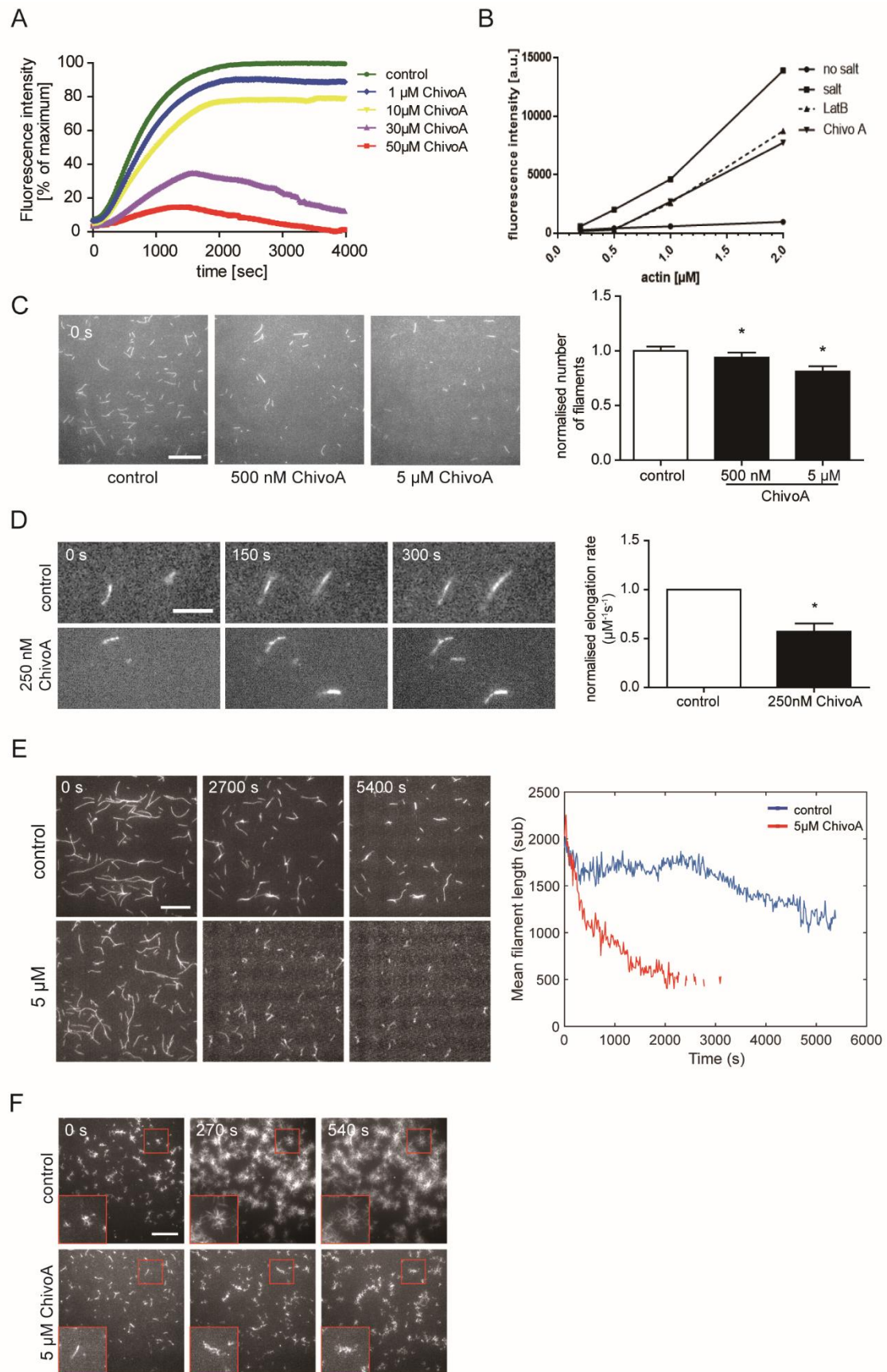
Figure 4.1 Chivosazole A sequesters G-actin, inhibits actin nucleation, polymerization and branch formation and destabilizes F-actin in vitro

(A) Chivosazole A inhibits polymerization of pyrene actin concentration dependently. (B) Chivosazole A (20 µM) and Latrunculin B (positive control, 20 µM) shift the critical concentration of actin for polymerization to a similar degree. (C) and (D) In TIRF assays, chivosazole A inhibits nucleation of actin and the elongation rate. (E) F-actin filaments are destabilized by chivosazole A in the TIRF assay. (F) Actin branch formation is triggered by addition of the Arp2/3 complex and GST-VCA during polymerization, and the process of branch formation is inhibited by chivosazole A. The representative time series of fluorescence images are shown. Red inserts in (F): Zoom-ins of single actin nuclei at 2✕ magnification. Scale bars in (C), (E) and (F) represent 15 µm. Scale bars in (D) represents 5 µm. Data are presented as mean ± SEM, n = 3, *p < 0.05 using Kruskal-Wallis test.

4.2 Chivosazole A inhibits proliferation and changes actin architecture in endothelial cells

In order to get insights into potential functional differences between the two compounds (in spite of their similar actions on actin alone), we performed comparative experiments on a cellular level. In HUVECs chivosazole A inhibited proliferation with an IC 50 of approximal 3 nM. This is in good accordance with previously published values in different mammalian cells[44], and demonstrates chivosazole A to be much more potent than latrunculin B (Fig. 4.2A). Morphologically, chivosazole A causes dissociation of F-actin fibers and formation of amorphous actin aggregates with increasing concentrations (Fig. 4.2B).
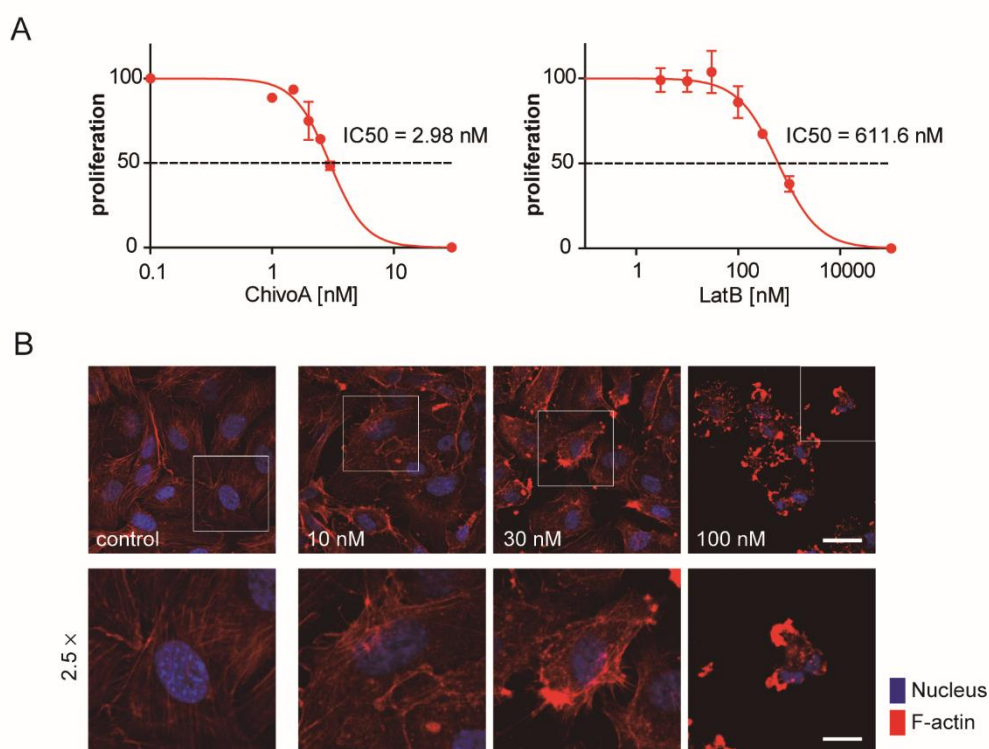
Figure 4.2 Chivosazole A inhibits proliferation and changes actin architecture in endothelial cells

(A) Chivosazole A (left panel) inhibits HUVEC cells proliferation much more potently than latrunculin B (right panel). (B) The actin cytoskeleton of HUVECs is rapidly rearranged by chivosazole A. Representative images in one experiment (out of triplicates in three independent experiments each) are shown. Lower panel: Zoom-in of the white frames indicated as boxes in the upper panels. Blue: nuclei stained with Hoechst, red: F-actin stained with rhodamine-phalloidin. Scale bars: 75 µm (upper panel), 30 µm (lower panel).

4.3 Chivosazole A inhibits HUVEC cell migration

Since cellular motility is a central aspect of actin function, we investigated the effects of the two compounds on migration of HUVECs in a scratch assay and specifically on directional migration (chemotaxis). The IC 50 value concerning migration was 10-fold higher than for proliferation (Fig. 4.3A). This is most likely due to the shorter duration of the migration assay (16 h vs. 72 h). With latrunculin B the difference in potency in comparison to chivosazole A was less in migration than in proliferation, indicating that latrunculin B loses potency over time more rapidly than chivosazole A. In 2D-chemotaxis assay, overall features of cell motility (velocity), and directional components of migration were assessed. Both

compounds caused a decrease of cell velocity, and, additionally, a loss of the "sense of direction" (Fig. 4.3B).
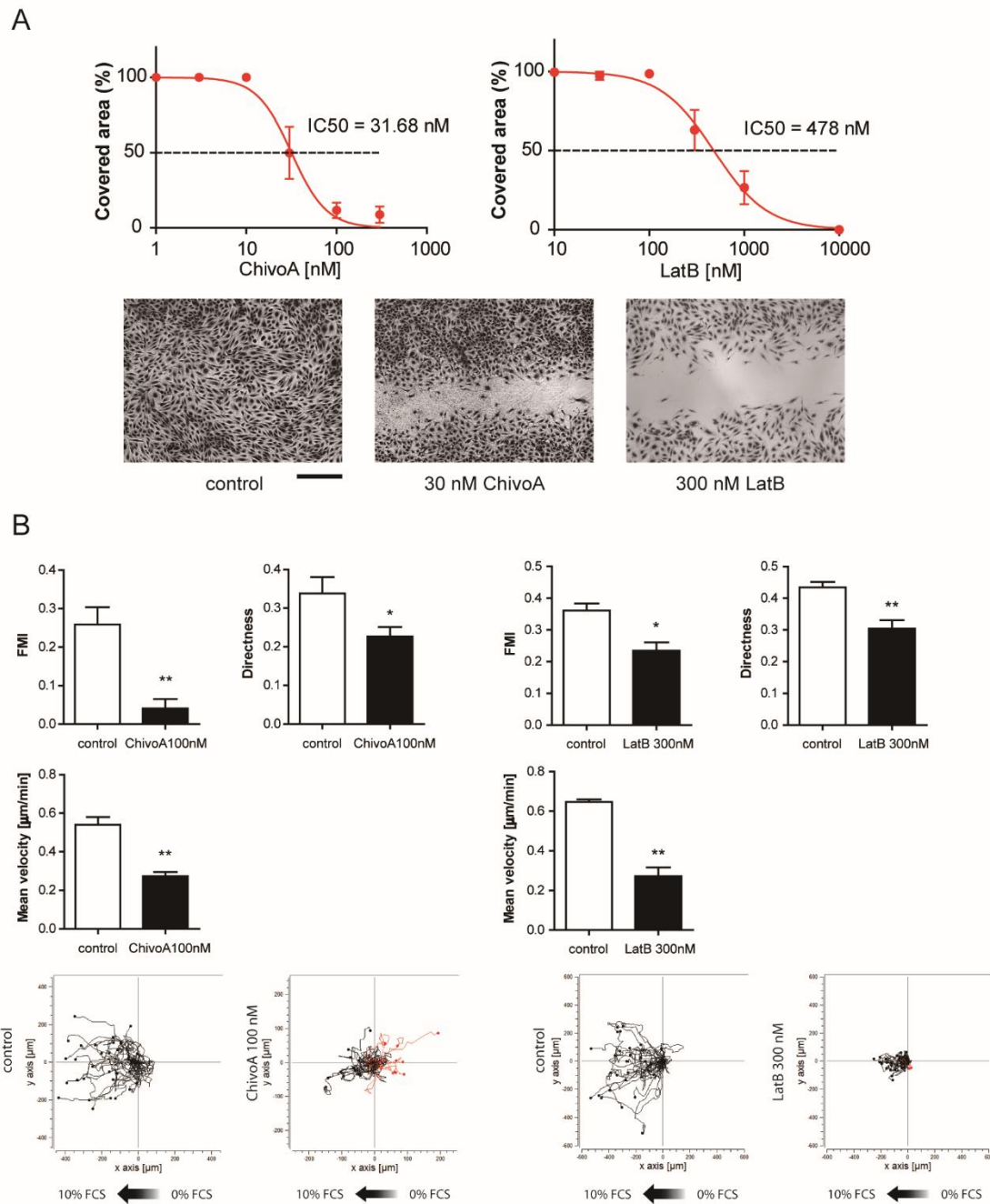
Figure 4.3 Chivosazole A inhibits migration in endothelial cells

(A) Upper panel: Dose response curves of cell migration after treatment with chivosazole A or latrunculin B in a scratch assay. Lower panel: representative images of scratches after migration. Scale bar: 200 µm. (B) In 2D-chemotaxis assay, quantitative evaluation of the parameters X-Forward migration index, directness and mean velocity are shown. Analysis of one representative experiment

(out of triplicates in three independent experiments) is shown. Data are presented as mean ± SEM, n = 3, *p < 0.05, **p < 0.01 using Kruskal-Wallis test.

4.4 Chivosazole A disturbs tube formation in endothelial cells

To study the effect of chivosazole A on a morphogenetic process in vitro, a tube formation assay on matrigel was performed. The tube structure when compared with control could not be established after 16 – 20 h incubation with either chivosazole A or latrunculin B (Fig. 4.4). Treatment led to a fragmented phenotype of the tubular network with a higher number of shorter tubes. The cell-cell contacts were disrupted. Thus, chivosazole A has same effect as latrunculin B, interfering with the stability of tubes and development of cell-cell contacts.
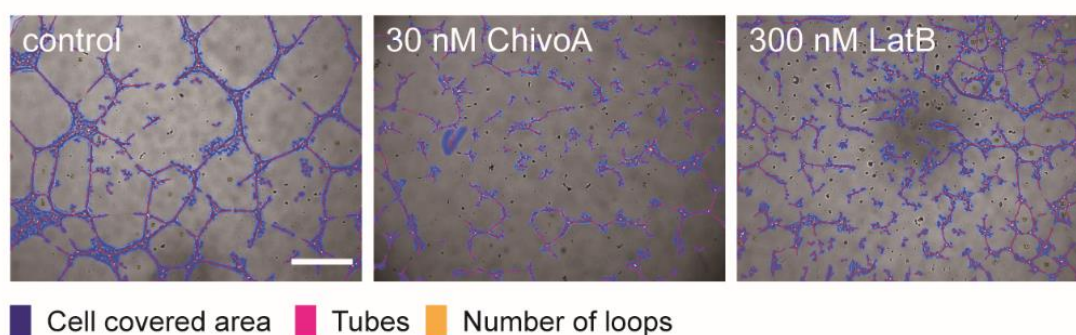
Figure 4.4 Chivosazole A disturbs tube formation in endothelial cells
(A) HUVECs were seeded on matrigel, treated with the indicated concentration of chivosazole A and latrunculin B respectively and incubated for 16 h. Images were taken and analyzed. Representative images in one experiment (out of triplicates in three independent experiments each) are shown. Cell covered areas recognized by software are indicated in blue, tubes are indicated in pink, and loops are indicated by yellow numbers. The scale bar represents 30 µm.

4.5 Chivosazole A competes with ABPs for binding to G-actin and causes dimerization of actin

Based on the surprising functional differences between the two compounds concerning transcription (Table S6, S7 and S8), and the fact that actin influences transcriptional regulation mainly by its interaction with ABPs, we tested the effects of the two compounds on the binding of several proteins (cofilin, gelsolin and profilin) to G-actin. We performed an actin pull-down assay with G-actin immobilized on beads and single ABPs in the absence and presence of chivosazole A or latrunculin B, then quantified the ABP binding to G-actin.

As seen in Fig. 4.5A-C (left panels), the total amount of the tested ABPs in G-actin pellets decreased with chivosazole A (molar ratio 1:100), indicating that it prevented binding of cofilin, gelsolin and profilin to G-actin. In contrast, latrunculin B had no such effect (Fig. 4.5A-C, right panels), which offers a potential explanation for the functional differences between these two compounds.
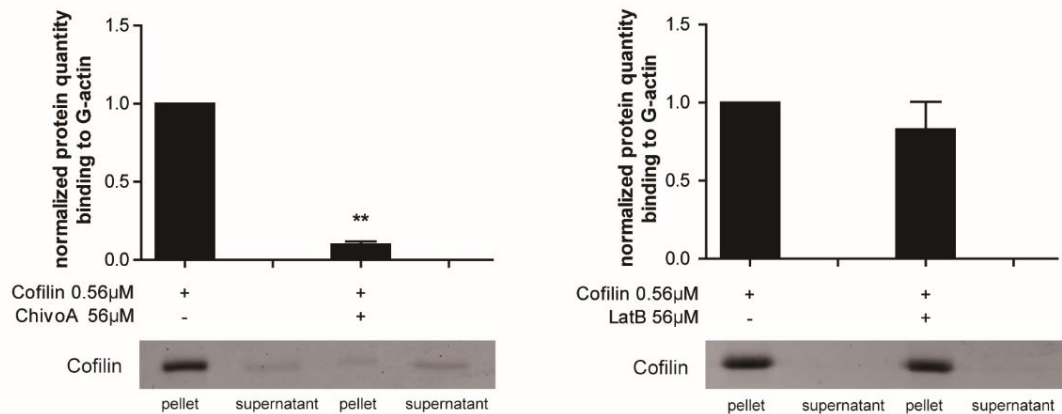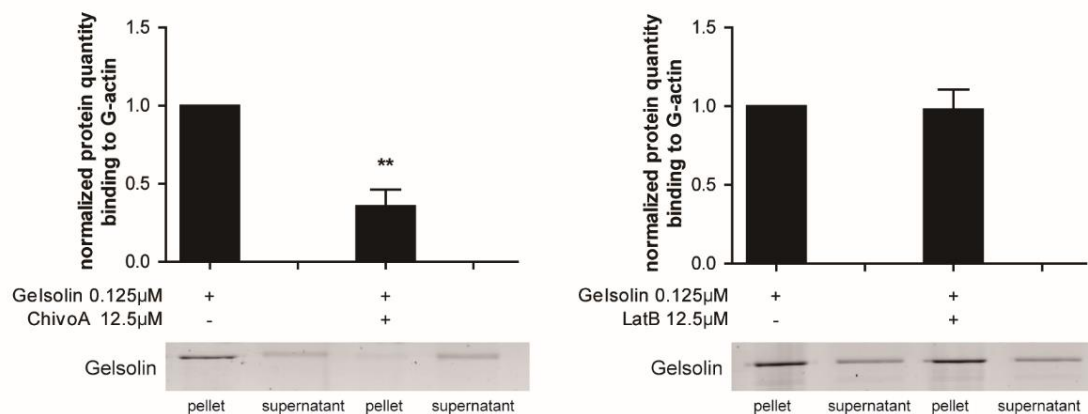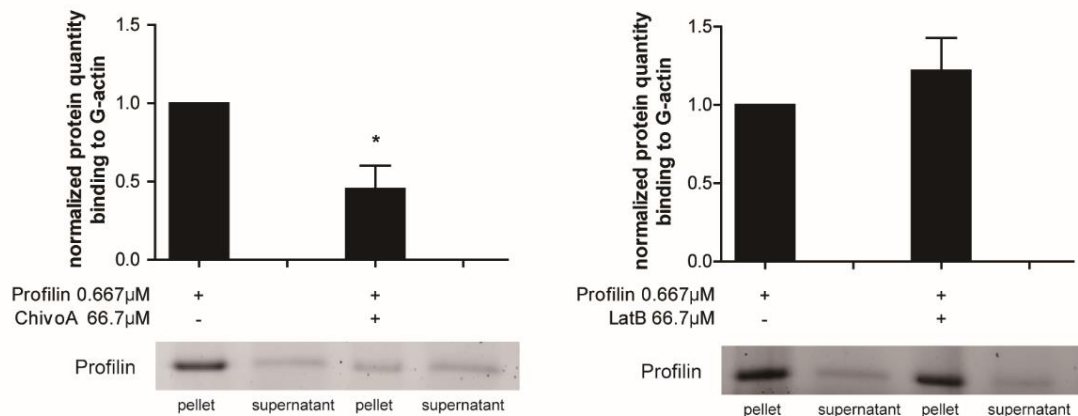
Figure 4.5 Chivosazole A prevents the binding of ABPs to G-acin, while latrunculin B does not

G-actin beads were pretreated with indicated concentrations of either chivosazole A or latrunculin B for 30 min at room temperature, then co-incubated with the G-actin binding proteins (A) cofilin, (B) gelsolin or (C) profilin at a molar ratio of 100:1 (compound: ABP). After 1 h, the mixture of actin beads and ligands was spun and only the ligands bound to G-actin will be co-precipitated in the pellet. The amount of ABP in pellet was quantified. Representative images of protein bands are shown. Data are presented as mean ± SEM, n = 3, *p < 0.05, **p < 0.01 using Kruskal-Wallis test.

Since the binding affinity of thymosin β4 is very weak, and we were not able to detect this protein in the pull-down assay, we crosslinked the bound protein as previously described[51]. With crosslinking, a 1:1 complex of thymosin β4 with G-actin at approximately 47.5 kDa is detectable (Fig, 4.6A, left panel). Chivosazole A reduced crosslink product formation (Fig. 4.6A, right panel). In addition, a high molecular weight complex (approximately 100 kDa) was formed in the presence of chivosazole A (Fig. 4.6A, left panel and also in the absence of thymosin β4, Fig. 4.6C), suggesting the formation of G-actin dimers. Latrunculin B decreased the formation of the thymosin β4/G-actin complex (Fig. 4.6B), but did not cause formation of actin dimers. Gel filtration experiments also showed an increase of actin dimers in the presence of chivosazole A under conditions of a different pH (Fig. 4.6D, experiments were performed by Dr. Sabine Schneider, Department of Chemistry, Technical University of Munich, Germany). However, the retention time of these dimers differs from that of spontaneously formed physiological dimers, indicating a different structure (Fig. 4.6D).

Figure 4.6 Chivosazole A prevents thymosin β4 binding to G-actin, and causes formation of unphysiological actin dimers

(A) This interaction was inhibited by chivosazole A. In the presence of chivosazole A actin dimers (~100 kDa, the boxed-in portion of protein bands) formed. (B) Binding of thymosin β4 to G-actin was also inhibited by latrunculin B, however, no actin dimers were formed in the presence of this compound. (C) The actin dimers formed by chivosazole A were not dependent on the presence of thymosin β4. Representative images of protein bands and quantitative densitometric analyses are

shown. (D) Size-exclusion chromatography at different pH values indicate the formation of actin-dimers in the presence of chivosazole A. Dimers formed spontaneously in the absence of chivosazole A elute at a time point different from the drug induced ones, hinting at an unphysiological conformation of the latter ones. Results of size-exclusion chromatography in (D) are provided by Dr. Sabine Schneider, Department of Chemistry, Technical University of Munich, Germany. (Data are presented as mean ± SEM, n = 3, *p < 0.05 using Kruskal-Wallis test)

Chivosazole F, a derivative which is structurally very similar to chivosazole A, and rhizopodin, an also structurally related compound, inhibited binding of profilin, gelsolin and cofilin to G-actin to a similar degree as chivosazole A (Fig. 4.7).

D
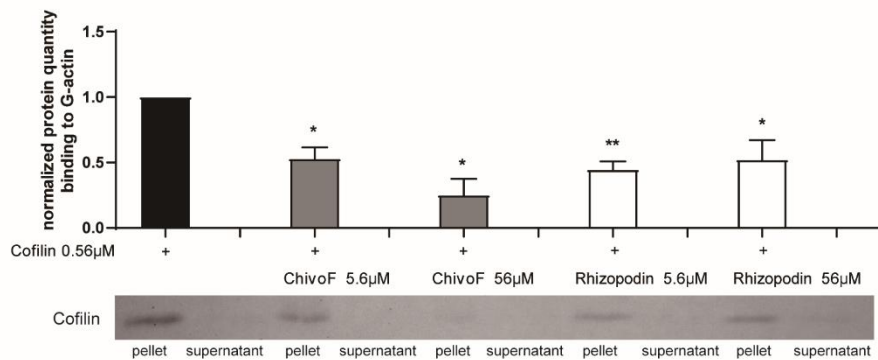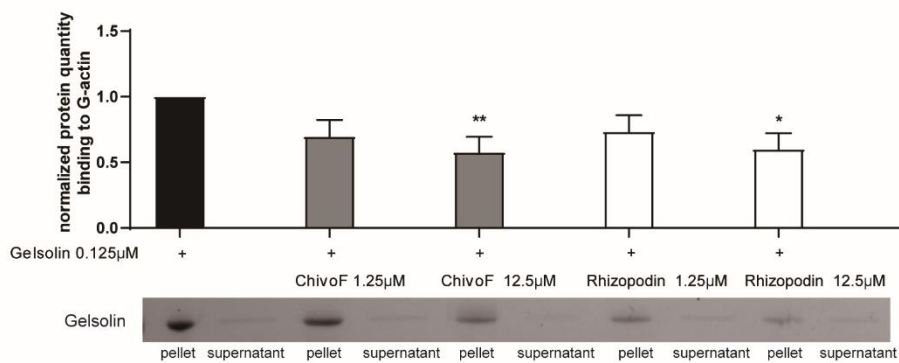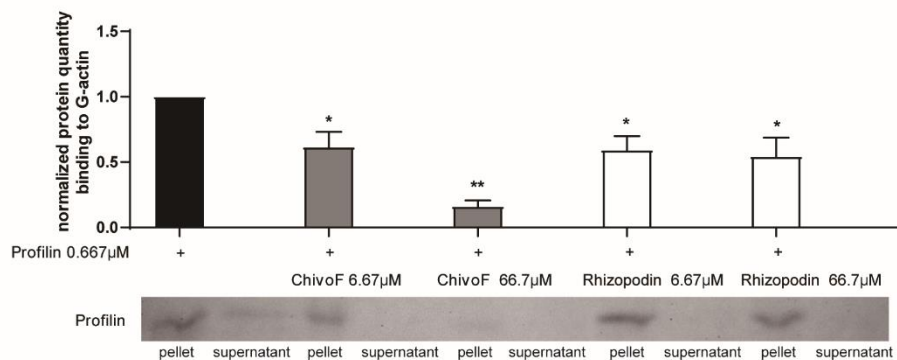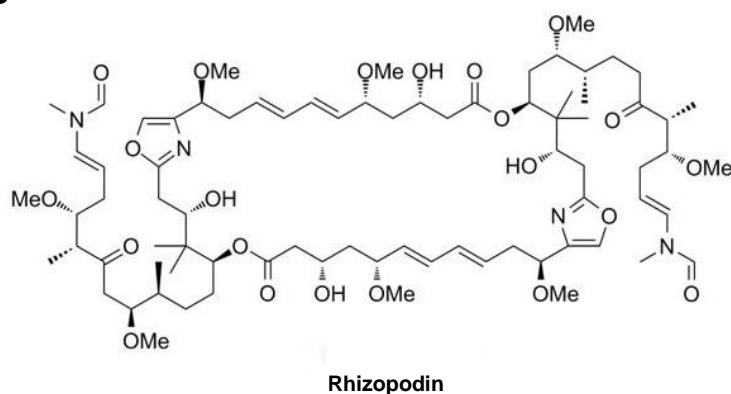
Rhizopodin

Figure 4.7 Chivosazole F and rhizopodin both compete with (A) cofilin, (B) gelsolin and (C) profilin binding to G-acin

G-actin beads were pretreated with either chivosazole F or rhizopodin for 30 min at room temperature, then co-incubated with each ABP at a molar ratio of 10:1 and 100:1 (compound: ABP). After 1 h, the mixture of actin beads and ligands was spun and only the ligands bound to G-actin will be co-precipitated in the pellet. The amount of ABP in pellet was quantified. Representative images of protein bands are shown. Data are presented as mean ± SEM, n = 3, *p < 0.05, **p < 0.01 using Kruskal-Wallis test. (D) Chemical structure of rhizopodin adapted from Patocka J et al. 2017.

5 Discussion

5.1 Actin targeting compounds: promising biological tools and therapeutic options

Actin is the most abundant protein in eukaryotic cells and the protein with the greatest variety of binding partners[3, 52, 53]. Due to its ubiquitous expression and its many biological functions, actin has not been pushed as a clinically relevant drug target. Especially the question how selective functional effects could be elicited by just increasing or decreasing overall actin polymerization by the use of small molecular binders has precluded the use of actin targeting natural compounds in a therapeutic setting for many years in spite of their availability[28, 30, 54]. In recent years, however, it has become increasingly clear that actin-binding proteins (ABPs) are the key to localized and specific regulation of actin polymerization and depolymerization. For example, it has been shown that JMY or WHAMM are needed to localize actin nucleation specifically to the autophagosome[55, 56]. Since the amount of G-actin in a cell is limited, a competition between actin monomers, F-actin filaments, and ABPs for binding to the available G-actin pool takes place, and turns out to be relevant for regulation of actin function[31, 52, 57]. Exploiting this level of regulation by using the concept of "biomolecular mimicry"[34, 58] would open a new field of biological tools or even therapeutic options by developing novel and much more specific actin targeting compounds.

5.2 Miuraenamide A, a novel actin stabilizing compound, selectively inhibits cofilin binding to F-actin

5.2.1 Miuraenamide A, an actin stabilizer, and its specific mode of binding

Miuraenamide A has been discovered in 2006 with high cytotoxicity to a range of tumor cell lines[41]. It is presumed to be an actin filament stabilizing agent[38]. The absolute stereostructure of miuraenamide A was determined soon in 2008[40]. Comparable biological effects were observed with other cyclodepsipeptides, such as chondramide[42] and jasplakinolide[35], which is not surprising on the basis of their closely related structure (Fig. 1.1). However, it is still poorly characterized and its influence on actin is still not clear. In this study, we have performed an in-depth characterization of miuraenamide A. The in vitro data on isolated actin indicate that miuraenamide A has a profile similar to phalloidin or jasplakinolide (increase of nucleation, enhanced polymerization, and stabilization). FCS assay result suggests that miuraenamide A favors polymerization by stabilizing the early

stage oligomers formed during nucleation (Fig. S1 and Fig. S2). This reveals the increasing nucleation and elongation effect of miuraenamide A in TIRF assay (Fig. 3.1). The competition with phalloidin for actin binding in the TIRF assay indicates binding sites of both compounds in close proximity (Fig. 3.2A).

To get an impression of the specific binding mode of miuraenamide A, we performed in silico studies (experiments were performed by the group of Prof. Iris Antes, Protein Modelling group, Technical University of Munich, Germany), which revealed that miuraenamide A binds to motifs similar, but different to the binding site of phalloidin, chondramide, or jasplakinolide[59-61]. Interaction of a compound with F-actin is complex, since the compound may bind to three actin molecules at the same time at different sites. For the sake of simplicity, we collapsed all binding sites of miuraenamide A, phalloidin and jasplakinolide on one actin monomer, respectively (Fig. S3). This simulation reveals that M4 is a binding site which miuraenamide A shared with phalloidin and jasplakinolide, which in part explains the competition of Miuraenamide A with phalloidin. M2 and M5 also show similar binding sites as phalloidin and jasplakinolide, but M1 and M3 address sites on the actin molecule, which are not bound by phalloidin or jasplakinolide. The mode of binding to M1 is unique in that the bromophenol substitution of the macrocycle and the three aromatic residues from actin (Tyr133, Phe352, and Tyr143) form an aromatic cyclic tetramer (Fig. S4A and B). Similar motives (involving more or less aromatic cycles) were shown to be frequently observed in proteins and contribute to the stabilization of their tertiary structure[62-64]. They were also recently identified as a key feature of metal centered cycloadducts[65]. This relatively strong interaction reveals the importance of the bromophenol ring as a crucial moiety of the macrocyclic miuraenamide A. The second phenyl ring bound to the macrocycle, on the other hand, is not engaged in any crucial interactions.

Analysis of the influence of miuraenamide A binding on the F-actin filament structure by simulation of actin-trimer complexes with and without bound miuraenamide A showed that the binding of miuraenamide A influences the overall structures of the actin timer, as for the apo-actin-trimer a different relative arrangement of the individual actin monomers was observed compared to the holo-trimer complex (Fig. S4C, D, E and F). A more detailed analysis of the structures (Fig. S4G and Fig. S5A) reveals that the miuraenamide A ligand bound to the actin DNAse I binding site triggers the migration of the D-loop in monomer 3 towards actin. This phenomenon increases the contact area between the monomers. Presumably miuraenamide A further acts as a buffer between these two monomers and stabilizes the compact trimer form. Comparisons between holo- and apo-structures show

that the interaction between monomers 2 and 3 is affected most by the binding of miuraenamide A (Fig. S4D, F, blue lines), although all monomers contain a ligand in the holo-system. This is consistent with the fact that only the ligand of monomer 2 is located at an inter-monomeric interface in the trimer simulation. This observation, together with the RMSD analysis, further highlights that the binding of miuraenamide A does not affect the individual integrity of the units but regulates the inter-monomeric interactions. Overall, miuraenamide A binding ensures a tighter and stronger packing of the actin monomers compared to the apo F-actin (Fig. S4H) by shifting the D-loop, which is indispensable for F-actin stabilization[59].

5.2.2 Miureanamide A has comparable effect on a cellular level as other actin stabilizer, but has a unique selectivity inhibition on cofilin binding to F-actin

To find out, whether this unique binding mode results into a different functional outcome, we investigated miuraenamide A also on a cellular level. Miuraenamide A had functional effects similar to chondramide, another actin nucleator (inhibition of proliferation, migration), and also the morphological changes were comparable[42, 66].

Since the hydrophobic cleft in the actin molecule, where M1 is situated, is the main hub for interaction of actin with other proteins, we analyzed interactions of ABPs with both, G- and F-actin. Interactions of ABPs with G-actin were not altered by miuraenamide A. Obviously, the compound does not bind to a single monomeric actin, or it does not directly interfere with protein binding. In contrast, we observed that miraenamide A inhibited ABP cofilin binding to F-actin. The interesting point here is that this observation was specific for cofilin – the binding of gelsolin or the Arp2/3 complex on F-actin were not affected. Even more interestingly, jasplakinolide did not have this effect. Consequently, the action of miuraenamide A seems to be due to its unique binding mode. Our molecular dynamics (MD) simulations offer an explanation for the inhibition of cofilin binding to F-actin by miuraenamide A: the shift of the D-loop by miuraenamide A leads to a clash between this loop and cofilin in its bound conformation (Fig. S5B).

It has already been sporadically described that actin binding compounds are able to influence binding of ABPs to G- or F-actin (e.g. cytochalasin D and MRTF[33, 67], or phalloidin and gelsolin[68]). Obviously, these small molecules can act as inhibitors of protein-protein interactions, and afford a certain specificity.

On a functional cellular level, the comparison between jasplakinolide and miuraenamide A was quite astounding. Though migration and proliferation were inhibited by miuraenamide A as was to be expected, the differences of transcriptional regulation in HUVEC cells after

treatment with both compounds were pronounced: 101 genes were regulated in a significantly different way (Table S1 and S3). When the regulated genes are classified into functionally relevant gene ontologies (Table S4 for Miuraenamide A and Table S5 for jasplakinolide), it becomes clear that most of the differences between Miuraenamide A treatment and jasplakinolide do not result from different extents of regulation of the same genes, but from regulation of different sets of genes (Table S2). This might be linked to the effects of miuraenamide A on binding of cofilin to F-actin (Fig.5.1), since cofilin directly modulates nuclear architecture[69], but also plays an important role in regulating nuclear actin levels[70], which, in turn, have an influence on transcriptional regulation[71]. However, due to the complexity of the role of actin and ABPs in transcriptional regulation, we cannot rule out other modes of action of miuraenamide A treatment.
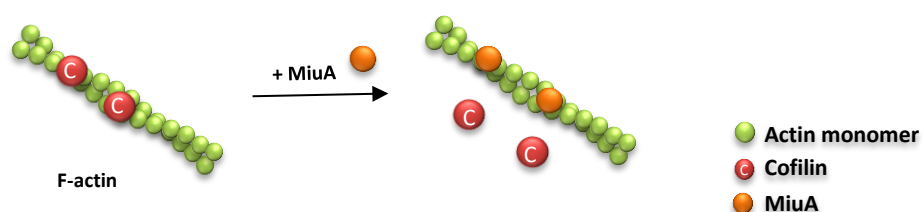
Figure 5.1 MiuA prevents cofilin binding to F-actin

5.3 Chivosazole A modulates protein-protein-interactions of actin

5.3.1 Is chivosazole A just another of many known natural compounds, which interfere with actin polymerization dynamics?

Chivosazole A has been initially described as cytotoxic agent in eukaryotic cells in 1995[43], and its absolute configuration has been resolved 12 years later[45]. Its actin interfering effects (inhibition of G-actin polymerization and depolymerization of F-actin) were identified 2009[44]. One could argue that chivosazole A is just another of many known natural compounds, which interfere with actin polymerization dynamics[72]. However, it turned out that each of these actin binding compounds has unique functional features, and that it is worthwhile to study their structure-activity-relationships.

Very recently, chivosazole F, a compound closely related to chivosazole A has been shown to directly interact with actin by chemoproteomics[73]. Based on genome-wide mutagenesis studies in yeast with chivosazole F it was proposed that the binding site for chivosazole F on actin would partially overlap the binding site for latrunculinA in the ATP-binding cleft [73]. However, here we present a crystal structure of an actin- ChivoA complex, revealing that it binds at the barbed end of actin, and not to a site close to the latrunculin A binding site. This discrepancy could be explained by the fact that we used chivosazole A, while chivosazole F was used in the other work. However, this seems unlikely, as both compounds are nearly identical (Fig. 1.2). It is feasible that the sequence of actin (which is evolutionary highly conserved) lacks flexibility, and mutations at the real binding site just do not yield functional protein. The described mutations (R183K and R335K) might have allosteric consequences, influencing binding of chivosazole F at a distant site[73].

In order to elucidate the previously unknown binding mode of chivosazole A to actin, we first determined the X-ray crystal structure of chivosazole A in complex with G-actin to 2.4 Å resolution (experiments were performed by Dr. Sabine Schneider, Department of Chemistry, Technical University of Munich, Germany). Chivosazole A binds to the barbed end (target binding cleft) of G-actin (Fig. S6A and Fig. S7). This binding site for chivosazole A is very close, but not identical to those of many actin binding macrolides (Fig. S6B): Despite the variation in ring size and decoration of the tail with different backbone substitutions present in actin-binding macrolides, they possess a common theme in their interaction with actin. In all reported actin complex-structures the macrolactone ring binds to subdomain 1, with the side chain/tail protruding into the hydrophobic cavity between subdomain 1 and 3[34, 74-81]. The oxazole ring of chivosazole A occupies an intermediate

position compared to the trisoxazole rings of jaspisamide A, kabiramide C and ulapulaide A[34, 81] (Fig. S6B). Albeit we cannot rule out that crystal lattice contacts impact on the binding mode of chivosazole A (Fig. S7), for jaspisamide A and kabiramide C identical interactions with actin were observed in structures obtained from different crystal symmetries.

Interestingly, the binding side of chivosazole A overlaps with that for a number of actin-binding proteins (ABPs). This might explain, why chivosazole A competes with cofilin, gelsolin, profilin or thymosin β4 for binding to G-actin, while latrunculin B does not. These proteins interact with actin by insertion of an amphiphilic helix into the target binding cleft as depicted in Fig. S8 [82-86].

Recently the cryo-EM structure of F-actin has been reported (PDB code 6BNO[87]), revealing an interface of 1,076 Å2 between the actin-monomers (theoretical gain of free energy of -6.9 kcal/mol). Here the D-loop (residue 40-50) slides into the target binding cleft between subdomain 1 and 3. Superposition of the F-actin structure and the actin-ChivoA complex shows that the ChivoA-tail partly occupies the binding site for the DNase-binding loop (Fig. 6C), and, in addition, slightly perturbs other structural elements involved in actin-actin interaction (Fig. S6C). This explains the F-actin-severing effect of chivosazole A, which does not occur with rhizopodin or cytochalasin D, other actin binding polyketides[44, 88]. Albeit actin-ChivoA complexes can still form dimers in vitro, their overall shape differs from that of physiological actin-dimers in solution as indicated by size-exclusion chromatography (Fig. 4.6D). The occurrence of actin dimers has already been described with rhizopodin and swinholide A[78, 80]. However, these compounds have two enamide side chains each, which explain their crosslinking activity, while chivosazole A has just one. It has recently been shown that the induction of unphysiological actin oligomers by toxins can cause dramatically altered affinity towards ABPs[89]. This effect could further contribute to the higher efficacy of chivosazole A in comparison to latrunculin B.

5.3.2 Chivosazole A selectively competes with ABPs

Chivosazole A has been previously described to inhibit actin polymerization and to induce F-actin depolymerisation[44]. In our work, we corroborate this finding, and additionally show that nucleation is inhibited and G-actin is sequestered in a similar way as with latrunculin B. This makes it understandable that at first glance both compounds have similar functional effects on eukaryotic cells (proliferation, migration, cytoskeletal architecture), which can be explained by an overall disturbance of actin turnover. However, when having a closer look at binding of ABPs to G-actin, as discussed above, we see striking differences between

both compounds, and a high selectivity: profilin, gelsolin and cofilin compete only with chivosazole A (Fig.5.2), while chivosazole A and latrunculin B both compete with thymosin β4. Influencing these interactions might have distinct consequences on downstream signaling, and ultimately on gene expression. Indeed, we see the differences of chivosazole A and latrunculin B on gene expression in endothelial cells: a number of genes that are only up- or downregulated by chivosazole A and not by latrunculin B, and vice versa (Table S6, S7 and S8).
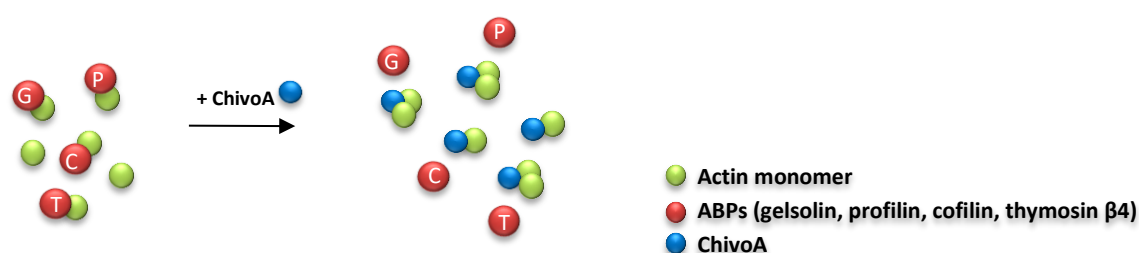
Figure 5.2 ChivoA prevents ABPs binding to G-actin

Consequently, our result reveals a previously unexpected layer of complexity in the mechanism of action of actin binding compounds: instead of just causing bulk stabilization or de-stabilization of actin fibers, distinct cellular functions could be preferentially addressed by single compounds. "Biomolecular mimicry"[58], the fact that compounds can selectively compete with ABPs, and the high structural diversity of actin binding compounds might team up to generate an unprecedented functional selectivity for pharmacologically targeting actin. Since the total synthesis of chivosazole F has been resolved[46], and chivosazoles can be produced biotechnologically, these compounds might be ideal candidates for derivatization and for exploring structure-activity-relationships with actin.

5.4 Summary and conclusion

In our work we show that

➢ Miuraenamide A has cellular effects and actin stabilizing effect in vitro comparable to jasplakinolide, owing to their closely related structure,

➢ Chivosazole A has cellular effects and actin destabilizing effect in vitro similar to latrunculin B.
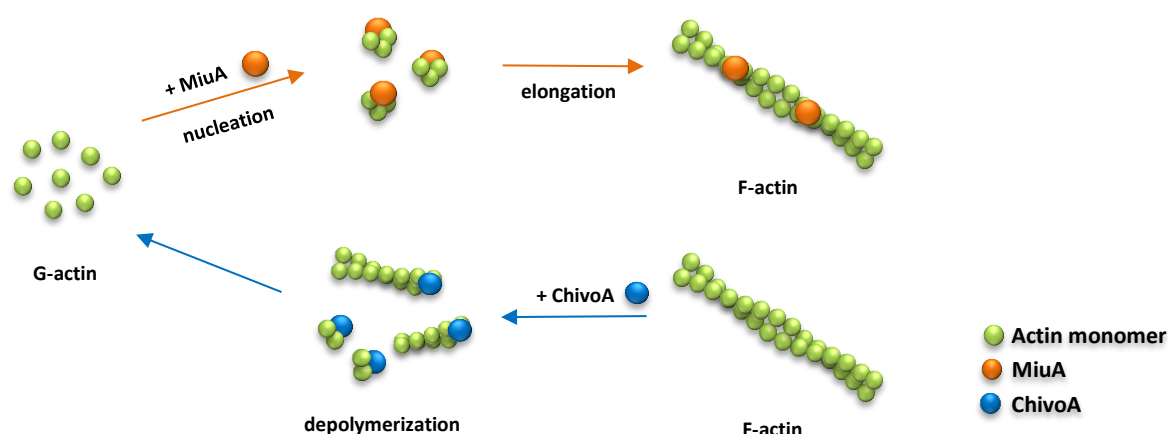
Figure 5.3 Effect of actin binding compounds on actin dynamics
Miuraenamide A induces actin nucleation, polymerization and stabilizes F-actin. Chivosazole A destabilizes F-actin, inducing actin depolymerization.

However, we identified the unique mode of actions of both miuraenamide A and Chivosazole A by structural data that

➢ Miuraenamide A selectively inhibits binding of cofilin to F-actin and causes transcriptional regulation different from that of jasplakinolide,

➢ Chivosazole A competes with ABPs for binding to G-actin in contrast to latrunculin B, and influences transcriptional activity in human primary cells in a different manner from latrunculin B.

Consequently, our findings reveal that small structural differences in actin binding compounds can cause functional selectivity (miuraenamide A and jasplakinolide), and the mechanisms of actions of actin binding compounds are much more complex than previously conceived which was not presumed in this class of molecules. The much better synthetic

accessibility of both miuraenamide A and chivosazole A, as compared to other actin binding compounds, makes them ideal candidates for studying structure-activity relationships. Ideally, it could be feasible to rationally create appropriate derivatives with improved activities that do not influence actin polymerization or depolymerization per se, but selectively modulate the binding of single ABP, and circumvent the selectivity issues, which hindered the development of actin-addressing drugs.

6 Summary

6.1 Part 1: Miuraenamide A, a novel actin stabilizing compound, selectively inhibits cofilin binding to F-actin

Actin binding compounds such as phalloidin, jasplakinolide and latrunculin are widely used tools in cell biology regulating actin dynamics. Jasplakinolide is a prototypic actin stabilizer which binds to F-actin with no effect on ABPs (cofilin, gelsolin, profilin). In contrast miuraenamide A, as a new actin stabilizer, competes exclusively with cofilin for binding to F-actin. Notably, the molecular basis for this difference still remains to be determined. To investigate whether this difference is due to a specific binding site in miuraenamide A we performed molecular dynamics simulations. These simulations suggest that the bromophenol group of miurenamide A interacts with actin residues Tyr133, Tyr143, and Phe352. This interaction shifts the D-loop of the neighboring actin, creating tighter packing of the monomers, and blocks the binding site of cofilin. We found that miuraenamide A shows activity similar to jasplakinolide both in vitro with respect to polymerization, depolymerization, branching, nucleation and in vivo with respect to cell proliferation, migration. However, gene expression in HUVEC cells was differentially affected by both compounds, indicating functional differences. We found that relatively small changes in the molecular structure give rise to this selectivity, suggesting that actin binding compounds might serve as promising scaffolds for creating actin binders with specific functionality instead of just "stabilizers".

6.2 Part 2: Chivosazole A modulates protein-protein-interactions of actin

Actin is a protein of central importance for many cellular key processes. Its function is regulated by local interactions with a large number of ABPs. To date, various compounds are known either increasing or decreasing polymerization dynamics of actin. However, no actin binding compound has been developed for clinical applications yet, due to selectivity issues. We provide a crystal structure of the natural product chivosazole A bound to actin, and show that – in addition to inhibiting nucleation, polymerization and severing of F-actin filaments – it selectively modulates binding of ABPs to G-actin: while unphysiological actin dimers are induced by chivosazole A, interaction with of gelsolin, profilin, cofilin and thymosin β4 is inhibited. Moreover, chivosazole A causes transcriptional effects differing from latrunculin B, an actin binder with a different binding site. Thus, our data show that chivosazole A and related compounds could serve as scaffolds for the development of actin binding molecules selectively targeting specific actin functions.

7 References

1. Holzinger, A., *Jasplakinolide: An Actin-Specific Reagent that Promotes Actin Polymerization*, in *Cytoskeleton Methods and Protocols*, R.H. Gavin, Editor. 2010, Humana Press: Totowa, NJ. p. 71-87.

2. Helal, M.A., S. Khalifa, and S. Ahmed, *Differential binding of latrunculins to G-actin: a molecular dynamics study.* J Chem Inf Model, 2013. **53**(9): p. 2369-75.

3. Dominguez, R., *Actin-binding proteins--a unifying hypothesis.* Trends Biochem Sci, 2004. **29**(11): p. 572-8.

4. dos Remedios, C.G., et al., *Actin binding proteins: regulation of cytoskeletal microfilaments.* Physiol Rev, 2003. **83**(2): p. 433-73.

5. Maciver, S.K. and P.J. Hussey, *The ADF/cofilin family: actin-remodeling proteins.* Genome Biol, 2002. **3**(5): p. reviews3007.

6. Winder, S.J. and K.R. Ayscough, *Actin-binding proteins.* J Cell Sci, 2005. **118**(Pt 4): p. 651-4.

7. Romero, S., et al., *Formin is a processive motor that requires profilin to accelerate actin assembly and associated ATP hydrolysis.* Cell, 2004. **119**(3): p. 419-29.

8. Pasic, L., T. Kotova, and D.A. Schafer, *Ena/VASP proteins capture actin filament barbed ends.* J Biol Chem, 2008. **283**(15): p. 9814-9.

9. Burke, T.A., et al., *Homeostatic actin cytoskeleton networks are regulated by assembly factor competition for monomers.* Curr Biol, 2014. **24**(5): p. 579-85.

10. Kunze, D. and B. Rustow, *Pathobiochemical aspects of cytoskeleton components.* Eur J Clin Chem Clin Biochem, 1993. **31**(8): p. 477-89.

11. Popova, E.N., et al., *Scavenging of reactive oxygen species in mitochondria induces myofibroblast differentiation.* Antioxid Redox Signal, 2010. **13**(9): p. 1297-307.

12. Suarez-Huerta, N., et al., *Actin depolymerization and polymerization are required during apoptosis in endothelial cells.* J Cell Physiol, 2000. **184**(2): p. 239-45.

13. Aida, N., et al., *Actin stabilization induces apoptosis in cultured porcine epithelial cell rests of Malassez.* Int Endod J, 2016. **49**(7): p. 663-9.

14. Smethurst, D.G., I.W. Dawes, and C.W. Gourlay, *Actin - a biosensor that determines cell fate in yeasts.* FEMS Yeast Res, 2014. **14**(1): p. 89-95.

15. Falahzadeh, K., A. Banaei-Esfahani, and M. Shahhoseini, *The potential roles of actin in the nucleus.* Cell J, 2015. **17**(1): p. 7-14.

16. Verschueren, H., et al., *Metastatic competence of BW5147 T-lymphoma cell lines is correlated with in vitro invasiveness, motility and F-actin content.* J Leukoc Biol, 1994. **55**(4): p. 552-6.

17. Fife, C.M., J.A. McCarroll, and M. Kavallaris, *Movers and shakers: cell cytoskeleton in cancer metastasis.* Br J Pharmacol, 2014. **171**(24): p. 5507-23.

18. Desmouliere, A. and G. Gabbiani, *Modulation of fibroblastic cytoskeletal features during pathological situations: the role of extracellular matrix and cytokines.* Cell Motil Cytoskeleton, 1994. **29**(3): p. 195-203.

19. Eira, J., et al., *The cytoskeleton as a novel therapeutic target for old neurodegenerative disorders.* Prog Neurobiol, 2016. **141**: p. 61-82.

20. Bamburg, J.R. and B.W. Bernstein, *Actin dynamics and cofilin-actin rods in alzheimer disease.* Cytoskeleton (Hoboken), 2016. **73**(9): p. 477-97.

21. Janmey, P.A. and C. Chaponnier, *Medical aspects of the actin cytoskeleton.* Curr Opin Cell Biol, 1995. **7**(1): p. 111-7.

22. Nurnberg, A., A. Kollmannsperger, and R. Grosse, *Pharmacological inhibition of actin assembly to target tumor cell motility.* Rev Physiol Biochem Pharmacol, 2014. **166**: p. 23-42.

23. Izdebska, M., et al., *The Role of Actin Dynamics and Actin-Binding Proteins Expression in Epithelial-to-Mesenchymal Transition and Its Association with Cancer Progression and Evaluation of Possible Therapeutic Targets.* Biomed Res Int, 2018. **2018**: p. 4578373.

24. Grzanka, D., et al., *The interactions between SATB1 and F-actin are important for mechanisms of active cell death.* Folia Histochem Cytobiol, 2015. **53**(2): p. 152-61.

25. Kullmann, J.A., et al., *Purkinje cell loss and motor coordination defects in profilin1 mutant mice.* Neuroscience, 2012. **223**: p. 355-64.

26. Dancker, P., et al., *Interaction of actin with phalloidin: polymerization and stabilization of F-actin.* Biochim Biophys Acta, 1975. **400**(2): p. 407-14.

27. Low, I., P. Dancker, and T. Wieland, *Stabilization of F-actin by phalloidin. Reversal of the destabilizing effect of cytochalasin B.* FEBS Lett, 1975. **54**(2): p. 263-5.

28. Bubb, M.R., et al., *Jasplakinolide, a cytotoxic natural product, induces actin polymerization and competitively inhibits the binding of phalloidin to F-actin.* J Biol Chem, 1994. **269**(21): p. 14869-71.

29. Longley, R.E., et al., *Evaluation of marine sponge metabolites for cytotoxicity and signal transduction activity.* J Nat Prod, 1993. **56**(6): p. 915-20.

30. Spector, I., et al., *Latrunculins: novel marine toxins that disrupt microfilament organization in cultured cells.* Science, 1983. **219**(4584): p. 493-5.

31. Davidson, A.J. and W. Wood, *Unravelling the Actin Cytoskeleton: A New Competitive Edge?* Trends Cell Biol, 2016. **26**(8): p. 569-576.

32. Goldschmidt-Clermont, P.J., et al., *The control of actin nucleotide exchange by thymosin beta 4 and profilin. A potential regulatory mechanism for actin polymerization in cells.* Mol Biol Cell, 1992. **3**(9): p. 1015-24.

33. Miralles, F., et al., *Actin dynamics control SRF activity by regulation of its coactivator MAL.* Cell, 2003. **113**(3): p. 329-42.

34. Klenchin, V.A., et al., *Trisoxazole macrolide toxins mimic the binding of actin-capping proteins to actin.* Nat Struct Biol, 2003. **10**(12): p. 1058-63.

35. Braekman, J.C., et al., *Jaspamide from the Marine Sponge Jaspis johnstoni.* Journal of Natural Products, 1987. **50**(5): p. 994-995.

36. Kopp, M., et al., *Production of the tubulin destabilizer disorazol in Sorangium cellulosum: biosynthetic machinery and regulatory genes.* Chembiochem, 2005. **6**(7): p. 1277-86.

37. Zhang, S., et al., *In vitro anti-cancer effects of the actin-binding natural compound rhizopodin.* Pharmazie, 2015. **70**(9): p. 610-5.

38. Sumiya, E., et al., *Cell-morphology profiling of a natural product library identifies bisebromoamide and miuraenamide A as actin filament stabilizers.* ACS Chem Biol, 2011. **6**(5): p. 425-31.

39. Iizuka, T., et al., *Miuraenamides A and B, novel antimicrobial cyclic depsipeptides from a new slightly halophilic myxobacterium: taxonomy, production, and biological properties.* J Antibiot (Tokyo), 2006. **59**(7): p. 385-91.

40. Ojika, M., et al., *Miuraenamides: antimicrobial cyclic depsipeptides isolated from a rare and slightly halophilic myxobacterium.* Chem Asian J, 2008. **3**(1): p. 126-33.

41. Karmann, L., et al., *Total syntheses and biological evaluation of miuraenamides.* Angew Chem Int Ed Engl, 2015. **54**(15): p. 4502-7.

42. Menhofer, M.H., et al., *The actin targeting compound Chondramide inhibits breast cancer metastasis via reduction of cellular contractility.* PLoS One, 2014. **9**(11): p. e112542.

43. Irschik, H., et al., *Chivosazol A, a new inhibitor of eukaryotic organisms isolated from myxobacteria.* J Antibiot (Tokyo), 1995. **48**(9): p. 962-6.

44. Diestel, R., et al., *Chivosazoles A and F, cytostatic macrolides from myxobacteria, interfere with actin.* Chembiochem, 2009. **10**(18): p. 2900-3.

45. Janssen, D., et al., *Chivosazole A--elucidation of the absolute and relative configuration.* Angew Chem Int Ed Engl, 2007. **46**(26): p. 4898-901.

46. Williams, S., et al., *An Expedient Total Synthesis of Chivosazole F: an Actin-Binding Antimitotic Macrolide from the Myxobacterium Sorangium Cellulosum.* Angew Chem Int Ed Engl, 2017. **56**(2): p. 645-649.

47. Breitsprecher, D., et al., *Analysis of actin assembly by in vitro TIRF microscopy.* Methods Mol Biol, 2009. **571**: p. 401-15.

48. Doolittle, L.K., M.K. Rosen, and S.B. Padrick, *Measurement and analysis of in vitro actin polymerization.* Methods in molecular biology (Clifton, N.J.), 2013. **1046**: p. 273-293.

49. Mentes, A., et al., *High-resolution cryo-EM structures of actin-bound myosin states reveal the mechanism of myosin force sensing.* Proc Natl Acad Sci U S A, 2018. **115**(6): p. 1292-1297.

50. Lee, E., E.A. Shelden, and D.A. Knecht, *Formation of F-actin aggregates in cells treated with actin stabilizing drugs.* Cell Motil Cytoskeleton, 1998. **39**(2): p. 122-33.

51. Carlier, M.F., et al., *Tbeta 4 is not a simple G-actin sequestering protein and interacts with F-actin at high concentration.* J Biol Chem, 1996. **271**(16): p. 9231-9.

52. Povarova, O.I., et al., *Actinous enigma or enigmatic actin: Folding, structure, and functions of the most abundant eukaryotic protein.* Intrinsically Disord Proteins, 2014. **2**(1): p. e34500.

53. Xue, B. and R.C. Robinson, *Guardians of the actin monomer.* Eur J Cell Biol, 2013. **92**(10-11): p. 316-32.

54. Katagiri, K. and S. Matsuura, *Antitumor activity of cytochalasin D.* J Antibiot (Tokyo), 1971. **24**(10): p. 722-3.

55. Coutts, A.S. and N.B. La Thangue, *Actin nucleation by WH2 domains at the autophagosome.* Nat Commun, 2015. **6**: p. 7888.

56. Merino, F., et al., *Structural transitions of F-actin upon ATP hydrolysis at near-atomic resolution revealed by cryo-EM.* Nat Struct Mol Biol, 2018. **25**(6): p. 528-537.

57. Suarez, C. and D.R. Kovar, *Internetwork competition for monomers governs actin cytoskeleton organization.* Nat Rev Mol Cell Biol, 2016. **17**(12): p. 799-810.

58. Tanaka, J., et al., *Biomolecular mimicry in the actin cytoskeleton: mechanisms underlying the cytotoxicity of kabiramide C and related macrolides.* Proc Natl Acad Sci U S A, 2003. **100**(24): p. 13851-6.

59. Pospich, S., et al., *Near-atomic structure of jasplakinolide-stabilized malaria parasite F-actin reveals the structural basis of filament instability.* Proc Natl Acad Sci U S A, 2017. **114**(40): p. 10636-10641.

60. Tannert, R., et al., *Synthesis and structure-activity correlation of natural-product inspired cyclodepsipeptides stabilizing F-actin.* J Am Chem Soc, 2010. **132**(9): p. 3063-77.

61. Waldmann, H., et al., *Total synthesis of chondramide C and its binding mode to F-actin.* Angew Chem Int Ed Engl, 2008. **47**(34): p. 6473-7.

62. Easter, D.C., D.A. Terrell, and J.A. Roof, *Monte Carlo studies of isomers, structures, and properties in benzene-cyclohexane clusters: computation strategy and application to the dimer and trimer, (C6H6)(C6H12)n, n = 1-2.* J Phys Chem A, 2005. **109**(4): p. 673-89.

63. Lanzarotti, E., et al., *Aromatic-aromatic interactions in proteins: beyond the dimer.* J Chem Inf Model, 2011. **51**(7): p. 1623-33.

64. Tauer, T.P. and C.D. Sherrill, *Beyond the benzene dimer: an investigation of the additivity of pi-pi interactions.* J Phys Chem A, 2005. **109**(46): p. 10475-8.

65. Ugur, I., et al., *1,3-Dipolar Cycloaddition Reactions of Low-Valent Rhodium and Iridium Complexes with Arylnitrile N-Oxides.* J Org Chem, 2017. **82**(10): p. 5096-5101.

66. Menhofer, M.H., et al., *In vitro and in vivo characterization of the actin polymerizing compound chondramide as an angiogenic inhibitor.* Cardiovasc Res, 2014. **104**(2): p. 303-14.

67. Sotiropoulos, A., et al., *Signal-regulated activation of serum response factor is mediated by changes in actin dynamics.* Cell, 1999. **98**(2): p. 159-69.

68. Allen, P.G. and P.A. Janmey, *Gelsolin displaces phalloidin from actin filaments. A new fluorescence method shows that both Ca2+ and Mg2+ affect the rate at which gelsolin severs F-actin.* J Biol Chem, 1994. **269**(52): p. 32916-23.

69. Wiggan, O., et al., *Cofilin Regulates Nuclear Architecture through a Myosin-II Dependent Mechanotransduction Module.* Sci Rep, 2017. **7**: p. 40953.

70. Munsie, L.N., C.R. Desmond, and R. Truant, *Cofilin nuclear-cytoplasmic shuttling affects cofilin-actin rod formation during stress.* J Cell Sci, 2012. **125**(Pt 17): p. 3977-88.

71. Fiore, A., et al., *Laminin-111 and the Level of Nuclear Actin Regulate Epithelial Quiescence via Exportin-6.* Cell Rep, 2017. **19**(10): p. 2102-2115.

72. Allingham, J.S., V.A. Klenchin, and I. Rayment, *Actin-targeting natural products: structures, properties and mechanisms of action.* Cell Mol Life Sci, 2006. **63**(18): p. 2119-34.

73. Filipuzzi, I., et al., *Direct Interaction of Chivosazole F with Actin Elicits Cell Responses Similar to Latrunculin A but Distinct from Chondramide.* ACS Chem Biol, 2017. **12**(9): p. 2264-2269.

74. Allingham, J.S., C.O. Miles, and I. Rayment, *A structural basis for regulation of actin polymerization by pectenotoxins.* J Mol Biol, 2007. **371**(4): p. 959-70.

75. Allingham, J.S., et al., *Absolute stereochemistry of ulapualide A.* Org Lett, 2004. **6**(4): p. 597-9.

76. Allingham, J.S., et al., *Structures of microfilament destabilizing toxins bound to actin provide insight into toxin design and activity.* Proc Natl Acad Sci U S A, 2005. **102**(41): p. 14527-32.

77. Blain, J.C., et al., *Two molecules of lobophorolide cooperate to stabilize an actin dimer using both their "ring" and "tail" region.* Chem Biol, 2010. **17**(8): p. 802-7.

78. Hagelueken, G., et al., *The absolute configuration of rhizopodin and its inhibition of actin polymerization by dimerization.* Angew Chem Int Ed Engl, 2009. **48**(3): p. 595-8.

79. Hirata, K., et al., *Structure basis for antitumor effect of aplyronine a.* J Mol Biol, 2006. **356**(4): p. 945-54.

80. Klenchin, V.A., et al., *Structural basis of swinholide A binding to actin.* Chem Biol, 2005. **12**(3): p. 287-91.

81. Pereira, J.H., et al., *Structural and biochemical studies of actin in complex with synthetic macrolide tail analogues.* ChemMedChem, 2014. **9**(10): p. 2286-93.

82. Choe, H., et al., *The calcium activation of gelsolin: insights from the 3A structure of the G4-G6/actin complex.* J Mol Biol, 2002. **324**(4): p. 691-702.

83. Dominguez, R. and K.C. Holmes, *Actin structure and function.* Annu Rev Biophys, 2011. **40**: p. 169-86.

84. Galkin, V.E., et al., *Remodeling of actin filaments by ADF/cofilin proteins.* Proc Natl Acad Sci U S A, 2011. **108**(51): p. 20568-72.

85. Irobi, E., et al., *Structural basis of actin sequestration by thymosin-beta4: implications for WH2 proteins.* Embo j, 2004. **23**(18): p. 3599-608.

86. Schutt, C.E., et al., *The structure of crystalline profilin-beta-actin.* Nature, 1993. **365**(6449): p. 810-6.

87. Gurel, P.S., et al., *Cryo-EM structures reveal specialization at the myosin VI-actin interface and a mechanism of force sensitivity.* Elife, 2017. **6**.

88. Shoji, K., et al., *Cytochalasin D acts as an inhibitor of the actin-cofilin interaction.* Biochem Biophys Res Commun, 2012. **424**(1): p. 52-7.

89. Heisler, D.B., et al., *ACTIN-DIRECTED TOXIN. ACD toxin-produced actin oligomers poison formin-controlled actin polymerization.* Science, 2015. **349**(6247): p. 535-9.

90. Laskowski, R.A. and M.B. Swindells, *LigPlot+: multiple ligand-protein interaction diagrams for drug discovery.* J Chem Inf Model, 2011. **51**(10): p. 2778-86.

8 Appendix

8.1 Supplementary Figures
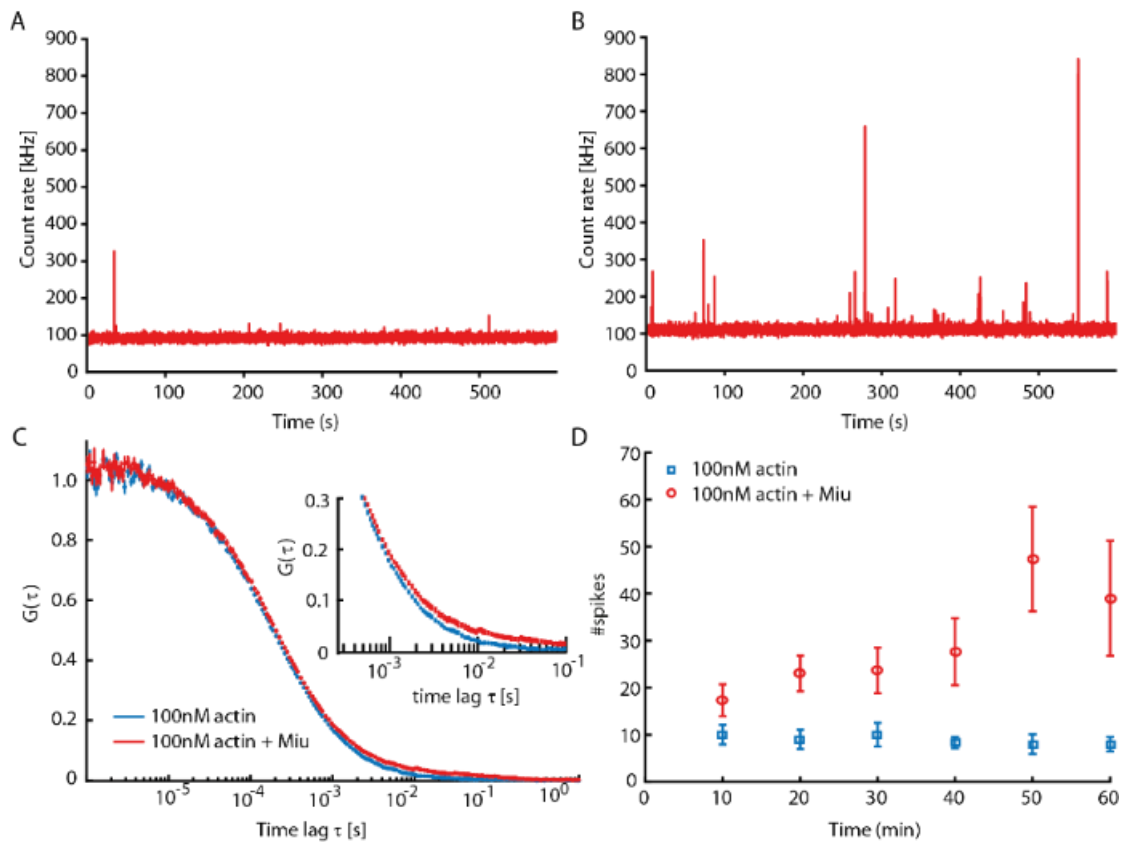
Figure S 1 Measurement of actin nucleation by Fluorescence correlation spectroscopy (FCS) experiment

The fluorescence signal of 100 nM actin-atto488 as a function of time after 1h incubation, without (A) and with (B) 10 × excess of Miuraenamide A. (C) FCS curves of 100 nM actin-atto488 with and without Miuraenamide A. Inset: detail of the autocorrelation function at longer timescales showing the formation of larger oligomers with Miuraenamide A. (D) Number of spikes due to filaments diffusing through the observation volume in 10 min time intervals. The data show that up to 6 times more spikes are observed during the course of one hour in the presence of Miuraenamide A. Error bars represent the standard error of the mean of three independent measurements. (Results were provided by Prof. Dr. Don C. Lamb, Department Chemistry, Ludwig-Maximilians University Munich, Germany)
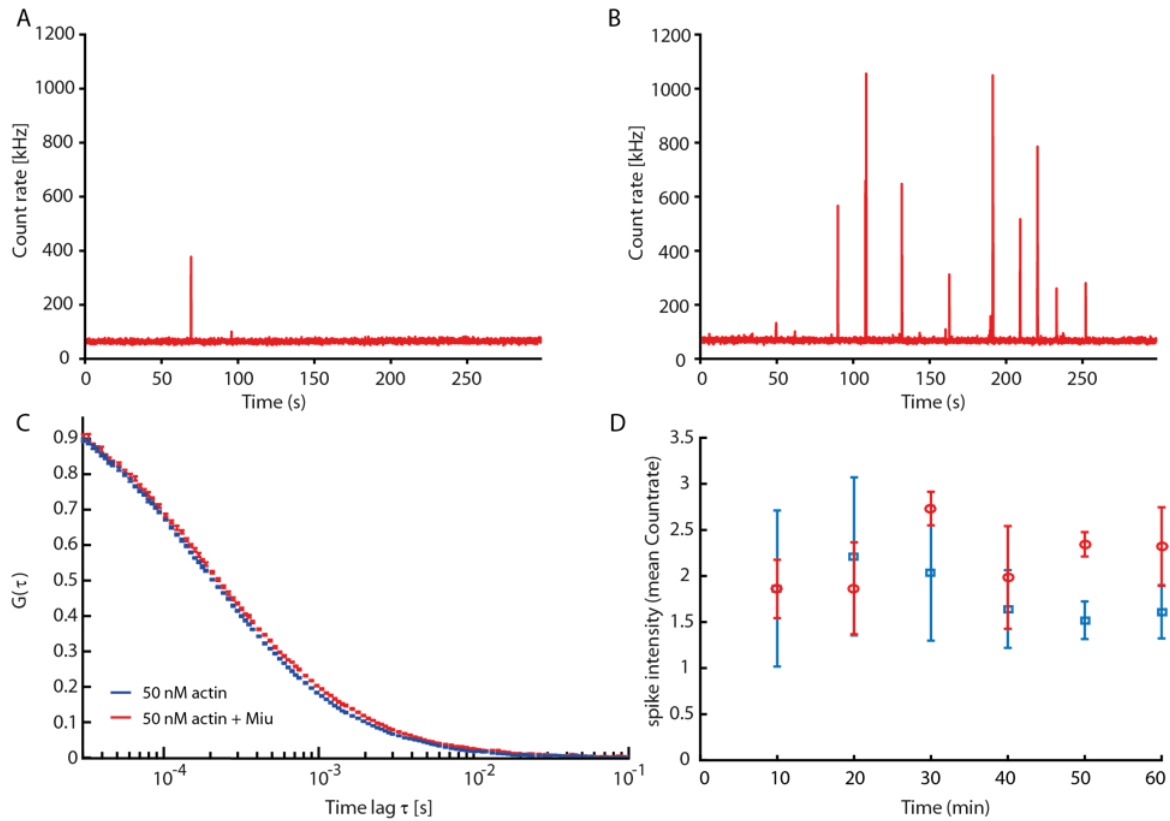
Figure S 2 Influence of MiuA on the formation of small oligomers of actin

(A, B) MiuA lowers the critical concentration of actin polymerization. The fluorescence intensity as a function of time is shown for 50 nM atto488 labeled actin after 1h incubation, without (A) and with (B) 10x excess of MiuA. (C) FCS curves of 50 nM actin-atto488 with and without MiuA, the emergence of a slowly diffusing component due to the formation of small oligomers is observed. (D) The Intensity of spikes (in units of the mean count rate) is shown for the respective measurements. Blue squares: 100 nM actin-atto488, red circles: 100 nM actin-atto488 and 1 µM MiuA. Error bars represent the standard error of the mean of three independent measurements. After 30 min of incubation, a higher spike intensity is observed for actin in the presence of MiuA. (Results were provided by Prof. Dr. Don C. Lamb, Department Chemistry, Ludwig-Maximilians University Munich, Germany)
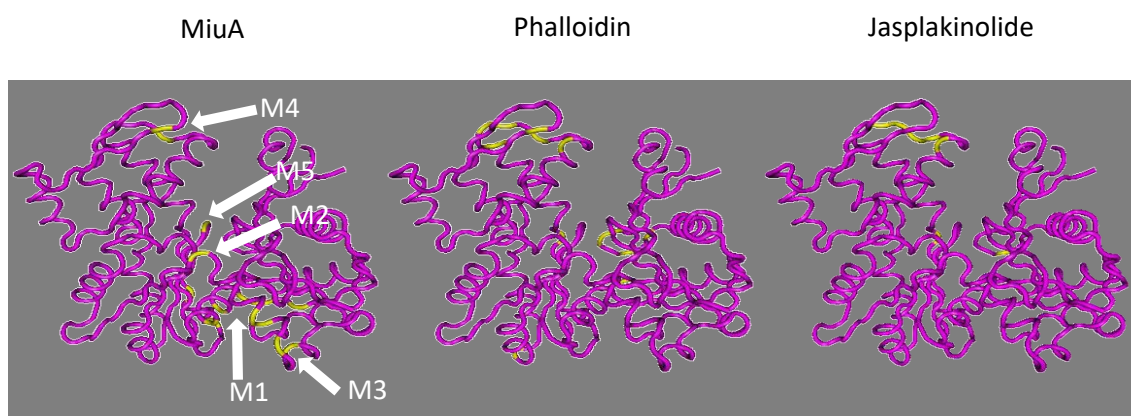
**Figure S 3 Binding sites for miuA, phalloidin and jasplakinolide**

Five potential binding sites for MiuA (M1 to M5) obtained by the computer-based docking simulations are projected into the G-actin monomer (Protein Data Bank: 3HBT). G-actin: magenta, respective binding sites of the compounds: yellow. (Data were provided by Prof. Iris Antes, Protein Modelling group, Technical University of Munich, Germany)
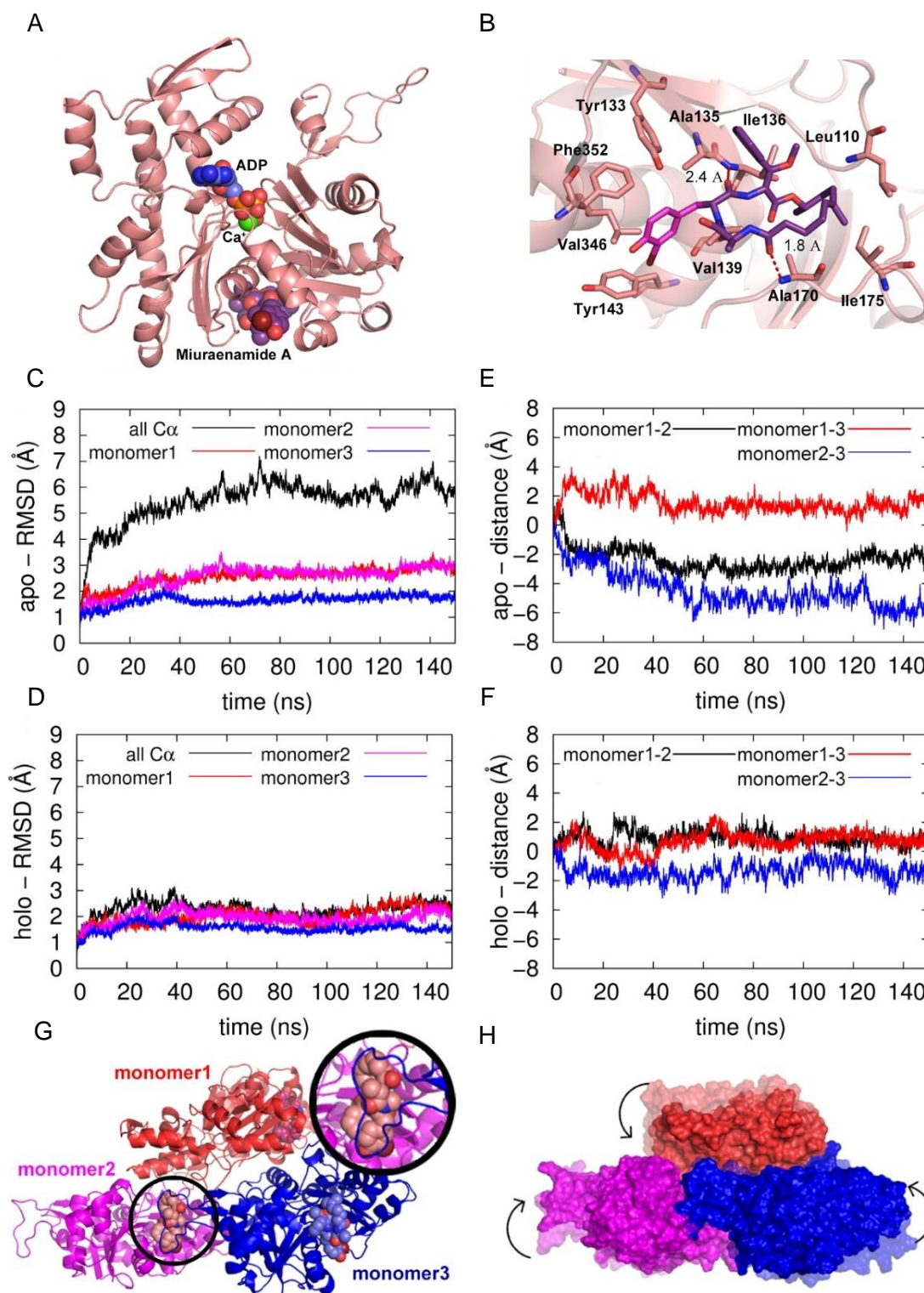
Figure S 4 Structures of the docked Miuraenamide A and after 25 ns of MD equilibration

A global view of the system is presented in (A) and (B) gives a detailed view of the binding site. Actin is shown in cartoon representation, ADP (blue), Ca+ (green) and Miuraenamide A (purple) are shown as van der Waals spheres (A) and as sticks (B). Residues interacting with the ligand are shown with

sticks. (C+D) RMSD time-series (Å) of the apo- (C) and holo- (miuraenamide A bound) (D) simulations. The black, red, magenta, and blue colors represent the deviations of α carbon atoms of the trimer, monomer1, monomer 2 and monomer 3 from the initial structures, respectively. (E+F) The deviation of the distances of pairs of monomers (based on the center of mass of the stable β-sheet regions of each monomer) from the initial structure as a function of time for the apo- (E) and holo- (F) systems. (G) The orientation of Miuraenamide A within the trimer is depicted with an additional focus on the interaction between the D-loop of monomer 3 and the ligand of monomer 2 in the inset. (H) The difference in packing between the apo- (transparent coloring) and holo- (solid coloring) trimer systems is illustrated for a representative structure of the two complexes. (Data were provided by Prof. Iris Antes, Protein Modelling group, Technical University of Munich, Germany)
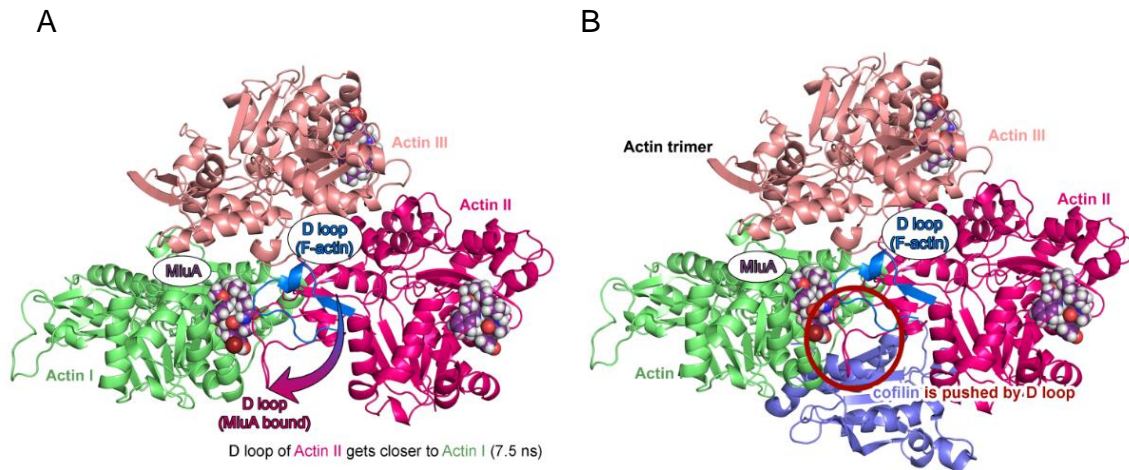
Figure S 5 Conformational changes induced by binding of MiuA

(A) Once MiuA binds to F-actin, the D-loop of monomer 3 moves closer to monomer 2 during the molecular dynamics simulation. (B) MiuA and cofilin bound to the F-actin (the position of cofilin is shown as bound in the apo-structure with F-actin). The new conformation of the D-loop overlaps with the bound conformation of cofilin. (Data were provided by Prof. Iris Antes, Protein Modelling group, Technical University of Munich, Germany)
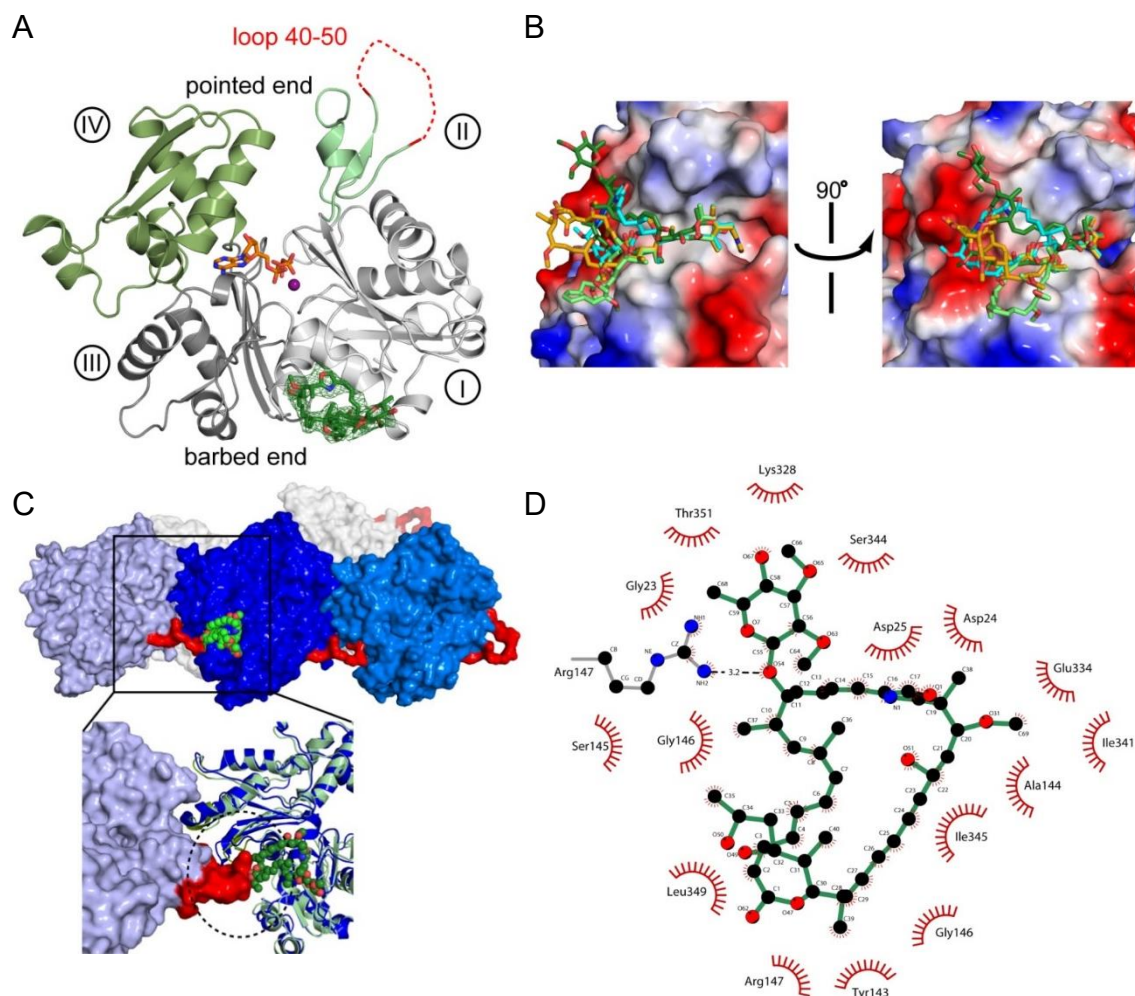
Figure S 6 X-ray crystal structure of G-actin in complex with chivosazole A

(A) Structure of the actin-chivosazole A complex, overall folding topology and domain structure. The actin is depicted as ribbon, with the four domains highlighted. The ATP (orange) and chivosazole A (green) are shown as stick model, the magnesium ion as sphere (purple). Overlaid, for chivosazole A the simulated annealing Fo-DFc difference electron density is contoured at 2.5 (green). (B) Superposition of actin structures in complex with macrolides. The actin surface is colored according to the surface residue charges and the macrolides are shown as stick models. Chivosazole A (dark green, this work), lobophorolide (light green, PDB code 3M6G), jasplakinolide A (cyan; PDB code 1QZ6) and sphinxolide B (golden; PDB code 2ASO). (C) Mapping of the chivosazole A (green space-fill model) binding side on the surface of the cryo-EM F-actin structure (PDB code 6BNO). Inset: zoom in the F-actin interface (blue) overlaid with the actin-chivosazole A complex (green). The DNase-binding loop (residues 40-50) of subdomain 2 interacting with subdomain 1 is shown in red. (D) Schematic diagram of the interactions between actin and chivosazole A. Hydrophobic interactions are indicated by the red half-circles. The 2D-plot was prepared with LigPlot[90]. (Data were provided by Dr. Sabine Schneider, Department of Chemistry, Technical University of Munich, Germany)
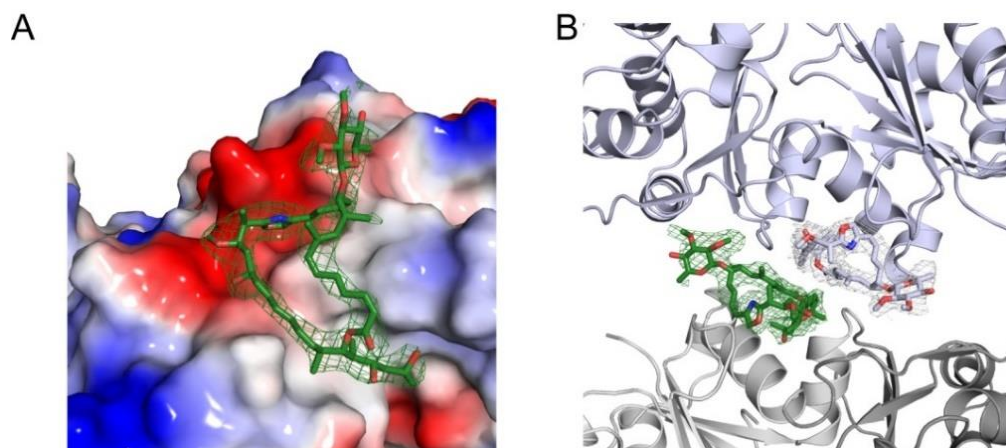
Figure S 7

(A) Simulated annealing Fo-DFc difference electron density (contoured at 2.5 σ; green) of Chivo A, with the actin surface coloured according to the surface residue charges. (B) Crystal-lattice contacts at the ChivoA binding site. (Data were provided by Dr. Sabine Schneider, Department of Chemistry, Technical University of Munich, Germany)
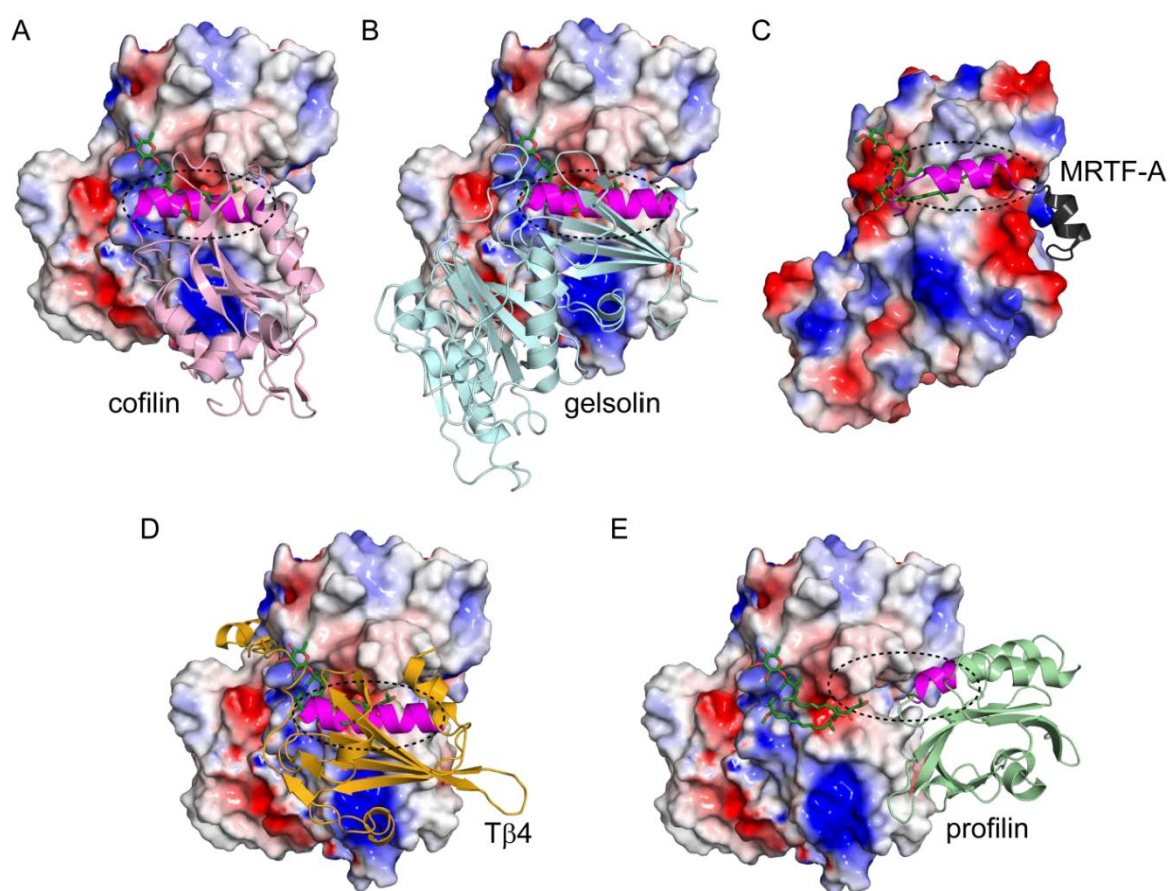
Figure S 8 Comparison of chivosazole A binding site and the interaction interface of actin binding proteins

(A) cofilin (light pink; PDB code 3J0S), (B) gelsolin (cyan; PDB code 1H1V), (C) MRTF-A (grey, PDB code 2V52), (D) thymosin β4 (Tβ4) (golden; PDB code 1T44) and (E) profilin (light green; PDB code 2BTF). The actin is shown as surface representation colored according to the surface charge. ChivoA is depicted as green stick model. The amphiphilic helices of the actin-binding proteins, which pack into the target binding grove, are highlighted in pink. (Data were provided by Dr. Sabine Schneider, Department of Chemistry, Technical University of Munich, Germany)

8.2 Supplementary Tables

Treatment	Total number of differentially regulated genes	Number of upregulated genes	Number of downregulated genes
Miuraenamide A (60 nM) vs. control	779	384	395
Jasplakinolide (120 nM) vs. control	224	132	92
Miuraenamide A (60 nM) vs. Jasplakinolide (120 nM)	101	55	46

Table S 1 Gene regulation by miuraenamide A and jasplakinolide after 4 h

Treatment of HUVECs with a well-tolerated concentration of Miuraenamide A (60 nM) or and equipotent concentration of jasplakinolide (120 nM) for 4 h caused dramatic effects on transcriptional regulation. Assessment of transcriptome was performed by Prof. Dr. Wolfgang Enard (Department Biology II, Ludwig-Maximilians University Munich, Germany).

GO, ID	Term	Annotated	Significant	Expected	Fisher
GO:0071456	cellular response to hypoxia	146	7	1,09	0,00011
GO:0030509	BMP signaling pathway	90	7	0,67	0,00015
GO:0030900	forebrain development	213	8	1,6	0,00018
GO:0045446	endothelial cell differentiation	74	5	0,55	0,00022
GO:0007568	aging	194	7	1,45	0,0006
GO:0043280	positive regulation of cysteine-type endopeptidase activity involved in apoptotic process	92	5	0,69	0,00061
GO:0045666	positive regulation of neuron differentiation	202	7	1,51	0,00077
GO:0043410	positive regulation of MAPK cascade	272	8	2,04	0,00094
GO:0006935	chemotaxis	295	8	2,21	0,00158
GO:0032496	response to lipopolysaccharide	177	6	1,33	0,00207
GO:0002064	epithelial cell development	124	5	0,93	0,00233
GO:0001558	regulation of cell growth	260	7	1,95	0,00325
GO:0071902	positive regulation of protein serine/threonine kinase activity	198	6	1,48	0,00361
GO:0051051	negative regulation of transport	265	7	1,99	0,00361
GO:0072593	reactive oxygen species metabolic process	149	7	1,12	0,00471
GO:0051216	cartilage development	110	6	0,82	0,00545
GO:0043405	regulation of MAP kinase activity	218	6	1,63	0,00576
GO:0071560	cellular response to transforming growth factor beta stimulus	155	5	1,16	0,00604
GO:0006979	response to oxidative stress	300	7	2,25	0,00706
GO:0051155	positive regulation of striated muscle cell differentiation	31	5	0,23	0,00727

Table S 2 Significant gene set enrichment (category "biological process", Fisher's exact test: <0.01) based on differentially regulated genes by Miuraenamide A compared to jasplakinolid The GOs (gene ontologies) marked in grey are unique for the comparison Miuraenamide A vs. jasplakinolide and do not show up in Miuraenamide A or jasplakinolide vs. control (provided by Prof. Dr. Wolfgang Enard, Department Biology II, Ludwig-Maximilians University Munich, Germany).

ENSEMBL	SYMBOL	baseMean	log2FoldChange	pvalue	padj
ENSG00000143869	GDF7	12.1612956	3.211230417	0.00066079	0.04390488
ENSG00000117707	PROX1	6.9950098	1.200773712	0.00038769	0.02984357
ENSG00000254409	NA	6.75172368	1.031068621	0.00075856	0.04826523
ENSG00000146592	CREB5	4.81387076	0.989692802	0.00214647	0.09695071
ENSG00000134070	IRAK2	13.4395225	0.85821141	0.00065576	0.04361793
ENSG00000138764	CCNG2	13.0686991	0.847376617	0.00013811	0.01398979
ENSG00000159167	STC1	22.7951994	0.837013708	1.71E-05	0.00295321
ENSG00000130522	JUND	41.7888712	0.767387825	3.31E-08	1.97E-05
ENSG00000196843	ARID5A	23.5057975	0.762749431	6.30E-06	0.00137834
ENSG00000147324	MFHAS1	15.1412852	0.732925029	0.00140356	0.0727488
ENSG00000185262	UBALD2	42.8586666	0.64487482	3.38E-07	0.00013123
ENSG00000131773	KHDRBS3	23.5340208	0.627094638	0.00023705	0.02070649
ENSG00000176907	C8orf4	26.9181463	0.616227006	6.12E-05	0.00760694
ENSG00000122861	PLAU	58.8854195	0.594281362	5.34E-07	0.0001904
ENSG00000102802	MEDAG	20.0934396	0.590968616	0.00142928	0.07353533
ENSG00000156030	ELMSAN1	64.7755138	0.572897126	8.00E-06	0.00166579
ENSG00000073756	PTGS2	36.0905195	0.570224831	7.02E-05	0.00836912
ENSG00000267519	LOC284454	41.4665223	0.560945617	6.59E-05	0.00792582
ENSG00000130513	GDF15	708.008436	0.517880532	1.74E-13	3.36E-10
ENSG00000114796	KLHL24	27.0924735	0.509324298	0.00116119	0.06431738
ENSG00000161940	BCL6B	43.7222369	0.50318591	6.45E-05	0.00786805
ENSG00000215788	TNFRSF25	32.6352593	0.496333564	0.00065528	0.04360987
ENSG00000102858	MGRN1	29.1883624	0.471525312	0.0018171	0.08659549
ENSG00000165434	PGM2L1	36.2370469	0.451787136	0.00092966	0.05523594
ENSG00000104419	NDRG1	65.4743738	0.433732745	5.07E-05	0.00656209
ENSG00000008513	ST3GAL1	52.2455518	0.40094068	0.00046526	0.03407745
ENSG00000173575	CHD2	47.917017	0.399692546	0.00113307	0.06351039
ENSG00000106144	CASP2	37.0511503	0.383660036	0.00149717	0.07580822
ENSG00000144580	CNOT9	90.3178913	0.37166965	3.39E-05	0.00489103
ENSG00000164938	TP53INP1	63.920527	0.370973762	0.00037737	0.0291967
ENSG00000171056	SOX7	54.8476519	0.360656701	0.00072401	0.04700333
ENSG00000137834	SMAD6	121.948355	0.3585581	0.0002086	0.01893161
ENSG00000130340	SNX9	66.2626525	0.355227145	0.00050724	0.03650922
ENSG00000138434	SSFA2	54.9343108	0.344254459	0.00101624	0.05874504
ENSG00000107438	PDLIM1	107.23865	0.332260672	0.00053902	0.03816533
ENSG00000197632	SERPINB2	78.299862	0.326985741	0.00160777	0.07936332
ENSG00000136802	LRRC8A	235.319363	0.325326803	1.92E-08	1.23E-05
ENSG00000183578	TNFAIP8L3	90.7877088	0.315874037	0.00036511	0.02855605

ENSG00000228470	NA	89.6018438	0.312031431	0.00029326	0.02442774
ENSG00000158769	F11R	82.0601165	0.302235223	0.00139272	0.07246435
ENSG00000151012	SLC7A11	82.7056378	0.301238012	0.00127783	0.06819069
ENSG00000087074	PPP1R15A	106.256495	0.27161909	0.00072546	0.04702655
ENSG00000213707	NA	140.893306	0.268136758	0.00222089	0.0992403
ENSG00000011422	PLAUR	148.981947	0.25625363	0.0005689	0.03952355
ENSG00000157191	NECAP2	119.240373	0.237760585	0.00166523	0.08146062
ENSG00000162407	PLPP3	172.539066	0.233707345	0.00183159	0.08711557
ENSG00000134294	SLC38A2	357.910122	0.232223562	0.00010455	0.01136282
ENSG00000124762	CDKN1A	319.443467	0.228764937	2.38E-05	0.00375222
ENSG00000229344	NA	5665.93474	0.211642945	9.01E-05	0.0100968
ENSG00000067082	KLF6	237.579626	0.193719487	0.00115517	0.06422145
ENSG00000124766	SOX4	1254.7448	0.18198231	0.00222527	0.09932691
ENSG00000131711	MAP1B	576.803941	0.176298073	3.93E-05	0.00547202
ENSG00000142192	APP	351.095286	0.162731651	0.00198436	0.0917555
ENSG00000198786	ND5	838.781205	0.150652582	0.00074444	0.04771955
ENSG00000125810	CD93	386.776359	0.146201722	0.00204198	0.0933214
ENSG00000151131	C12orf45	268.382041	-0.21024775	0.00214708	0.09695071
ENSG00000138385	SSB	185.094093	-0.214006338	0.00142173	0.07334747
ENSG00000149357	LAMTOR1	139.431261	-0.239179547	0.00079173	0.04957737
ENSG00000133226	SRRM1	375.102906	-0.272147429	0.00051291	0.0367654
ENSG00000115875	SRSF7	119.235007	-0.297525344	0.00020567	0.01881552
ENSG00000139168	ZCRB1	131.131784	-0.304510218	0.0014063	0.07282885
ENSG00000133773	CCDC59	85.2291742	-0.307601768	0.00201229	0.09246211
ENSG00000238072	NA	69.5976404	-0.307819146	0.00215496	0.09707743
ENSG00000048162	NOP16	134.341148	-0.313659024	2.15E-05	0.00348392
ENSG00000240298	NA	62.3763571	-0.319876639	0.00191628	0.08974243
ENSG00000179131	NA	77.2328996	-0.331069114	0.00216514	0.09750007
ENSG00000164741	DLC1	51.9483834	-0.345891822	0.00185087	0.08762236
ENSG00000142871	CYR61	235.361041	-0.370878102	0.00016354	0.01591759
ENSG00000266086	NA	71.1093436	-0.392386662	5.06E-05	0.00655592
ENSG00000155850	SLC26A2	45.6745027	-0.444084894	0.000238	0.02074545
ENSG00000179144	GIMAP7	73.1894221	-0.469074649	4.46E-05	0.00597939
ENSG00000080608	PUM3	104.021307	-0.474190625	1.08E-05	0.0020823
ENSG00000099260	PALMD	77.5489432	-0.483968208	9.46E-06	0.00187135
ENSG00000237049	NA	30.5010276	-0.493060911	0.00108841	0.06171657
ENSG00000137463	MGARP	24.9273743	-0.521143856	0.00154892	0.077368
ENSG00000196873	CBWD3	26.5944043	-0.552697818	0.00045917	0.03376768
ENSG00000117152	RGS4	33.6028624	-0.589116209	0.00013311	0.01361863

ENSG00000120738	EGR1	15.7402692	-0.629288447	0.0019559	0.09096887
ENSG00000099860	GADD45B	22.2964557	-0.635534712	0.00030033	0.02486209
ENSG00000107984	DKK1	99.9401769	-0.650902736	6.50E-05	0.0078897
ENSG00000078401	EDN1	260.830597	-0.680275946	7.62E-09	5.73E-06
ENSG00000244756	NA	23.7608697	-0.767663412	1.30E-05	0.00241149
ENSG00000157168	NRG1	20.6776412	-0.778532334	2.79E-05	0.00420651
ENSG00000180104	EXOC3	15.8029714	-0.797772381	0.00011715	0.01231661
ENSG00000125378	BMP4	24.0942604	-0.826740033	6.51E-05	0.0078897
ENSG00000124523	SIRT5	8.94292235	-0.852466902	0.0010919	0.06182819
ENSG00000118523	CTGF	679.769853	-0.85885136	1.07E-14	2.38E-11
ENSG00000148677	ANKRD1	3885.6597	-0.889321614	9.17E-13	1.55E-09
ENSG00000178882	RFLNA	23.2346925	-1.022347951	3.40E-07	0.00013141
ENSG00000243537	NA	4.24821161	-1.286558947	0.00148006	0.07533573
ENSG00000128383	APOBEC3A	3.57717737	-1.405510384	0.00144089	0.07392863
ENSG00000171016	PYGO1	3.26208156	-1.439309644	0.00132005	0.06963448
ENSG00000218472	NA	5.56373608	-1.588729529	0.00032532	0.02634036
ENSG00000275757	LOC100008587	10.1139674	-1.765498882	2.05E-05	0.00338016
ENSG00000235332	NA	2.51970313	-1.860462883	0.00089551	0.05386374
ENSG00000109846	CRYAB	5.56763057	-2.016951635	5.58E-06	0.0012453
ENSG00000166165	CKB	9.31435082	-2.276836856	3.17E-05	0.00467047
ENSG00000250397	NA	1.89401328	-2.543100155	0.00187365	0.08825596
ENSG00000231034	NA	2.01281478	-2.603037911	0.00179789	0.08591501
ENSG00000234576	NA	7.74783861	-3.140189044	0.00080679	0.05013368
ENSG00000278806	NA	10.140733	-4.458140103	1.89E-05	0.00316203

Table S 3 List of the genes that are differently regulated in HUVEC cells treated with Miu A vs. Jaspla

(provided by Prof. Dr. Wolfgang Enard, Department Biology II, Ludwig-Maximilians University Munich, Germany).

GO,ID	Term	Annotated	Significant	Expected	Fisher	ratio
GO:0071260	cellular response to mechanical stimulus	56	11	2.87	0.00011	19.6
GO:0045987	positive regulation of smooth muscle contraction	11	5	0.56	0.00012	45.5
GO:0042273	ribosomal large subunit biogenesis	57	11	2.92	0.00012	19.3
GO:0045214	sarcomere organization	18	6	0.92	0.00019	33.3
GO:0030335	positive regulation of cell migration	265	31	13.59	0.0002	11.7
GO:0038096	Fc-gamma receptor signaling pathway involved in phagocytosis	62	11	3.18	0.00027	17.7
GO:0010592	positive regulation of lamellipodium assembly	13	5	0.67	0.00032	38.5
GO:0007015	actin filament organization	253	39	12.97	0.00036	15.4
GO:0045601	regulation of endothelial cell differentiation	20	6	1.03	0.00037	30
GO:0090151	establishment of protein localization to mitochondrial membrane	14	5	0.72	0.00047	35.7
GO:2001222	regulation of neuron migration	21	6	1.08	0.00049	28.6
GO:0030220	platelet formation	15	5	0.77	0.00068	33.3
GO:0030901	midbrain development	59	10	3.03	0.00075	16.9
GO:0002064	epithelial cell development	124	19	6.36	0.00081	15.3
GO:0032970	regulation of actin filament-based process	231	34	11.84	0.00092	14.7
GO:0007254	JNK cascade	130	16	6.67	0.00097	12.3
GO:0060996	dendritic spine development	61	10	3.13	0.00098	16.4
GO:0070423	nucleotide-binding oligomerization domain containing signaling pathway	32	7	1.64	0.00098	21.9
GO:0071347	cellular response to interleukin-1	51	9	2.61	0.00101	17.6
GO:0008361	regulation of cell size	107	14	5.49	0.00109	13.1
GO:0048146	positive regulation of fibroblast proliferation	33	7	1.69	0.00119	21.2
GO:0001503	ossification	240	24	12.31	0.00131	10
GO:0060333	interferon-gamma-mediated signaling pathway	53	9	2.72	0.00134	17
GO:0071417	cellular response to organonitrogen compound	341	31	17.48	0.00136	9.1

GO:0006954	inflammatory response	312	29	16	0.00137	9.3
GO:0034332	adherens junction organization	98	13	5.02	0.00143	13.3
GO:0007163	establishment or maintenance of cell polarity	123	15	6.31	0.00152	12.2
GO:0002181	cytoplasmic translation	44	8	2.26	0.00156	18.2
GO:0006937	regulation of muscle contraction	66	14	3.38	0.00166	21.2
GO:1900026	positive regulation of substrate adhesion-dependent cell spreading	26	6	1.33	0.00169	23.1
GO:0016601	Rac protein signal transduction	26	6	1.33	0.00169	23.1
GO:0007588	excretion	18	5	0.92	0.00171	27.8
GO:1902905	positive regulation of supramolecular fiber organization	120	18	6.15	0.00174	15
GO:0022618	ribonucleoprotein complex assembly	177	19	9.08	0.0018	10.7
GO:2000146	negative regulation of cell motility	154	18	7.9	0.00229	11.7
GO:0017148	negative regulation of translation	129	15	6.61	0.00245	11.6
GO:0002262	myeloid cell homeostasis	104	13	5.33	0.00246	12.5
GO:0051092	positive regulation of NF-kappaB transcription factor activity	93	12	4.77	0.00273	12.9
GO:0030260	entry into host cell	93	12	4.77	0.00273	12.9
GO:0035094	response to nicotine	20	5	1.03	0.00284	25
GO:0043123	positive regulation of I-kappaB kinase/NF-kappaB signaling	133	15	6.82	0.0033	11.3
GO:0071356	cellular response to tumor necrosis factor	187	19	9.59	0.00337	10.2
GO:0043542	endothelial cell migration	122	14	6.26	0.0038	11.5
GO:0051216	cartilage development	110	13	5.64	0.00404	11.8
GO:0030216	keratinocyte differentiation	62	9	3.18	0.00409	14.5
GO:0007179	transforming growth factor beta receptor signaling pathway	123	14	6.31	0.00409	11.4
GO:0000187	activation of MAPK activity	86	11	4.41	0.00432	12.8
GO:0034314	Arp2/3 complex-mediated actin nucleation	31	6	1.59	0.00434	19.4
GO:0061028	establishment of endothelial barrier	31	6	1.59	0.00434	19.4

GO:0048333	mesodermal cell differentiation	22	5	1.13	0.00442	22.7
GO:0010470	regulation of gastrulation	22	5	1.13	0.00442	22.7
GO:0003206	cardiac chamber morphogenesis	75	10	3.85	0.00474	13.3
GO:0045446	endothelial cell differentiation	74	15	3.79	0.00479	20.3
GO:0030048	actin filament-based movement	67	12	3.44	0.00503	17.9
GO:0002009	morphogenesis of an epithelium	341	29	17.48	0.00505	8.5
GO:1901185	negative regulation of ERBB signaling pathway	42	7	2.15	0.00505	16.7
GO:0008064	regulation of actin polymerization or depolymerization	123	20	6.31	0.00516	16.3
GO:0097421	liver regeneration	23	5	1.18	0.00542	21.7
GO:0030198	extracellular matrix organization	182	18	9.33	0.00565	9.9
GO:0001525	angiogenesis	269	28	13.79	0.00613	10.4
GO:0061842	microtubule organizing center localization	24	5	1.23	0.00656	20.8
GO:0030195	negative regulation of blood coagulation	24	5	1.23	0.00656	20.8

Table S 4 List of the gene ontologies (GO) that are significantly regulated by MiuA treatment

(provided by Prof. Dr. Wolfgang Enard, Department Biology II, Ludwig-Maximilians University Munich, Germany).

GO,ID	Term	Annotated	Significant	Expected	Fisher	ratio
GO:0030335	positive regulation of cell migration	265	14	4.39	0.00013	5.3
GO:0007015	actin filament organization	253	22	4.19	0.00014	8.7
GO:0034314	Arp2/3 complex-mediated actin nucleation	31	5	0.51	0.00014	16.1
GO:0007163	establishment or maintenance of cell polarity	123	9	2.04	0.0002	7.3
GO:0002576	platelet degranulation	80	7	1.33	0.00035	8.8
GO:0007229	integrin-mediated signaling pathway	61	6	1.01	0.00049	9.8
GO:0071346	cellular response to interferon-gamma	71	6	1.18	0.00111	8.5
GO:0003206	cardiac chamber morphogenesis	75	8	1.24	0.00116	10.7
GO:0006937	regulation of muscle contraction	66	8	1.09	0.00194	12.1
GO:0032956	regulation of actin cytoskeleton organization	210	17	3.48	0.00198	8.1
GO:0003014	renal system process	55	5	0.91	0.00209	9.1
GO:2000379	positive regulation of reactive oxygen species metabolic process	55	5	0.91	0.00209	9.1
GO:0045165	cell fate commitment	110	7	1.82	0.0023	6.4
GO:0048145	regulation of fibroblast proliferation	57	5	0.94	0.00246	8.8
GO:0019221	cytokine-mediated signaling pathway	320	13	5.3	0.00253	4.1
GO:0000910	cytokinesis	113	7	1.87	0.00268	6.2
GO:0030509	BMP signaling pathway	90	6	1.49	0.00374	6.7
GO:0032970	regulation of actin filament-based process	231	20	3.83	0.00375	8.7
GO:0051092	positive regulation of NF-kappaB transcription factor activity	93	6	1.54	0.00439	6.5
GO:0009612	response to mechanical stimulus	124	7	2.05	0.00449	5.6
GO:0002064	epithelial cell development	124	7	2.05	0.00449	5.6
GO:0048812	neuron projection morphogenesis	344	13	5.7	0.00468	3.8
GO:0032535	regulation of cellular component size	236	17	3.91	0.00547	7.2
GO:0051017	actin filament bundle assembly	98	6	1.62	0.00567	6.1

GO:0045860	positive regulation of protein kinase activity	312	12	5.17	0.00568	3.8
GO:0043588	skin development	130	7	2.15	0.00581	5.4
GO:0034333	adherens junction assembly	71	5	1.18	0.00634	7
GO:0002009	morphogenesis of an epithelium	341	17	5.65	0.00637	5
GO:0006936	muscle contraction	153	15	2.53	0.00639	9.8
GO:0030307	positive regulation of cell growth	103	6	1.71	0.0072	5.8
GO:0001525	angiogenesis	269	13	4.46	0.00737	4.8
GO:0071560	cellular response to transforming growth factor beta stimulus	155	10	2.57	0.00753	6.5
GO:0045446	endothelial cell differentiation	74	5	1.23	0.00755	6.8
GO:0071158	positive regulation of cell cycle arrest	74	5	1.23	0.00755	6.8
GO:0007160	cell-matrix adhesion	139	7	2.3	0.00829	5
GO:0008360	regulation of cell shape	108	6	1.79	0.00901	5.6
GO:0001933	negative regulation of protein phosphorylation	292	11	4.84	0.00925	3.8
GO:0003231	cardiac ventricle development	78	7	1.29	0.00926	9
GO:0008217	regulation of blood pressure	78	5	1.29	0.00938	6.4

Table S 5 List of the gene ontologies (GO) that are significantly regulated by Jaspla treatment

(provided by Prof. Dr. Wolfgang Enard, Department Biology II, Ludwig-Maximilians University Munich, Germany).

ENSEMBL	symbol	log2 fold change	adjusted p value
ENSG00000278806	NA	-4,711252094	0,00139022
ENSG00000234576	NA	-4,564728721	0,00011785
ENSG00000225718	NA	-3,510179757	0,00229876
ENSG00000231034	NA	-3,41544532	0,00626786
ENSG00000229735	NA	-3,127949743	0,01961863
ENSG00000166165	CKB	-2,704005339	9,92E-05
ENSG00000236571	NA	-2,654571366	0,04171752
ENSG00000233829	NA	-2,651032822	0,05329787
ENSG00000268391	NA	-2,381502657	0,03993551
ENSG00000251340	MTCYBP35	-2,175472007	0,04915397
ENSG00000266920	NA	-1,851983819	0,03641245
ENSG00000156466	GDF6	-1,765741656	8,92E-08
ENSG00000255266	NA	-1,676356622	0,05183135
ENSG00000109846	CRYAB	-1,669887718	0,00381191
ENSG00000078401	EDN1	-1,589883974	3,40E-39
ENSG00000165702	GFI1B	-1,569041341	0,03693842
ENSG00000118523	CTGF	-1,485906037	1,37E-38
ENSG00000125378	BMP4	-1,476586972	2,56E-13
ENSG00000107984	DKK1	-1,451643699	8,46E-19
ENSG00000235387	SPAAR	-1,345679574	1,47E-07
ENSG00000144647	POMGNT2	-1,296480359	0,00338969
ENSG00000146674	IGFBP3	-1,271827367	0,04492982
ENSG00000148677	ANKRD1	-1,264103878	7,10E-22
ENSG00000243256	NA	-1,176852375	0,00091206
ENSG00000081692	JMJD4	-1,134625587	0,00650101
ENSG00000176697	BDNF	-1,12664306	0,00611232
ENSG00000163739	CXCL1	-1,106669894	6,90E-08
ENSG00000159399	HK2	-1,100730212	0,01758736
ENSG00000142871	CYR61	-1,084531632	2,88E-23
ENSG00000120217	CD274	-1,042662377	0,05106095
ENSG00000226915	NA	-1,018300709	0,04277393
ENSG00000112029	FBXO5	-0,977233153	0,0032306
ENSG00000235045	NA	-0,954167559	0,01668169
ENSG00000117152	RGS4	-0,932751547	4,15E-08
ENSG00000151093	OXSM	-0,930204096	0,02212105
ENSG00000226860	NA	-0,921720286	0,01930647

ENSG00000104833	TUBB4A	-0,920009066	0,02173595
ENSG00000164815	ORC5	-0,898115897	0,01709753
ENSG00000178882	RFLNA	-0,891361029	0,00022723
ENSG00000157168	NRG1	-0,767036575	0,00232789
ENSG00000132436	FIGNL1	-0,736941866	0,01385136
ENSG00000115875	SRSF7	-0,716940606	1,32E-15
ENSG00000183741	CBX6	-0,713469689	0,00359312
ENSG00000092098	RNF31	-0,708179646	0,04327808
ENSG00000127824	TUBA4A	-0,704994591	0,02647267
ENSG00000179431	FJX1	-0,68995993	0,01579507
ENSG00000182253	SYNM	-0,688613397	0,01951484
ENSG00000146834	MEPCE	-0,686588486	0,02601277
ENSG00000214870	NA	-0,682478229	0,00570223
ENSG00000099860	GADD45B	-0,678618177	0,01501352
ENSG00000144120	TMEM177	-0,67293138	0,00121859
ENSG00000122971	ACADS	-0,665025042	0,01780188
ENSG00000214289	NA	-0,65332803	0,00238371
ENSG00000189369	GSPT2	-0,646458553	0,01410789
ENSG00000155438	NIFK	-0,635431774	4,79E-05
ENSG00000137267	TUBB2A	-0,605154126	3,09E-07
ENSG00000244756	NA	-0,604714512	0,01422129
ENSG00000099260	PALMD	-0,585014555	1,28E-05
ENSG00000119408	NEK6	-0,572140637	0,00839702
ENSG00000188229	TUBB4B	-0,558492083	2,43E-10
ENSG00000228495	NA	-0,555991338	0,00017305
ENSG00000137285	TUBB2B	-0,555309058	1,21E-07
ENSG00000130340	SNX9	0,747090146	5,69E-11
ENSG00000275023	MLLT6	0,747468252	0,01765458
ENSG00000166510	CCDC68	0,748366521	0,00787823
ENSG00000130513	GDF15	0,749992949	3,82E-25
ENSG00000173575	CHD2	0,752044832	2,49E-08
ENSG00000088826	SMOX	0,761299352	0,00209826
ENSG00000257242	LINC01619	0,761719758	1,23E-13
ENSG00000144560	VGLL4	0,769596185	0,00090707
ENSG00000023287	RB1CC1	0,778228714	3,01E-05
ENSG00000215788	TNFRSF25	0,794904425	6,90E-06
ENSG00000188559	RALGAPA2	0,796218801	0,02130162
ENSG00000174718	KIAA1551	0,802010826	0,00870919

ENSG00000157514	TSC22D3	0,806541361	0,02471592
ENSG00000167106	FAM102A	0,811860557	0,01293999
ENSG00000168916	ZNF608	0,82181994	0,03610715
ENSG00000101445	PPP1R16B	0,826356979	0,00650101
ENSG00000159167	STC1	0,833760609	0,0019435
ENSG00000100784	RPS6KA5	0,885357525	0,00575559
ENSG00000245532	NEAT1	0,891768378	1,02E-21
ENSG00000140199	SLC12A6	0,893582467	0,02629094
ENSG00000162852	CNST	0,896329093	0,01267482
ENSG00000152518	ZFP36L2	0,91337122	2,86E-13
ENSG00000119138	KLF9	0,916987276	0,00128791
ENSG00000109787	KLF3	0,951547018	8,52E-05
ENSG00000161940	BCL6B	0,970565409	4,99E-14
ENSG00000127528	KLF2	0,97722175	3,91E-13
ENSG00000073756	PTGS2	1,01561324	2,43E-10
ENSG00000100916	BRMS1L	1,039595297	0,03534367
ENSG00000136630	HLX	1,067377216	2,26E-08
ENSG00000164463	CREBRF	1,149750682	0,00069663
ENSG00000158859	ADAMTS4	1,178642387	4,23E-23
ENSG00000183337	BCOR	1,183057282	0,00381859
ENSG00000138061	CYP1B1	1,271957146	2,58E-06
ENSG00000154734	ADAMTS1	1,277419617	8,97E-20
ENSG00000246451	NA	1,306544402	0,02269402
ENSG00000136826	KLF4	1,407640121	0,00367329
ENSG00000154240	CEP112	1,572562073	0,01110282
ENSG00000266010	GATA6-AS1	2,120515199	0,03267041
ENSG00000134323	MYCN	2,493810056	0,03274506

Table S 6 List of genes significantly regulated in HUVECs by treatment with ChivoA

62 genes were downregulated and 39 genes were upregulated after treatment with chivosazole A (20 nM ChivoA for 4h). Orange: down regulated genes, green: upregulated genes. (provided by Prof. Dr. Wolfgang Enard, Department Biology II, Ludwig-Maximilians University Munich, Germany).

ENSEMBL	symbol	log2 fold change	adjusted p value
ENSG00000234576	NA	-5,44594474	2,64E-05
ENSG00000278806	NA	-4,5534863	0,01021061
ENSG00000225718	NA	-3,65942707	0,0083952
ENSG00000166165	CKB	-3,64435677	4,33E-05
ENSG00000231034	NA	-3,45474852	0,02475462
ENSG00000229735	NA	-3,29860145	0,0383754
ENSG00000125378	BMP4	-1,84640849	4,19E-13
ENSG00000171388	APLN	-1,75669329	1,38E-08
ENSG00000156466	GDF6	-1,65336517	5,28E-05
ENSG00000118523	CTGF	-1,5886176	5,97E-37
ENSG00000148677	ANKRD1	-1,50746647	2,70E-27
ENSG00000078401	EDN1	-1,49884512	2,73E-28
ENSG00000142871	CYR61	-1,48015156	1,25E-31
ENSG00000176697	BDNF	-1,30977432	0,01587802
ENSG00000107984	DKK1	-1,21745678	2,50E-10
ENSG00000157168	NRG1	-1,09048674	0,00032156
ENSG00000099860	GADD45B	-1,08030402	0,00090707
ENSG00000176641	RNF152	-1,03290295	5,77E-06
ENSG00000162614	NEXN	-1,0081072	5,65E-05
ENSG00000117152	RGS4	-0,93498945	1,91E-05
ENSG00000214289	NA	-0,9112063	0,00032483
ENSG00000235926	NA	-0,83259571	0,0310095
ENSG00000074590	NUAK1	-0,82519552	0,02770423
ENSG00000235387	SPAAR	-0,81742293	0,03057397
ENSG00000275342	PRAG1	-0,81729627	0,00468475
ENSG00000178882	RFLNA	-0,80660113	0,01668169
ENSG00000144120	TMEM177	-0,74529577	0,00346445
ENSG00000065613	SLK	0,55832331	0,00321601
ENSG00000173210	ABLIM3	0,56917767	0,04387971
ENSG00000119899	SLC17A5	0,57109907	0,04076403
ENSG00000173575	CHD2	0,57492698	0,00229876
ENSG00000198873	GRK5	0,58148422	0,01506679
ENSG00000106537	TSPAN13	0,5816018	0,02516905
ENSG00000123094	RASSF8	0,5971009	0,03210881
ENSG00000138434	SSFA2	0,59797009	0,00017947
ENSG00000023287	RB1CC1	0,60298942	0,02400581
ENSG00000120875	DUSP4	0,60568084	3,11E-06
ENSG00000115993	TRAK2	0,61059133	0,03266839
ENSG00000173218	VANGL1	0,61273784	0,03479464
ENSG00000114796	KLHL24	0,61950604	0,02182263

ENSG00000169554	ZEB2	0,61984925	0,00360596
ENSG00000083223	ZCCHC6	0,62899774	0,02330445
ENSG00000073756	PTGS2	0,62948363	0,0153939
ENSG00000270106	TSNAX-DISC1	0,62954492	0,02547031
ENSG00000081189	MEF2C	0,63448471	3,93E-05
ENSG00000130766	SESN2	0,63581621	0,02701907
ENSG00000153885	KCTD15	0,64004924	0,04305272
ENSG00000102802	MEDAG	0,64634328	0,03720889
ENSG00000198844	ARHGEF15	0,646879	0,00113829
ENSG00000182208	MOB2	0,64897713	0,02193628
ENSG00000128284	APOL3	0,66574637	0,00966076
ENSG00000057704	TMCC3	0,66910573	0,0240483
ENSG00000136237	RAPGEF5	0,67799611	0,04259377
ENSG00000147421	HMBOX1	0,68095517	0,00398138
ENSG00000245532	NEAT1	0,68596589	2,29E-10
ENSG00000173706	HEG1	0,68962416	7,28E-05
ENSG00000185262	UBALD2	0,6984385	4,00E-05
ENSG00000270087	NA	0,69973386	0,03080426
ENSG00000176438	SYNE3	0,70446053	0,03633968
ENSG00000182704	TSKU	0,71198787	0,00389128
ENSG00000106829	TLE4	0,71776541	0,00855571
ENSG00000139117	CPNE8	0,71785387	0,0302548
ENSG00000008294	SPAG9	0,72305503	7,15E-07
ENSG00000139112	GABARAPL1	0,73052906	1,35E-05
ENSG00000162522	KIAA1522	0,73605251	0,04171752
ENSG00000127528	KLF2	0,73714378	3,44E-05
ENSG00000148120	C9orf3	0,74059138	0,0180949
ENSG00000031081	ARHGAP31	0,75725126	0,0002442
ENSG00000174718	KIAA1551	0,76454041	0,04466995
ENSG00000134954	ETS1	0,78045459	0,00354444
ENSG00000235750	KIAA0040	0,79040678	0,0053003
ENSG00000152518	ZFP36L2	0,79056843	3,09E-07
ENSG00000111276	CDKN1B	0,79946036	0,0124363
ENSG00000139679	LPAR6	0,82781059	0,00228863
ENSG00000161940	BCL6B	0,83129616	1,71E-07
ENSG00000166510	CCDC68	0,88179459	0,00270354
ENSG00000100784	RPS6KA5	0,92198304	0,01353423
ENSG00000108840	HDAC5	0,93221944	0,01147244
ENSG00000144560	VGLL4	0,93995395	9,12E-05
ENSG00000154734	ADAMTS1	0,95255394	1,10E-07
ENSG00000157514	TSC22D3	0,9609219	0,00971846

ENSG00000106546	AHR	0,9998206	3,92E-07
ENSG00000143127	ITGA10	1,00085755	0,00029991
ENSG00000136630	HLX	1,09595384	3,49E-07
ENSG00000090776	EFNB1	1,1885352	1,09E-10
ENSG00000159167	STC1	1,36864162	1,77E-09
ENSG00000158859	ADAMTS4	1,4528086	3,95E-31
ENSG00000138061	CYP1B1	1,75541074	7,36E-12
ENSG00000143869	GDF7	3,15558201	0,03633968

Table S 7 List of genes significantly regulated in HUVECs by treatment with LatB

27 genes were downregulated and 62 upregulated with latrunculin B (250 nM LatB for 4h). Orange: down regulated genes, green: upregulated genes. (provided by Prof. Dr. Wolfgang Enard, Department Biology II, Ludwig-Maximilians University Munich, Germany).

ENSEMBL	ChivoA	ENSEMBL	LatB
ENSG00000251340	MTCYBP35	ENSG00000171388	APLN
ENSG00000109846	CRYAB	ENSG00000176641	RNF152
ENSG00000165702	GFI1B	ENSG00000162614	NEXN
ENSG00000144647	POMGNT2	ENSG00000074590	NUAK1
ENSG00000146674	IGFBP3	ENSG00000275342	PRAG1
ENSG00000081692	JMJD4	ENSG00000065613	SLK
ENSG00000163739	CXCL1	ENSG00000173210	ABLIM3
ENSG00000159399	HK2	ENSG00000119899	SLC17A5
ENSG00000120217	CD274	ENSG00000198873	GRK5
ENSG00000112029	FBXO5	ENSG00000106537	TSPAN13
ENSG00000151093	OXSM	ENSG00000123094	RASSF8
ENSG00000104833	TUBB4A	ENSG00000138434	SSFA2
ENSG00000164815	ORC5	ENSG00000120875	DUSP4
ENSG00000132436	FIGNL1	ENSG00000115993	TRAK2
ENSG00000115875	SRSF7	ENSG00000173218	VANGL1
ENSG00000183741	CBX6	ENSG00000114796	KLHL24
ENSG00000092098	RNF31	ENSG00000169554	ZEB2
ENSG00000127824	TUBA4A	ENSG00000083223	ZCCHC6
ENSG00000179431	FJX1	ENSG00000270106	TSNAX-DISC1
ENSG00000182253	SYNM	ENSG00000081189	MEF2C
ENSG00000146834	MEPCE	ENSG00000130766	SESN2
ENSG00000122971	ACADS	ENSG00000153885	KCTD15
ENSG00000189369	GSPT2	ENSG00000102802	MEDAG
ENSG00000155438	NIFK	ENSG00000198844	ARHGEF15
ENSG00000137267	TUBB2A	ENSG00000182208	MOB2
ENSG00000099260	PALMD	ENSG00000128284	APOL3
ENSG00000119408	NEK6	ENSG00000057704	TMCC3
ENSG00000188229	TUBB4B	ENSG00000136237	RAPGEF5
ENSG00000137285	TUBB2B	ENSG00000147421	HMBOX1
ENSG00000130340	SNX9	ENSG00000173706	HEG1
ENSG00000275023	MLLT6	ENSG00000185262	UBALD2
ENSG00000130513	GDF15	ENSG00000176438	SYNE3
ENSG00000088826	SMOX	ENSG00000182704	TSKU
ENSG00000257242	LINC01619	ENSG00000106829	TLE4
ENSG00000215788	TNFRSF25	ENSG00000139117	CPNE8
ENSG00000188559	RALGAPA2	ENSG00000008294	SPAG9

ENSG00000167106	FAM102A	ENSG00000139112	GABARAPL1
ENSG00000168916	ZNF608	ENSG00000235750	KIAA0040
ENSG00000101445	PPP1R16B	ENSG00000111276	CDKN1B
ENSG00000119138	KLF9	ENSG00000139679	LPAR6
ENSG00000109787	KLF3	ENSG00000108840	HDAC5
ENSG00000100916	BRMS1L	ENSG00000106546	AHR
ENSG00000164463	CREBRF	ENSG00000143127	ITGA10
ENSG00000183337	BCOR	ENSG00000090776	EFNB1
ENSG00000136826	KLF4	ENSG00000143869	GDF7
ENSG00000154240	CEP112		
ENSG00000266010	GATA6-AS1		
ENSG00000134323	MYCN		

Table S 8 List of genes significantly regulated in HUVECs only by ChivoA or only by LatB
29 genes were only downregulated by chivosazole A, but not by latrunculin B, and 19 were only upregulated by chivosazole A and not by latrunculin B. 5 genes were specifically downregulated and 40 upregulated by latrunculin B in contrast to chivosazole A. Orange: down regulated genes, green: upregulated genes (provided by Prof. Dr. Wolfgang Enard, Department Biology II, Ludwig-Maximilians University Munich, Germany).

8.3 List of Figures and Tables

8.3.1 Figures

8.3.2 Tables

8.4 Abbreviations

Table 1 List of Abbreviations

2D	two-dimensional
3D	three-dimensional
Å	Ångstrom, 10^{-10} meter
ABPs	Actin binding proteins
ADF	actin-depolymerizing factor
ANOVA	Analysis of variance between groups
APS	Ammoniumpersulfate
ADP	Adenosine diphosphate
ATP	Adenosine triphosphate
BSA	Bovine serum albumin
Cc	Critical concentration
CFL1	Cofilin-1
ChivoA	Chivosazole A
ChivoF	Chivosazole F
cm, cm^2	Centimetre, Square centimetre
COM	Center-of-masses
DE	Differential expression
DMEM	Dulbecco's Modified Eagle Medium
DMSO	Dimethyl sulfoxide
DNA	Deoxyribonucleic acid
DTT	Dithiothreithol
ECGM	Endothelial cell growth medium
EDC	1-ethyl-3-(3-dimethylaminopropyl)- carbodiimide
EDTA	Ethylenediaminetetraacetic acid
EGTA	Ethylene glycol-bis(2-aminoethylether)-N,N,N′,N′-tetraacetic acid
EM	Electron microscopy
EMT	Epithelial-to-mesenchymal transition

et al.	And others
FCS (1)	Fetal calf serum
FCS (2)	Fluorescence correlation spectroscopy
Fig.	Figure
FMI	Forward migration index
g	Gram
GOs	Gene ontologies
h	Hour
HUVECs	Human umbilical vein endothelial cells
IC 50	Half maximal inhibitory concentration
i.e.	*Id est* (that is)
Jaspla	Jasplakinolide
kcal/mol	Kilocalorie per mole
kDa	Kilodalton
L	Liter
LatB	Latrunculin B
M	Molar
MD	Molecular dynamics
MES	2-(N-morpholino)-ethanesulfonic acid
MET	Mesenchymal-to-epithelial transition
mg, ml, mM, mm	Milligram, milliliter, millimolar, millimetre
min	Minute
MiuA	Miuraenamide A
MRTF	Myocardin related transcription factor
nM, nm	Nanomolar, Nanometre
PBS	Phosphate Buffered Saline
Pen / Strep	Penicillin/Streptomycin
PFA	Paraformaldehyde
pH	Potential of hydrogen

RMSD	Root mean square deviations
rpm	Revolutions per minute
RT	Room temperature
s	Second
SATB1	special AT-rich sequence-binding protein 1
SEM	Standard error of the mean value
SDS	Sodium dodecyl sulfate
SDS-PAGE	Sodium dodecyl sulfate-polyacrylamide gel electrophoresis
Tβ4	Thymosin β4
TCE	2,2,2-Trichloroethanol
T/E	Trypsin/EDTA
TEMED	N, N, N', N' tetramethylethylene diamine
TIRF	Total internal reflection fluorescence
Tris	Trishydroxymethylaminomethane
V	Volt
v/v	Volume per volume
w/v	Weight per volume
µg, µl, µM, µm	Microgram, microliter, micromolar, micrometre
°C	Degree Celsius

8.5 Publications

Karine Pozo, Stefan Zahler, Keisuke Ishimatsu, Angela M. Carter, Rahul Telange, Chunfeng Tan, **Shuaijun Wang**, Roswitha Pfragner, Junya Fujimoto, Elizabeth Gardner Grubbs, Masaya Takahashi, Sarah C. Oltmann and James A. Bibb
Preclinical characterization of tyrosine kinase inhibitor-based targeted therapies for neuroendocrine thyroid cancer
Oncotarget. 2018; 9:37662-37675.

Shuaijun Wang, Florian Gegenfurtner, Alvaro H. Crevenna, Christoph Ziegenhain, Zane Kliesmete, Wolfgang Enard, Rolf Müller, Angelika M. Vollmar, Sabine Schneider and Stefan Zahler
Chivosazole A modulates protein-protein-interactions of actin
Journal of Natural Products. 2019 Jul 1.

Shuaijun Wang, Alvaro H. Crevenna, Ilke Ugur, Antoine Marion, Iris Antes, Uli Kazmaier, Maria Hoyer, Don C. Lamb, Florian Gegenfurtner, Zane Kliesmete, Christoph Ziegenhain, Wolfgang Enard, Angelika Vollmar and Stefan Zahler
Actin stabilizing compounds show specific biological effects due to their binding mode
Scientific Reports. 2019.

8.6 Presentations

8.6.1 Oral presentations

Shuaijun Wang, Uli Kazmaier, Rolf Müller, Angelika Vollmar, Stefan Zahler
Chivosazole A, a novel actin-binding macrolide from myxobacterium, modulates protein-protein-interactions
Graduate School Life Science Munich (LSM) retreat 2019
30th April – 3rd May, June, 2019, Munich, Germany

8.6.2 Poster presentations

Shuaijun Wang, Uli Kazmaier, Rolf Müller, Angelika Vollmar, Stefan Zahler
Biological activities of actin binding compounds in endothelial cells
EMBO | EMBL Symposium: Actin in Action: from Molecules to Cellular Functions
7th -10th, September, 2016, Heidelberg, Germany

Shuaijun Wang, Uli Kazmaier, Rolf Müller, Angelika Vollmar, Stefan Zahler
Biological activities of actin binding compound Miuraenamide A in endothelial cells
Graduate School Life Science Munich (LSM) retreat 2018
25th - 28th, June, 2018, Munich, Germany

8.7 Curriculum vitae

Personal data

Name	**Shuaijun Wang**
Date of birth	06.08.1989
Place of birth	Changchun, Jilin Province, P.R. China
Nationality	Chinese

Contact

Pharmaceutical Biology

Department of Pharmacy - Center for Drug Research

Ludwig-Maximilians-University Munich

Butenandtstr. 5-13, Haus B

81377 Munich Germany

E-mail : crystaljadav@gmail.com

Education

09.2015 - now	PhD study in Pharmaceutical Biology,
	Department of Pharmacy,
	Ludwig-Maximilians-University Munich, Germany
	Prof. Dr. Stefan Zahler
09.2012 - 06.2015	Master study in Pharmacology,
	Department of Pharmacology,
	School of Pharmaceutical Sceinces,
	Jilin University, P.R. China,
	Prof. Dr. Dayuan Sui
09.2004 - 06.2008	Bachelor study in Pharmaceutical Sciences,
	School of Pharmaceutical Sceinces,
	Jilin University, P.R. China,

Grants/Funding

Since 09.2015	financial support by China Scholarship Council
Since 01.2018	Life Science Munich doctoral programme

8.8 Acknowledgements